EFFECTS OF LOW-FREQUENCY VIBRATION ON MECHANICAL PROPERTIES AND MICROSTRUCTURE OF ALUMINIUM EUTECTICS

by

SÜHEYL BAYBALI

B.S. in M.E., Boğaziçi University, 1982

Submitted to the Institute of Graduate Studies in Science and Engineering in Partial fullfillment of the requirements for the degree of

Master of Science

in

Mechanical Engineering

Boğaziçi University

1984

EFFECTS OF LOW-FREQUENCY VIBRATION ON MECHANICAL PROPERTIES AND MICROSTRUCTURE OF ALUMINIUM EUTECTICS

APPROVED BY

Doç.Dr.Sabri ALTINTAŞ.....S.Altıntaş.....

Doç.Dr.Başar CİVELEK..M.Başar Civelek

Dr.Vahan KALENDEROĞLU...V.Kalenderoğlu....

Doç.Dr.Öktem VARDAR.....Vardar.....

DATE OF APPROVAL 26/11/1984

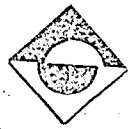

ACKNOWLEDGEMENT

I would like to express my sincere gratitude to my thesis supervisor Doç.Dr.Sabri Altıntaş for his precious guideance and invaluable contributions throughout the preperation of this study.

I express my appreciation to Aytanç Makina for their helps in building the apparatus of the experiments.

I am also indepted to Adnan Koru for his precious guiadence in my works and to Hakan Örüç, Murat Taşman and Kenan Doğaç for their helps during the experiments.

Süheyl Baybalı

October, 1984

EFFECTS OF LOW-FREQUENCY VIBRATION ON MECHANICAL PROPERTIES AND MICROSTRUCTURE OF ALUMINIUM EUTECTICS

In this study, the effects of low-frequency vibration on mechanical properties and microstructure of aluminium eutectics, Al-% 33 Cu, Al-% 12.6 Si, Al-% 5.7 Ni, were investigated.

A brief rewiev of the eutectic solidifying structures and the theory of the applied low-frequency vibration were presented to-gether with the effects of low-frequency vibration on lamellar, dendritic solidifying structures and on pure metals, solid solutions and eutectics.

In the experimental work, unvibrated and vibrated aluminium eutectic ingot castings were treated to differant rate of solidification and then the mechanical properties were measured with tensile and hardness testing. The resulting microstructure was investigated in detail to reveal the effects produced by variable solidification rate and low-frequency vibration.

Finally, the obtained ultimate tensile strength and Vickers hardness data have been correlated to the increasing mould temperature, casting temperature and vibration amplitude.

ÖZET

Bu çalışmada düşük frekanslı titreşimin,ötektik aluminyum alaşımlarının, Al-% 33 Cu, Al-% 12.6 Si, Al-% 5.7 Ni, mekanik özelliklerine ve mikro yapısına etkisi incelenmiştir.

Ötektik katılaşma ile ortaya çıkan yapının kısa bir özeti ve düşük frekanslı titreşim uygulamasının teorisi, düşük frekanslı titreşimin lamellar, dendritik katılaşmaya ve saf metallere,alaşımlara ve ötektiklere etkisi ile beraber sunulmuştur.

Deneysel çalışmada, titreşimli ve titreşimsiz aluminyum ötektik ingot dökümlerine değişik katılaşma hızları uygulanmıştır ve mekanik özellikleri çekme ve sertlik deneyleri ile ölçülmüştür. Sonuçta elde edilen mikroyapı değişik katılaşma hızlarının ve düşük frekanslı titreşimin etkilerini açıklamak üzere detaylarına kadar incelenmiştir.

Deneyler sonunda elde edilen çekme mukavemeti ve Vickers sertlik değerleri ile kalıp sıcaklığı, döküm sıcaklığı ve titreşim genliği arasında ilişki sunulmuştur.

TABLE OF CONTENTS

LIST OF FIGURES

LIST OF SYMBOLS

a	acceleration, m
a_o	maximum amplitude, m
b	dendrite root width, m
c	velocity of sound, ms^{-1}
d_1	liquid depth, m
d_2	mold height, m
d_3	height of ejection of drop, m
d_4	dendrite length or width of solidifying zone, m
d_5	dendite arm diameter, m
d_6	diameter of grain, m
d_7	diagonal length of intended pryramid in hardness test
d_8	diagonal length of intended pryramid in hardness test
D_m	diameter of melted region, m
D_b	diameter of bubble, m
D	ingot diameter, m
E	modulus of elasticity, Nm^{-2}
f	frequency, Hz
f_s	fraction of solid
G	temperature gradient, Km^{-1}
H	latent heat of fusion, J
ΔH	change in entalphy on melting, J
L	distance parameter for Re, m
m	mass, kg
n	integral odd number
P_a	applied pressure, pas
P_g	equilibrium gas pressure in liquid, pas
P_d	pressure at depth d_1, pas
P_{max}	maximum pressure, Nm^{-2}
P_{vibr}	$\pm \rho_L d_1 a_o$
P	pressure, pas
ΔP	change in pressure, pas
r_1	radius of bubble, m
r_2	radius of drop, m
S_{LR}, S_{HR}, S_{MI}	bending stresses, N/m^2
t	time, s
TD	thermal diffusivity, m^2s^{-1}
ΔT_f	change in freezing point, ^oK

T	Temperature, ^{o}K
ΔV	change in volume, m^3
v	velocity, ms^{-1}
w	angular velocity, s^{-1}
x	vibration amplitude variable, m
x_1	diffusivity distance, m
λ	wavelength, m
λ_1	interphase or particle distance
γ_L	surface tension of liquid, Nm^{-1}
γ_{LS}	interfacial tension, Nm^{-1}
γ	surface tension, Nm^{-1}
ρ	density, kgm^{-3}
ρ_L	density of liquid, kgm^{-3}
ρ_S	density of solid, kgm^{-3}
$\Delta\rho_1$	$\rho_S-\rho_L$, kgm^{-3}
η	viscosity, Nsm^{-2}

CHAPTER I

INTRODUCTION

The idea of improving the quality of cast metal either by chemical or mechanical means is a very old one. Therefore the structural or mechanical properties of the cast metals are tried to be improved by many mechanisms, i.e use of mould coating, catalyst or by electro-magnetic stirring, oscillation, rotation and vibration(1,2,3). In the present work the effect of low frequency vibration to the solidifying aluminium eutectic ingot castings, Al-% 33 Cu, Al-% 12.6 Si and Al-% 5.7 Ni are examined and the improvements brought to the mechanical properties and microstructure of the alloys stated.

Vibration, sonic as well as ultrasonic, is known to impart a number of notable effects into metals when applied during solidification that, suppression of columnar and dentritic growth fromation of equiaxed grains, degassification and emulsification of immissible phases were observed and as a consequence of this there was a marked improvement in mechanical properties, and structural properties(3,4,5,6). Also eutectic and near eutectic alloys, both normal and anamolous, exhibit refined dendritic growth, decreased eutectic cell size and coarsenning of the intermetallic eutectic phases by application of vibration(7,8,9) that both lamellar and dendritic growing aluminium alloys were studied to predict the effects produced on mechanical properties and microstructure of the alloys.

At present there is not a single theory which is completely successful in explaining the metallurgical effects produced by vibration on eutectic alloys. The encouraged nucleation rate due to the fragmentation of dendrite arms, formation of cavitation collapse and the reduced undercooling together with the growth rate produced by vibration is considered to be responsible for the effects pointed above. The theories concentrated on mostly induced nucleation, as for solidification to occur nucleation and subsequent growth of

the solid phase in a supercooled liquid must be initiated.

As the micro-structure and mechanical properties of the studied eutectic alloys were investigated, it was found that the vibrated ingot castings casted with increasing mould temperature presented an improved tensile strength, hardness and elongution data for Al-% 33 Cu and Al-% 5.7 Ni. Also vibrated ingots casted with increasing casting temperature showed an improved tensile strength and elongation data for Al-% 12.6 Si, while Al-% 33 Cu, Al-% 12.6 Si and Al-% 5.7 Ni showed on improved hardness data. The coarsening of the eutectic constituents also observed in ingot castings casted with increasing casting and mould temperature and vibration amplitude.

In the following chapters, chapter II and chapter III a brief rewiev of the eutectic solidifying structures and low-frequency vibration application will be given. Next, effects of low frequency vibration to the lamellar and dendritic solidifying structures and pure metals, solid solutions and eutectics will be presented. In chapter V results obtained in previous studies and in chapter VI experimental work of the present study will be given.

CHAPTER II
EUTECTIC SOLIDIFYING STRUCTURES

The complicated structure of eutectics has been investigated by many workers(7) in the past years. Beyond the studies prepared on kinetics and mechanism of the eutectic growth, many workers concentrated on the subject of the modification of eutectic structures either by chemical or mechanical effects(8,9,10). Before focusing on the effects produced by low-frequency vibration on the solidifying aluminium eutectics, a brief rewiev of the eutectic solidification will be presented.

A. EUTECTIC ALLOY STRUCTURES

A variety of structures are encountered in the metallographic examination of binary eutectic alloys, the only common feature is that two phases can always be seen. The eutectic structures that are observed can be classified into lamellar, in which both phases are lamellar, rod type, in which one phase is rod shaped and embedded into the other phase, and discontinious in which one phase consist of the isolated crystals embedded in a matrix of the other phase. There are various modifications of these basic structures sometimes caused by the tendency of interface between the two phases to conform to specific low index planes of one phase or the other.

1- Degenerated Lamellar Structures

When a lamellar binary eutectic liquid between two metals cools to its melting point and beyond, both phases will tend to form nuclei, but it is reasonable to suppose that the tendency will be intrinsically different for the two phases, so that one phase is more likely to form a nucleus than the other at any given degree of supercooling. Therefore it is concluded that only one of the two phases will be capable of

initiating eutectic crystallization.

If the second phase other than the primary of the eutectic is present in slight excess, the eutectic liquid undercools until a substantial envelope of the favorable (first) phase is formed round the primaries and this envelope initiates the lamellar growth from its surface as observed in the case of Al-% 33 Cu(7) (Figure 1).

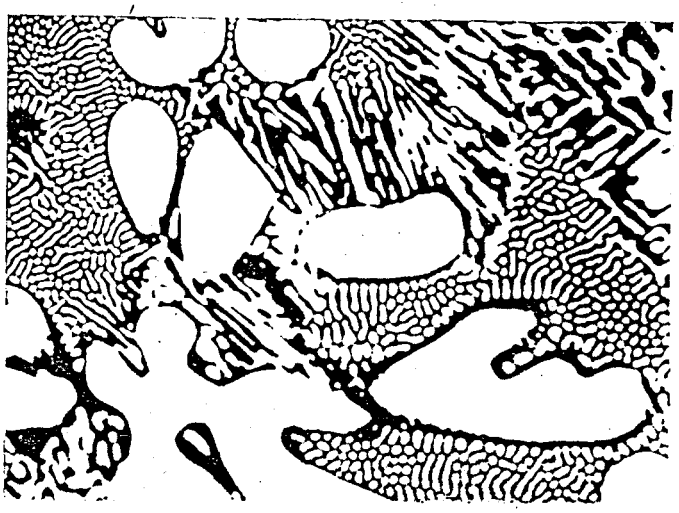

Figure 1- Primary crystals in an eutectic matrix which can not create entectic crystallization(7)

If formation of a eutectic is a secondary process, i.e predominantly primary crystallization is followed by secondary crystallization of small amount of remaining liquid, the lamellar symmetry degenerates as in the case of Al-% 5.7 Ni(11) (Figure 2). This seems to be a situation when growth of the eutectic phases on to the existing crystal substitudes for independent nucleation.

2- Discontinious Eutectic Structures

When a discontinious eutectic is investigated it is observed that one of the phases must renucleate repeatedly owing to the termination of growth of the crystals of that phase. The discontinuity of the eutectic is appearently a result of the very specific morphology of the crystals of the discontinious phase which nucleate in random orientations and

Figure 2- Predominantly primary crystallization is folloved by secondary crystallization as formation of eutectic is a secondary process. The shape and form of the degenerated lamellar structure have lost its distructive nature as illustrated above(11)

therefore grew in directions which are randomly oriented with respect to the growth interface as in the case of Al-% 12.6 Si(7) (Figure 3). Therefore the general explanation of discontinuity in eutectics is the existence of strong anisotropy in the growth characteristics of one of the phases.

Figure 3- Unmodified Al-% 12.6 Si(24), which exhibit a discontinious form of eutectic phase

CHAPTER III

LOW-FREQUENCY VIBRATION APPLICATION

The effects of vibration on solidifying metals has been investigated by many workers(3,4,6,7), and different results obtained and many theories built about the behavior of metals casted with controlled variables. Much of the confusion, in reporting has originated from the mixing of the solidification structures. These structures which are totally dissimiliar and should not be mixed can be listed as follows.

i dendrites and dentrite arms
ii grains
iii second phase as one constituent of eutectics.

Therefore taking these structures into account, a general theoretical background which would enable to correlate experimental and theoretical parameters is provided by J.Champbell(13) after the rewiev prepared by Hiedeman(14) few decades before.. This chapter is provided with the theoretical background prepared by previous workers for better understanding of low-frequency vibration effects.

A. BASIC SINE-FUNCTION RELATIONS

Since the rectilinear travel of the mould and casting is generated by rotary movement, the vibration is of simple harmonic type. So that it may be analyzed in terms of a sinusoidal wave form. Therefore it is important to remind the basic sine-function relations.

A definition of simple harmonic motion is given by,

$$a = -w^2 x \qquad (1)$$

$$w = 2\pi f \qquad (2)$$

where a is acceleration, w is angular relocity, f is frequency and x is vertical displacement.

Then the maximum acceleration is given as a_{max},

$$a_{max} = -4\pi^2 f^2 a_o \tag{3}$$

and velocity v and v_{max}

$$v = w\sqrt{a_o^2 - x^2} \tag{4}$$

$$v_{max} = 2\pi f a_o \tag{5}$$

for maximum amplitude a_o.

The power required to force a mass m, to follow the sinusoidal motion obtained as,

$$\text{force} = -mw^2 x \tag{6}$$

$$\text{work} = -mw^2 \int_o^{a_o} x\,dx = 1/2\ mw^2\ a_o^2 \tag{7}$$

and for a period f/4 the generated power is,

$$\text{power} = 1/2\ mw^2\ a_o^2\ 4f = 8\pi^2\ ma_o^2\ f^3 \tag{8}$$

B. PRESSURE VARIATIONS IN THE MELT

1- Cavitation Formation

Transmission of the wave through the molten metal under-treatment takes place by alternate compression and rarefaction of the liquid. The exerted force on the first bulk region of the liquid produced a compression zone. The reverse progress of the wave introduces a rarefied zone. These zones then travel into the liquid with gradually reducing intensity. This sinusoidal motion and generation of compression and rarefaction cycles shown in figure 4(9).

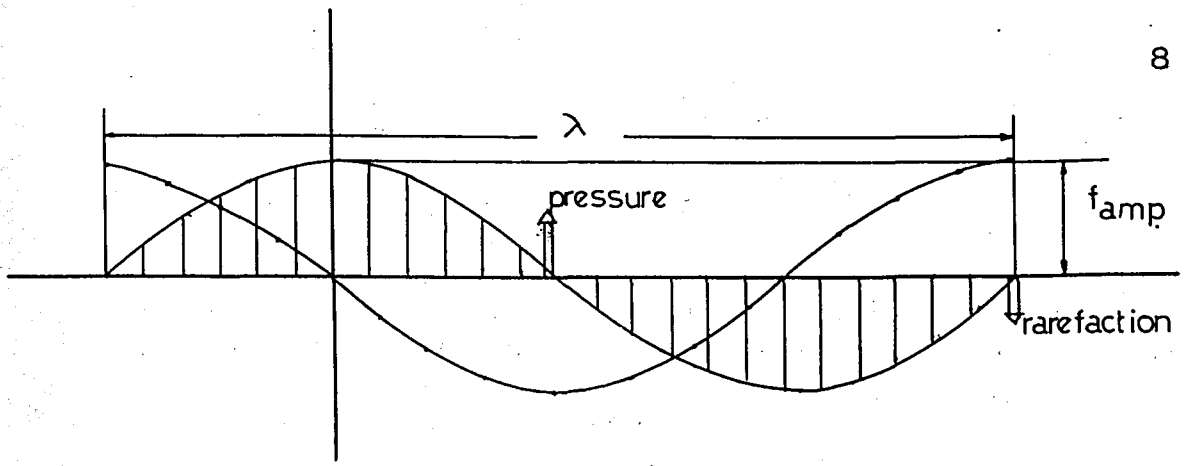

Figure 4- Sinusoidal table movement and generation of compression and rarefaction cycles(9)

During rarefaction part of the cycle cavitation may occur if the stress is high enough for the given conditions of gas and nuclei content. The possibility of cavitation occurence can be controlled from the given set of vibration conditions depending on the formulation given below.

$$P_{d_1} = P_a + \rho_L g d_1 \pm \rho_{vibr.} \tag{9}$$

$$P_{vibr.} = \pm \rho_L d_1 a_o \tag{10}$$

$$P_{d_1} = \underline{\rho}_a + \rho_L d_1 \ (\underline{a} \pm g) \tag{9-i}$$

where as P_{d_1} is the pressure experienced at height d_1, d_1 is the hight of the vibrating liquid column and ρ_L is the liquid density. Normal atmospheric pressure P_a is neglected and the maximum pressure fluctuation, P_{max}, is

$$P_{max} = \rho_L d_1 \ (g \pm a_{max}) \tag{11}$$

$$P_{max} = \rho_L d_1 \ (g \pm 4\pi^2 f^2 a_o^2) \tag{11-i}$$

when

$$g = 4\pi^2 f^2 a_o \tag{12}$$

the pressure indicated by equation 11-i becames zero throughout the liquid at one point in the cycle. If nucleation is easy cavitation may occur at that point. However if nucleation is not easy the increase of frequency or amplitude beyond this

point will cause tensile stresses in the liquid which will result in a cavitation threshold (Figure 5)(13).

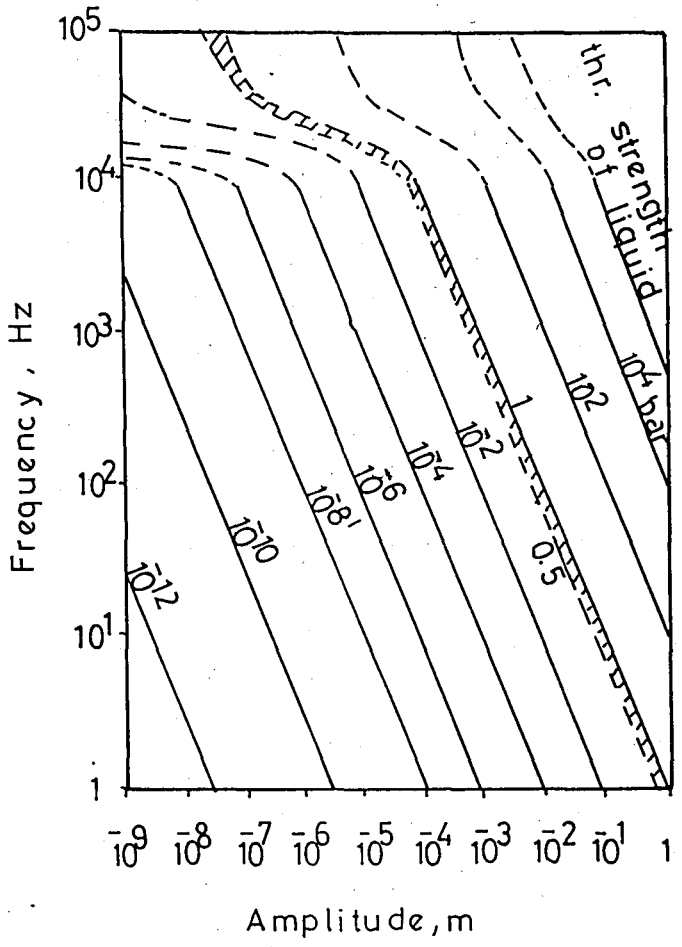

Figure 5- Frequency-amplitude map showing the peak pressures generated in casting when whole casting is vibrated(13). Shaded region indicates the theoretical cavitation threshold.

2- Cavitation Threshold

For any cavitation nucleus or bubble, to be in mechanicle equilibrium with a liquid the pressure difference, ΔP, across its liquid/gas interface must be equal;

$$\text{Internal pressure-External pressure} = 2\gamma/r_1 \qquad (13)$$

$$\Delta P = 2\gamma/r_1 \qquad (13\text{-i})$$

$$\underbrace{P_g - (P_{gh} + P_a + P_{vibr.})}_{\text{L.H.S}} = 2\gamma_{LS}/r_1 \qquad (13\text{-ii})$$

P_g is the equilibrium gas pressure in the liquid, γ_{LS} is the liquid/gass interface energy and r_1 is the diameter of the gas bubble.

The mechanical equilibrium between a bubble and a liquid no longer holds when $2\gamma_{LS}/r_1$ is smaller than L.H.S of the above equation (13-ii). The bubble grows from its original embryonic size to macroscopic dimensions and this effect can easily be produced during the negative half of the pressure cycle that $P_{vibr.}$ becomes a negative value. When the nucleation of a bubble easy due to the presence of a large nuclei and gassy metal, maximum pressure needed for bubble formation, cavitation threshold, decreases, but when nucleation of a buble is not easy, i.e liquid is very clean, cavitation tureshold increases and it is known that for very clean metals liquid can with stand 10 to 100 atmosphere multiaxial tensile stresses.

Example: Neglecting $\rho_L d_1 g$ and taking $2\gamma/r_1 = 0$ for eassy nucleation and taking $P_g = 0.5$ atm. for gassy metals, 13-ii becames

$$P_g = P_{max} \text{ and}$$

$$P_{max} = 0.5 \text{ atm.}$$

For clean metals $P_g = 1$ atm and

$$P_{max} = 1 \text{ atm.}$$

Therefore it is understood that ultimate tensile strength of the liquid is dictated by the probability of formation of a cluster of vacancies of sufficient size to exceed the critical radius. These theoretical problems of homogeneous nucleation of gaseous cavities are solved by Fisher(13) as referenced by J.Champbell(13).

3- Cavitation Collapse

The nucleated bubbles expand rapidly conserving its spherical shape under the favorable conditions of growth. When these favorable conditions disappear the bubble start to collapse. The acceleration of this collapse is increased by surface tension forces and mostly an unsymetrical explosion is observed. Theoretical calculations of the collapse pressure made by previous workers and West and Howlet(13) proved that shock waves are definitely emitted by collapse not by bubble growth. On the other hand it is proved by Hunt and Jackson(13) that the formation and the collapse of a bubble does induce the nucleation of solid from the liquid, which is being in accondance with Le Chatelier's principle, as melting point is raised by an increase in pressure for materials decrease in volume on solidification.

Using Claypeyron Equation the melting point of a metal can be calculated as a function of pressure. If it is assumed that the equation can also be used to calculate the temperature of nucleation of a supercooled melt as a function of pressure, the amount of supercooling will be constant at all pressures shown in figure 6(15). It is obvious that isothermal change which results in an increase in melting point results in an equal increase in supercooling. This increase in supercooling may now be sufficient for nucleation. Claypeyron equation is;

$$\Delta T_f / \Delta P = T.\Delta V / \Delta H \qquad (14)$$

where ΔV volume change is positive on contraction and ΔP is the change is pressure, ΔT_f is the change in freezing point temperature, ΔH change in entalphy and T is the temperature.

A pressure of 80,000 atm. was calculated using Claypeyron equation as the pressure required to increase the temperature of nucleation of nickel by $200^{o}K$. According to Lord Rayleigh(15) this very large pressure could be generated for a very brief period of time by the collapse of cavity and once nucleation occurs growth becomes the main driving force of this solidification process.

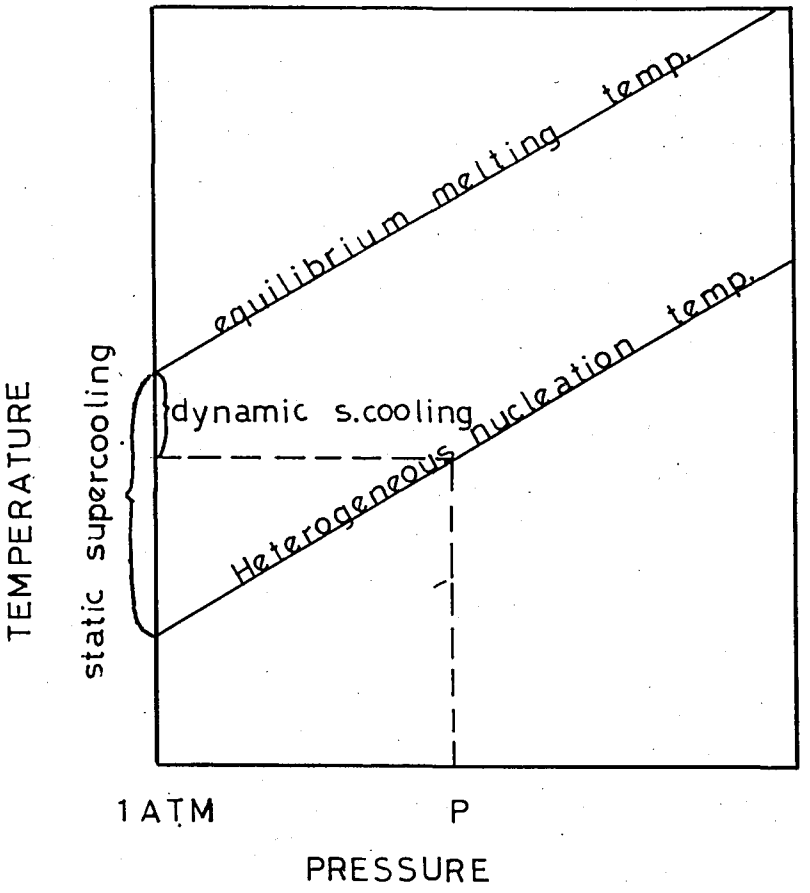

Figure 6- Melting temperature and heterogeneous nucleation temperature v.s pressure (schematic)(15)

The pressure generated by the collapse of cavitation will nucleate the solid from the liquid and sufficiently large crystal must be obtained so that it will not remelt on passing through the intermediate pressure region. The theories involve pressure changes resulting from the formation and collapse of cavities and for the case where density of solid is larger than that of liquid, the pressure wave of vibration cavitation would tend to reduce the size of critical stable solid nucleus. By the time the collapse wave would increase the solid size.

On the other hand Garlick and Wallace(4) showed the relation between solidification contraction and grain refinement depending upon the pressure cycles created during vibration, itself, not by cavitation. But the pressures obtained during the cycle itself is observed by J.Champbell to be underestimate by a factor 10^4-10^5 when the pressure needed for nucleation is considered.

4- High Rate Solidification

There are evidences that large pressures both positive and negative can arise in the liquid under conditions of rapid solidification.Few decades before Walter discovered the change in solidification structure from coarse to fine grained when nickel was supercooled more than 175^{o}K below its freezing point. Then it was suggested that at high rates of solidification cavitation can occur in the tension field ahead of the growing interface as a consequence of viscous and inertial restraints against the inrush of the liquid feed the contraction on solidification.

Horway(13) examined the tensile stresses at the growing tip and stated that 2000 atm pressure of tension was present for a period of 10^{-11}s at a solidification velocity of 100 m^{s-1}.

Therefore it is concluded that the cavitation will lead the nucleation of new solid producing a multiplication effect in ingots solidified quickly. Glicskman and Schaffer(13) related also the grain refinement due to high rate of solidification to the fragmented dendrites due to the under cooling observed.

C. FLOW EFFECTS

1- Reynolds Number Considerations

It is important to determine of the vibrating flow caused by the vibration around dendrite arms to be laminar or turbulent, since corresponding forces on the arm will be calculated from different formulae. It may be assumed that below Re number of 10 flow is laminar and above 10^{3}, flow is turbulent.

By definition,

$$Re = v\rho d_{5}/\eta \qquad (16)$$

and as the vibration is simple harmonic,

$$Re = 2\pi f a_o \gamma d_5 / \eta \qquad (17)$$

where η is liquid viscosity, d_5 is dendrite arm diameter and ρ is density. The thresholds of $Re=10^3$ and $Re=10$ are plotted in figure 7(13) to illustrate the extreme cases, i) for a heavy metal $\eta=10^4$ kgm^{-3}, $\eta=10^{-3}$ Nms^{-2} with coarse dendrite arms d=1 mm, ii) a light metal $\eta=2\times10^{+3}$ kgm^{-3}, $\eta=5\times10^{-3}$ and fine dendrite arm d=100 μm. The threshold values changes up to a factor 100 by varying flow conditions during vibration, and the flow is mostly mixed during vibration that variables are not easily controlled.

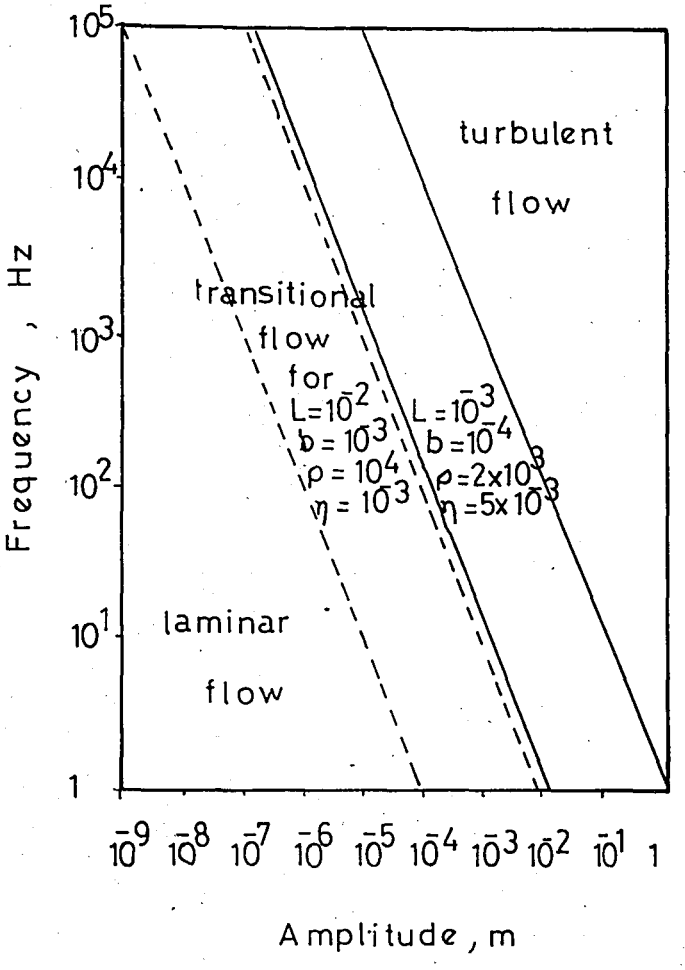

Figure 7- Thresholds of the flow regimes round dendrite arms(13). Re=10 for laminar flow and $Re=10^3$ for turbulent flow.

1- Interior Standing Wave Pattern

There is a possibility that the wave length of sound within a casting is smaller than the dimensions of the casting if the applied frequency is high or casting dimension is large. If by chance the dimension of the casting is corresponding to the quarter of the wave length, $\lambda/4$, than a standing wave patterns is possible as shown in figure 8(13).

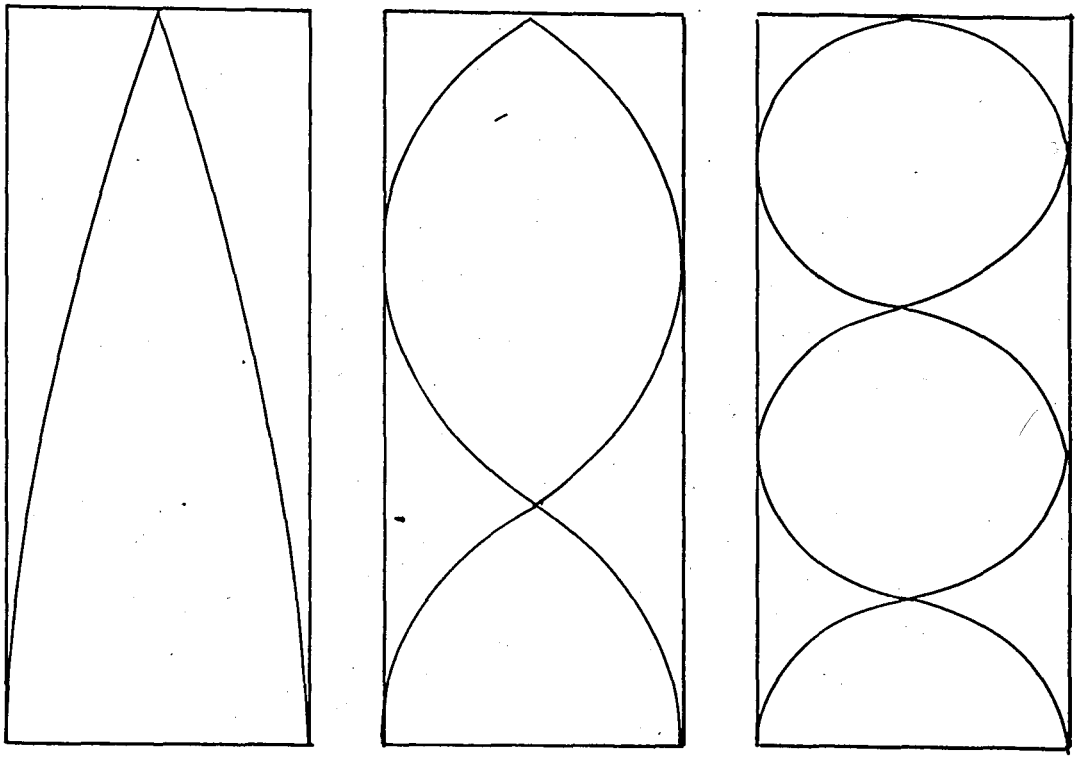

Figure 8- Standing wave pattern within an casting vibrated from its base(13)

The stationary wave pattern will occur for,

$$d_2 = n\,\lambda/4 \qquad (18)$$

$f = nc/4d_2$ where d_2 is the mold height and c is the velocity of the sound in the liquid. The approximate conditions for f-a plot for which above resonant conditions are satisfied

is illustrated in figure 9(13). If the mold dimension is choosen as 100 mm. for sound velocity of $5x10^4$ ms^{-7} in aluminium alloys, resonance can occur at 10 kHz frequency. In resonant conditions parts of the castings (antinodes) experience intense and continious vibration while neighboring regions (the nodes) remain permenantly quiescent.

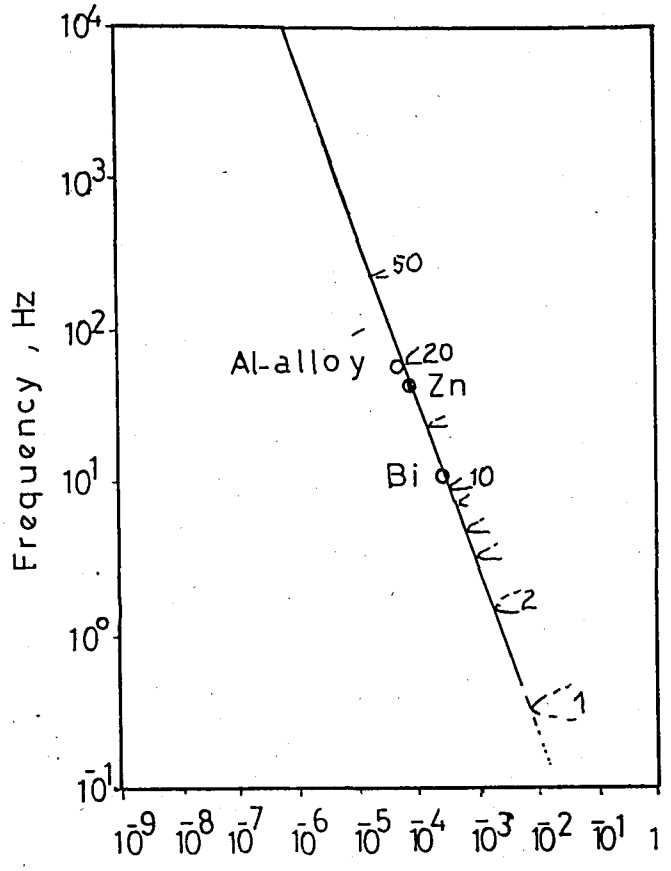

Figure 9- f-a map showing standing wave conditions within a casting and at free surface at top of casting(13). Harmonic number of resonances is shown. The experimental evidences where sufficient energy for liquid to be ejected is shown, which are satisfactorily agree with above limits(5,6,15)

2- Surface Standing Wave Pattern

The various symmetrical wave patterns which are possible for a liquid surface bounded by a circular wall is shown in figure 10(13). Velocity, u, of the standing waves,

$$u = (2\gamma\pi/\lambda\rho)^{1/2} \qquad (19)$$

and as $f.\lambda=4$

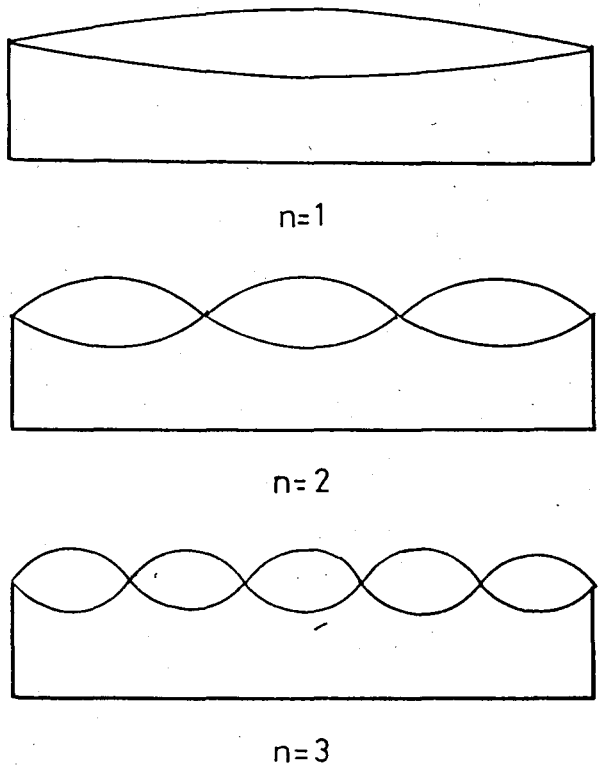

Figure 10- Axially symmetric standing wave patterns in free surface liquid(13)

$$\lambda^3 = 2\pi\gamma/\rho f^2 \qquad (20)$$

From geometrical conditions for an ingot with diameter D,

$$\lambda = 2(D/(2n+1))^{2/3} \quad \text{for} \quad n = 0,1,2...$$

the obtained frequencies of resonant surface standing waves given as

$$f^2 = \frac{\pi\gamma}{4\rho}\left(\frac{2n+1}{D}\right)^2 \qquad (21)$$

This made of standing wave pattern was reported(13) to cause the ejection of metal from the surface.

3- Droplet Ejection

The problem of ejection of metal from the surface is a serious effect since it can limit the power that can be put into the casting. The subject is examined and an energy

threshold is stated for its occurence. This threshold is in relation with the surface standing waves discussed above.

Some assumptions were made when stating the threshold;

i radius of the ejected drop, r_1, is v $\lambda/16$

ii total energy needed for drop ejection to height d_3, is $(md_3g + 4\ r_2^2\gamma)$

iii available energy from vibration,

$$2\pi^2 f^2 a_o^2\ m$$

Equating the needed energy with the available energy,

$$2\pi^2 f^2 a_o^2\ m = md_3g + 4\pi r_2^2\gamma \qquad (22)$$

and neglecting potential energy energy near surface energy and using $m = 4\pi r_2^3\rho/3$ and $r_2 = \lambda/16$

$$a_o = \left(\frac{24}{2^{1/3}\ \pi^{7/3}}\right)^{1/3} \left(\frac{\gamma}{\rho}\right)^{1/2} \cdot f^{-2/3} \qquad (23)$$

$$a_o \tilde{=} \left(\frac{\gamma}{\rho}\right)^{1/2} \cdot f^{-2/3} \qquad (23\text{-i})$$

Although the threshold for ejection of metal is passed, ejection of droplet may not be observed if conditions of surface-standing wave resonant is not full-filled.

CHAPTER IV

EFFECTS OF LOW FREQUENCY VIBRATION ON SOLIDIFICATIONS STRUCTURES, PURE METALS, SOLID SOLUTIONS AND EUTECTICS

The nucleation of new solid in front of a planar interface and the break up of dendrites occur by a number of possible mechanisms. All these possible mechanisms require the action of collapsing cavity when the theoretical background is considered. But the experimental evidences on refinement and other resultant effects with the onset of cavitation are not as clear as the theory.

The experimental evidences about the refinement of the planar and dendritic front solidifying metals are illustrated in figure 11(13). From the experimental data presented it is understood that all though significant refinement predicted in pure metals and eutectics, such as Al, Sb and Al-Si respectively, some metals do not show any refinement. Also significant coarsening of the eutectic constituents and refinement of eutectic cells observed by some workers(4,7,14).

Therefore the effect of vibration to the planar and dendritic front solidifying metals will be examined together with the effects produced in pure metals, solid solutions and eutectics (Figure 11 and 12)(13).

A. THE EFFECTS OF LOW-FREQUENCY VIBRATION TO THE PLANAR FRONT SOLIDIFICATION

1- Nucleation of New Solid

The generation of enormous local pressures during the collapse of the cavities formed during cavitation does seem capable of causing nucleation of fresh solid from the liquid, where as this newly nucleated fresh solid also succesful in surviving in the melt due to the effects of thermal spike associated with collapse. This nucleation of the fresh solid

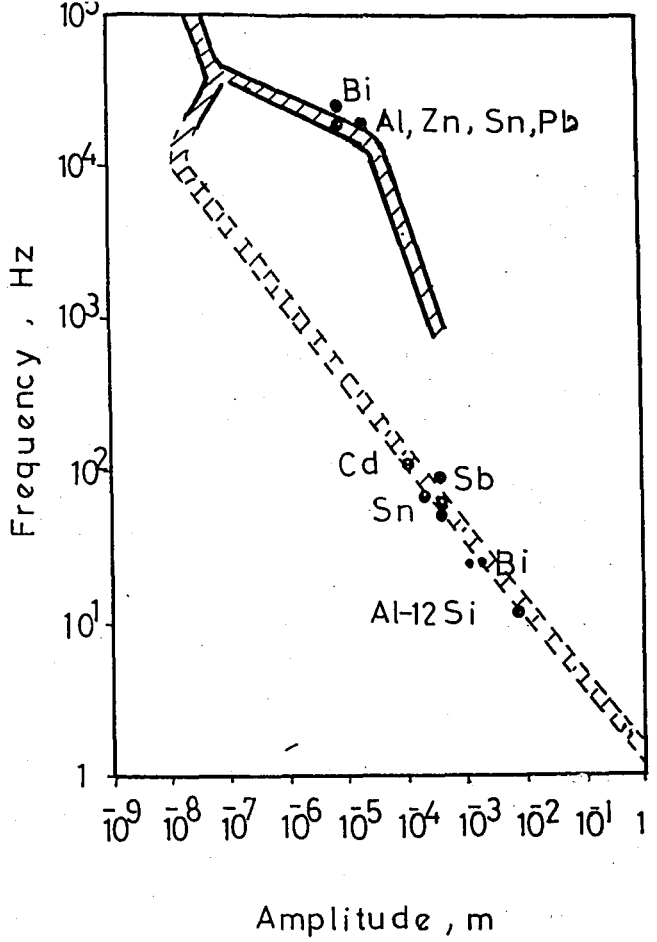

Figure 11- f-a map showing grain refinement data dealing with cellular or planar front solidification, where continious lines denoting the investigated regions with successful refinement. Discontinious lines denoting the cavitation threshold generated by transducer dipped into metal for vibration, with successfull refinement points(13)

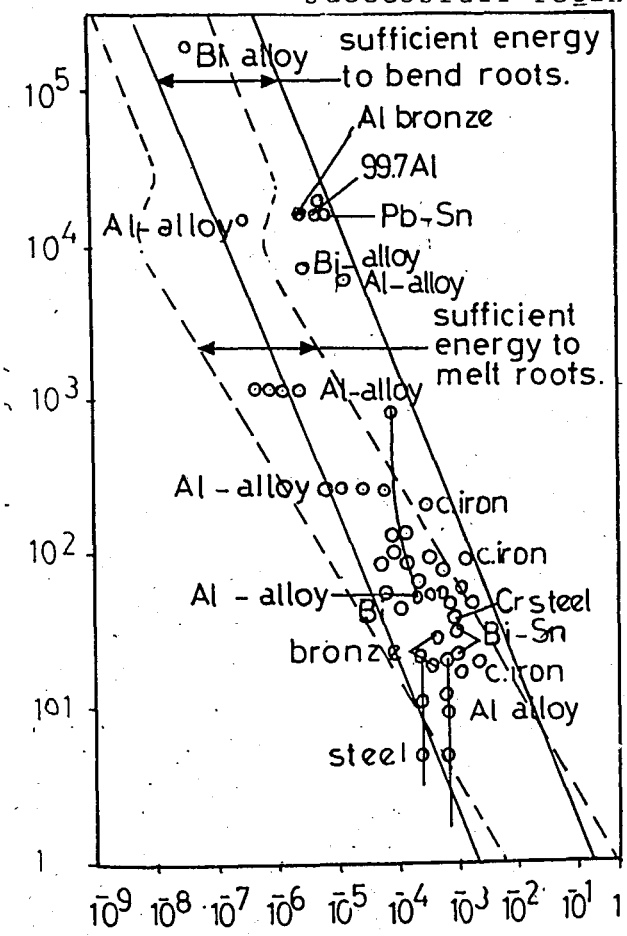

Figure 12- Experimental data from literature for grain refinement of dendritically freezing alloys(13)

o previous successful refinement points

— unsuccessful studies

from the liquid is considered to be induced by vibration, due to the formation of cavitation, that greatly discussed in section III.B.3.

2- Fracture of Existing Solid Interface

Due to the collapse of cavitation near the interface inordinary mechanical damages could be expected. Although the solid interface at temperatures near melting point highly ductile, the fracture produced by the collapse of cavitation have a local prittle character.

This may be due to a probable phase change to somehow less deformable solid product induced during the deformation, in which the expected brittle fracture could be explained with. But there is no information about the deformation of crystals at high temperatures which we can use to explain the above brittle fracture considerations, who act as individual nucleants in the liquid.

3- Melting Erosion of the Existing Solid Interface

Non-wetted particles are carried to the solid liquid interface during solidification that, these are concentrated infront of the growing interface. Therefore repeated formation and collapse of vapour bubbles infront of the interface will be expected due to the easy formation of cavitation. A gradual erosion of the interface front will be the result of these repeated formation and collapses. Then an irregular interface front formed due to erosion which might be subjected to mechanicle damage such as bending, shearing and detachment.

The evidence of erosion proved by the calculated energy emission during the cavitation collapse. The diameter of the solid melted D_m, during cavitation collapse lead to erosion calculated as following.

PdV contained within a bubble equated to the energy needed for melting;

$$PD_b^3 = (H/\rho)\, D_m^3 \qquad (24)$$

assuming P=1 atm.

$$D_b^3 = (H/\rho)\, D_m^3$$

$$D_b = (H/\rho)^{1/3}\, D_m$$

and

$$D_m = (\rho/H)^{1/3}\, D_b \simeq 10^{-1}\, D_b \qquad (24\text{-}i)$$

where p is the local pressure, H is latent heat of fusion and D_b is the bubble diameter. For a small bubble of 0.1 mm diameter the melted metal diameter is 10 m, which is comparable with the dimensions of the dendrite arms illustrated in figure 13(13).

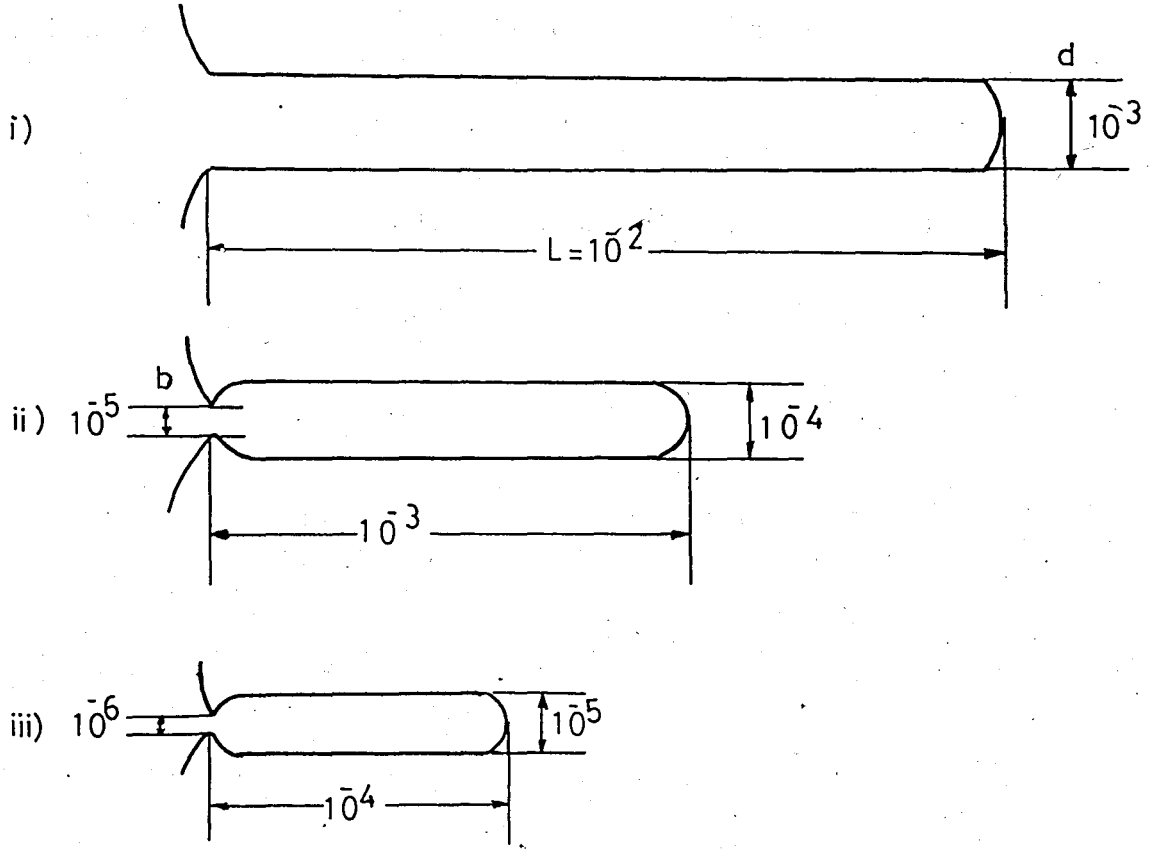

Figure 13- The three dendrite arm models used in evaluation of fragmentation stresses. i) slow, ii) medium and, iii) fast solidification rates are shown(13).

2- Dendrite Damage Models

a) Dendrite Root Shearing

At low Re the viscous drag on a dendrite arm is given Lamb's equation;

$$\text{drag force} = L\eta v/0.507 + 1.18323 \log(\eta/vd_5\rho) \quad (26)$$

where L is the distance parameter.

Neglecting logaritmic term and using v_{max} from equation(5)

$$\text{max. drag force} = 40\ \pi\eta L\acute{f}a_o \quad (27)$$

Subsequently Schmid and Roll derived the maximum shear experienced by the root, using b as dendrite width,

$$\text{max. shear stress} = 40\ \pi\eta L f a_o/b^2 \quad (28)$$

For high Re the viscous drag force on dendrite arm given as,

$$\text{drag force} = Ld_5\rho v^2 \quad (29)$$

$$\text{max. shear stress} = Ld_5\rho\ 4\pi^2 f^2 a_o^2/b^2 \quad (30)$$

The inertial force experienced by the dendrite arms is inertial force = $m_{eff} \cdot a_{max}/\text{area}$

$$\text{mertial force} = \Delta\rho L\ d_5^2\ 4\pi^2 f^2 a_o^2/b^2 \quad (31)$$

Equating the inertial and drag forces, for low Re

$$f = 10\ \eta/\pi\Delta\rho d_5^2 \quad (32)$$

and for high Re

$$P = 2/3\ \Delta\rho/\rho . d_5 \quad (33)$$

Above frequencies and amplitudes are brought together in a series of graphs to reveal the working regimes, where as the graphs prepared for different solidification rates as illustrated in figures 14-15-16(13) for Bismuth alloys.

The energy required to shear arms equated to the available energy to define a threshold for dendrite shearing. It is assumed that 2 $m/d_6^3\rho$ new interfaces are created in an interval t, having an area b^2 and surface energy γ_{LS}. Using the available energy from equation(8);

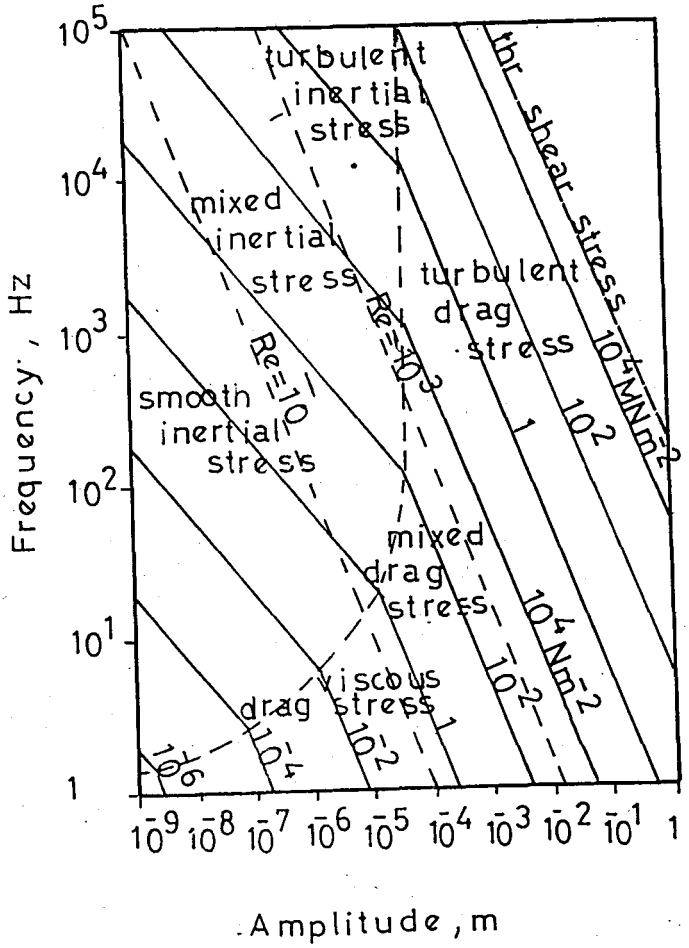

Figure 14- f-a map showing dendrite-root shearing stresses in slow freezing Bi Alloy(13)

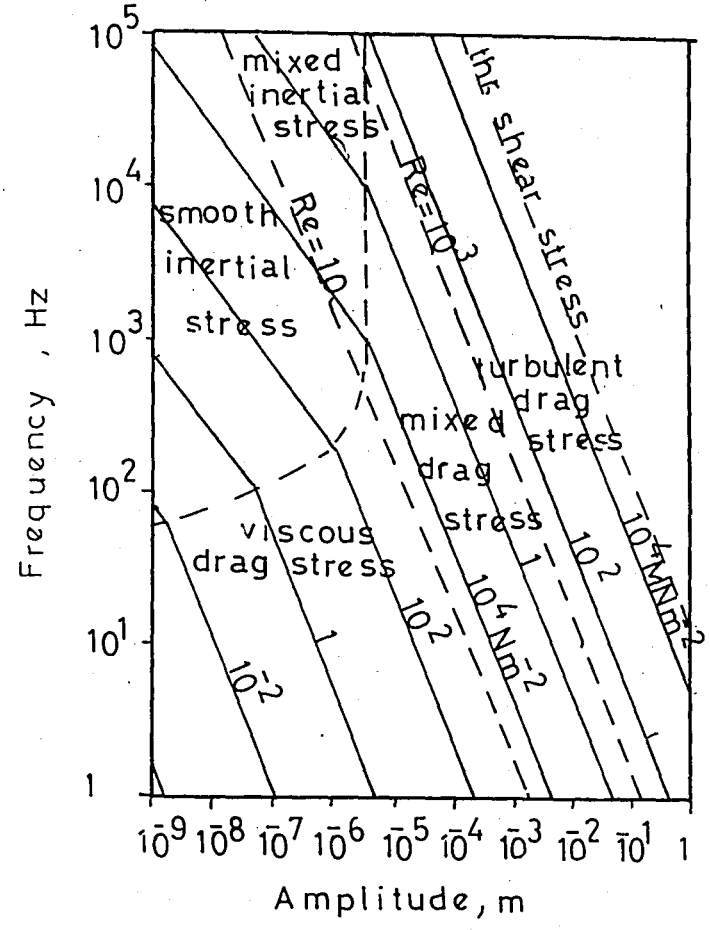

Figure 15- f-a map showing shearing stresses in narrowed roots of dendrites in Bi alloy cooled at intermediate rate(13).

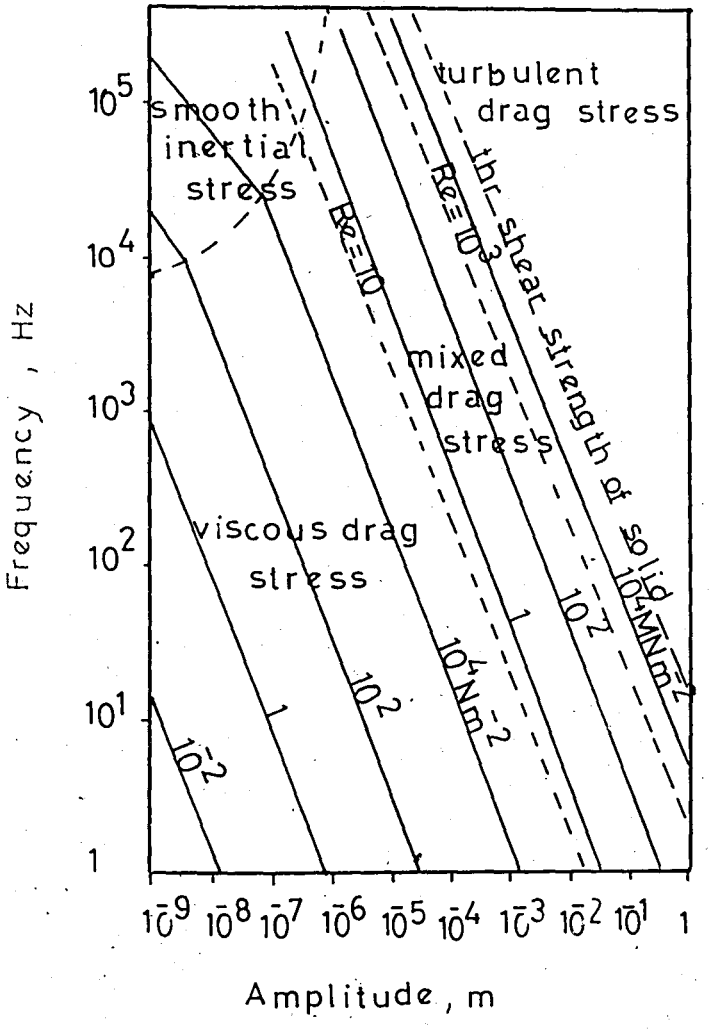

Figure 16- f-a map showing stresses in narrowed roots of dendrites in Bi alloy solidified quickly(13)

$$8\,\pi^2 f^3 a_o^2 = 2\gamma_{LS}\, b^2/\rho d_6^3\, t \qquad (34)$$

using d_6 as grain diameter.

The above defined threshold value too low when experimental data given in figure 13(13) by J.Champbell, is considered, and to match with data, γ_{LS} must be increased by a factor 10^3, during which this increase is not feasible as the energy level will reach just to the level of other failure mechanisms that will be explained in further sections.

b) Dendrite Root Bending

To obtain the maximum stress acting on the dendrite root, the moment produced by viscous-drag-force is equated with the bending moment on the dendrite root For low-Re; bending stress S_{LR} is

$$S_{LR} \cdot b^2/2 \cdot b/2 = 40\,\pi\eta L\, a_o L/2 \qquad (35)$$

$$S_{LR} = \pi\eta L^2 f a_o\, 80/b^3 \qquad (35\text{-i})$$

For high-Re; bending stress S_{HR} is

$$S_{HR} = 8\pi^2\, L^2 d_5 \rho\, f\, a_o^2/b^3 \qquad (36)$$

and the maximum mertial stress, S_{MI} ,

$$S_{MI} = 8\pi^2 f^2 L^2 a_o d_5^2\, \Delta\rho/b^3 \qquad (37)$$

When the above equations 35, 36 and 37 are compared with the ones obtained for shear stress of 28, 30 and 31 respectively, it is observed that bending stresses are larger then shear stresses at least by a factor L/b. If the dendrite models given in section IV.A.3 is considered, it is understood that L/b will lead to a factor 10 to 100 which makes dendrite bending mechanism active before any other type of damages.

Figures 17, 18 and 19(13) are constructed to reveal the working regimes of bending mechanism for different dendrite models of aluminium for three different solidification rates.

c) Dendrite Root Crystallization and Detahcment

Vogel at all(13) observed that dendrites of aluminium alloys subject to damage usually show low angle boundaries across the roots of secondary arms. Depending on this result it is concluded that near melting temperatures of solid, the dislocations created due to the bending of the root quickly climb into a low energy array resulting in a low-angle boundary. This angle will increase by the increasing bending force subjected to the root until the surrounding liquid penetrate into the boundary to detach it.

When the detachment is investigated from the point of energy it is assumed that energy needed for creating two new surfaces and for little plastic work is similar to that of ductile shear. The energy supplied by bending is much more that of shearing that the subsequent detahcment after bending of the roots is obvious.

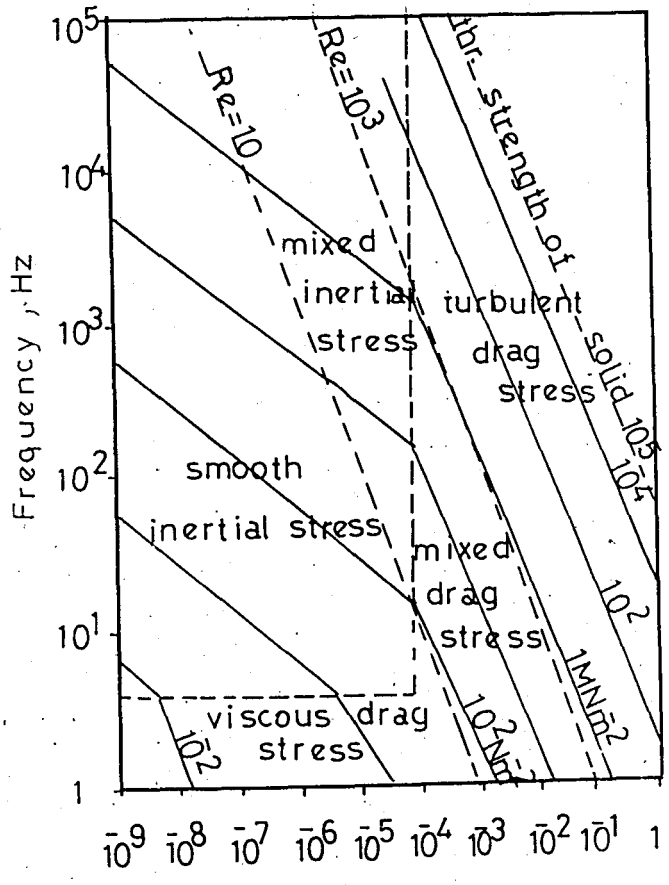

Figure 17- f-a map showing bending stresses in roots of aluminium solidified slowly(13)

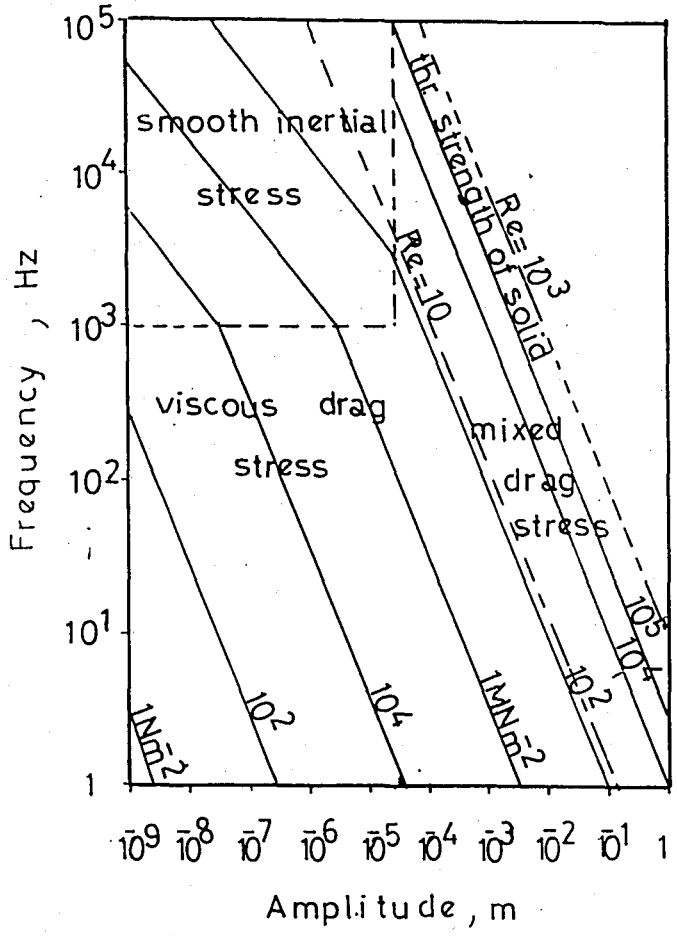

Figure 18- f-a map showing bending stresses in narrowed roots of aluminium alloy solidified at intermediate rate(13)

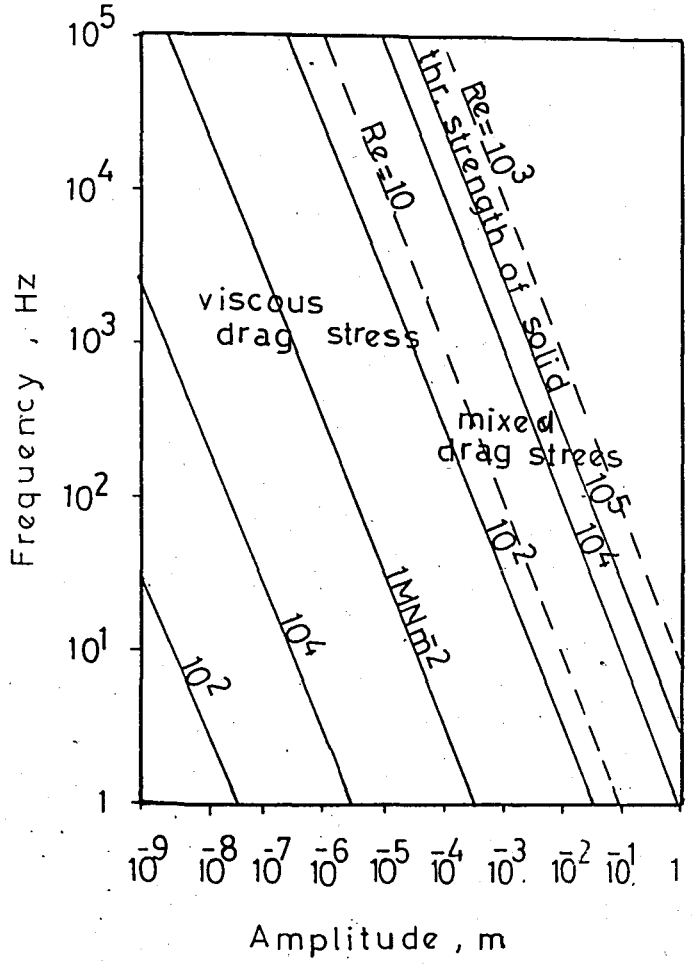

Figure 19- f-a map showing bending stresses in narrowed roots of aluminium alloy solidified quickly(13)

d) Dendrite Root Melting

Tiller and O'Hara(13) investigated the vibrated ingots and stated that heating as a result of dendrite bending is possible with a dislocation slip model. They also assesed the presence of the heat concentrations at the dendrite roots and concluded that remelting mechanism for the roots was probable. But this mechanism was regretted, as the stated heat concentration to remelt the roots, with assumed relations between thermal diffusivity TD, time and distance x_1, could not be obtained from equation 38.

$$x_1 = (TD.t)^{1/2} \qquad (38)$$

for 20 kHz, x_1 = 30 μm in a half cycle and
for 50 kHz, x_2 = 600 μm in a half cycle.

However for high energy inputs the general increase in temperature can cause the melting of the whole casting. This is predicted by equating the energy needed to remelt a fraction solid f_s of a mass m with the available vibrational energy from equation(8).

There fore;

$$8\pi^2 f^2 a_o^2 m = mHf_s/t \qquad (39)$$

defining $f_s = b^3/d_6^3$

$$8\pi^2 a_o^2 f^2 = Hb^3/d_6^3.t$$

The energy thresholds of the dendrite root melting and whole melting is shown in figure 20(13).

Allthough there are some solutions for root melting or remelting of castings, J.Champbell(13) concluded that there are many complexities in this subject and predicted them as follows.

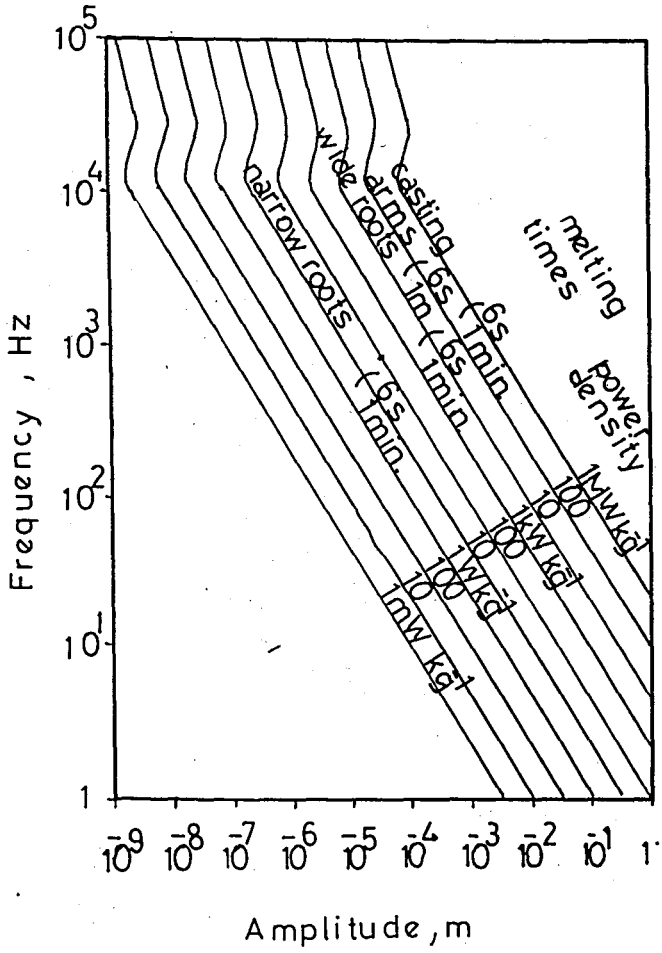

Figure 20- f-a map showing maximum power densities obtained in a liquid(13)(Theoretical)

i In the remelting of roots when bending, shearing and detachment is considered, root melting is energitically unfavorable

ii local adiabatic heating within the roots contributes negligibly to remelting

iii general heating of the castings at high energy inputs will remelt roots.

iv due to the temperature increase produced by collapse on cavitation nucleus, such as an inclusion, eroding of the neighboring dendrites may be expected.

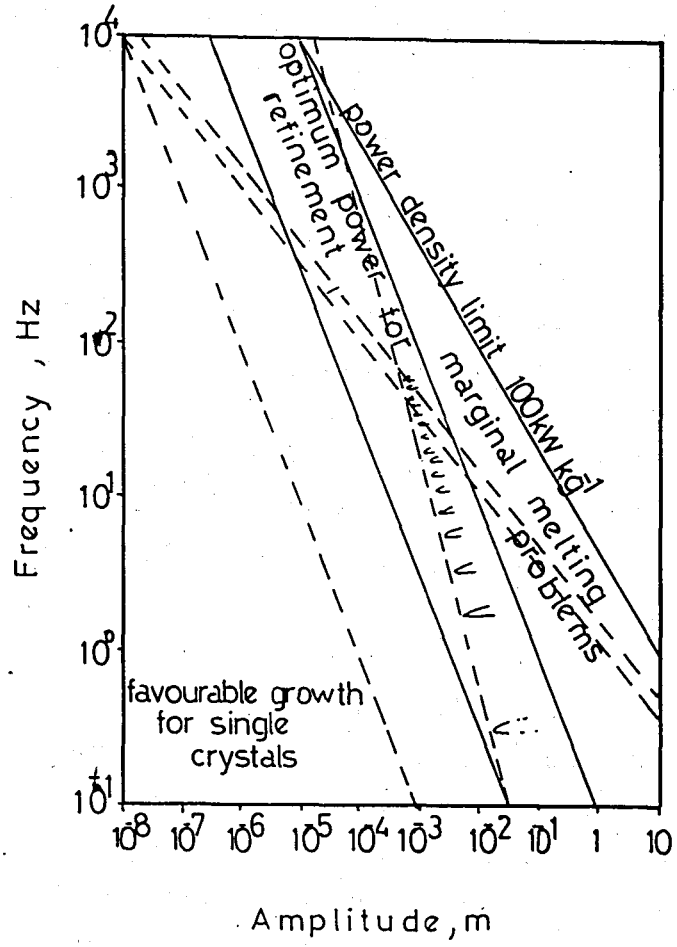

Figure 21- Summary of conditions for vibration of whole casting

C. THE EFFECT OF LOW-FREQUENCY VIBRATION ON PURE METALS

If the metals employed were commercial purity, it is anticipated that these metals will solidify by heteregenous nucleation. Under these circumstances a small amount of undercooling is necessary for stable nuclei to form, so that solidification can proceed. The mechanism became active during vibration application, could be explained in a manner similar to solid-solution solidification because of the impurities present.

If it is assumed that the metalsare of sufficient purity to avoid appreciable concentrations of solute in the liquid metal near the solidifying wall, another mechanism is offered. The thermal conditions during static solidification of the columnar zone in an ingot of pure metals is shown in figure 22(4). The growth of the columnar grains from the wall observed, since less undercooling is necessary for continued growth of the columnar grains than the nucleation of new grains and the thermal gradient in the liquid is positive.

But it is believed that thermal gradient in the liquid is not positive throughout the liquid and the heat of fusion from the solidifying chill or columnar zone increases the temperature in the immediate vicinity of the solid wall. Once this higher growth observed in pure metals, the grain refining effect or interruption of columnar growth observed in puremetals can be explained. This condition under which nucleation of new nuclei will occur during vibration of a solidifying pure metal with a greater solid then liquid density are shown in figure 23(4).

The pressure wave produced by vibration, due to the collapse of cavitation, has the effect of increasing the stability of the solid or denser phase, as explained in section III.C.3. This means that applied vibrations effectively increase the melting temperature, temperature for continued grain growth, and nucleation temperature for new grains. The continued grain growth as illustrated in figure 23(4), during

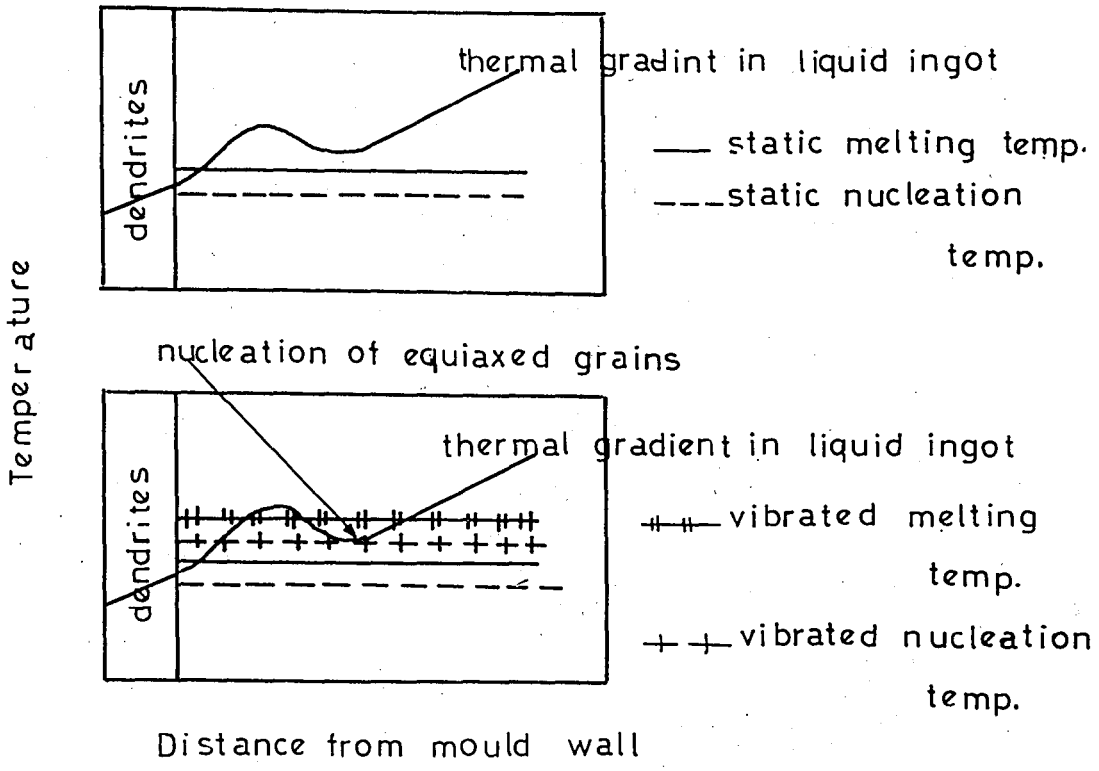

Figures 22 and 23- Influence of vibration on melting and nucleation temperature in pure metals and nucleation of new grains(4)

the high pressure formation, i.e collapse, is interrupted by the raise in temperature produced by heat of fusion at the solid metal wall. The high pressure wave incerases the nucleation temperature sufficiently permit nucleation of stable grains in the lower temperature region as indicated in figure 23(4) and refinement of the grain structure is observed.

D. THE EFFECT OF LOW FREQUENCY VIBRATION ON SOLID-SOLUTIONS

The solidification of solid-solutions occurs with a concentration of solute immediately adjacent to the solidifying wall of solid. This concentration of solute results in a reduced liquidus temperature immediately adjacent to this wall. These conditions can account for a grain refinement and interruption of a growth of column dendrites when a shallow thermal gradient exists. The solute and impurity concentration,

and conditions which favor nucleation of new grains in the melt so that columnar dendritic growth is stopped in a statically cast ingot is shown in figure 24(4). With the sharp thermal gradient t_1 columnar solidification will continue but with the shallow thermal gradient t_2, the nucleation temperature is attained and stable new grains solidify as indicated in figure 24(4).

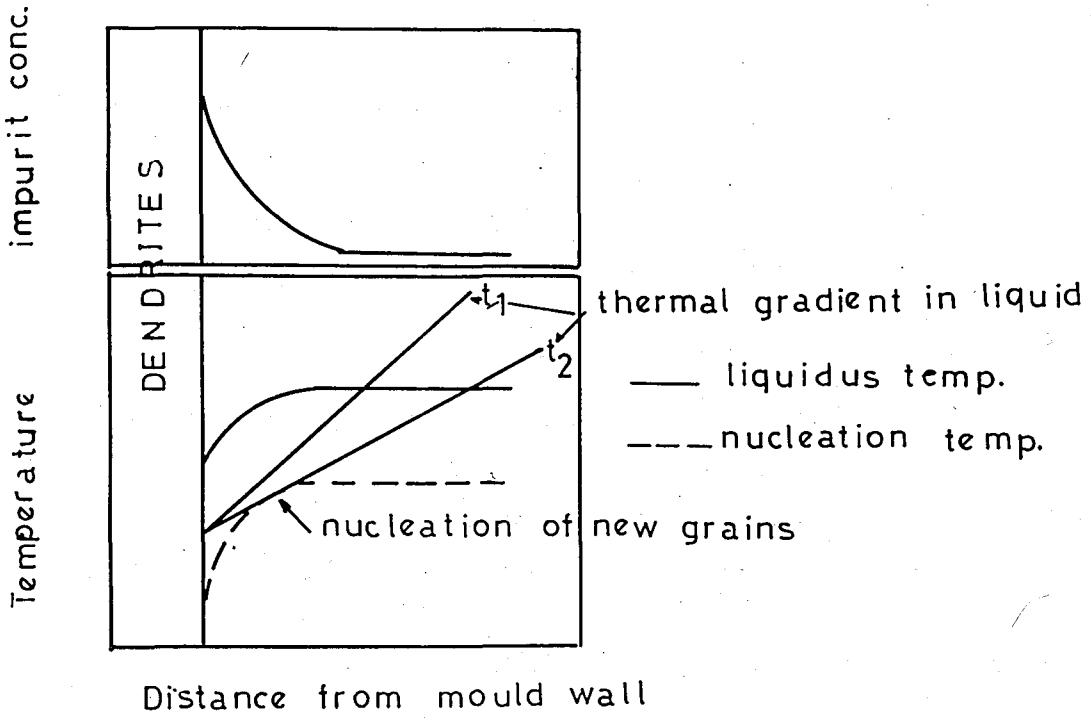

Figure 24- Impurity concentration and thermal conditions during transition from columnar to equiaxed solidification without vibration(4)

Superimposing the pressure waves of vibration, either pressure or rarefaction, will cause a change from columnar to equiaxed solidification with a steeper thermal gradient than the unvibrated condition. The mechanism by which vibrations produce this finer more equiaxed structure is illustrated in figure 25(4). Both liquidus and nucleation temperature are raised sufficiently by the pressure waves of vibration to produce the above stated effects.

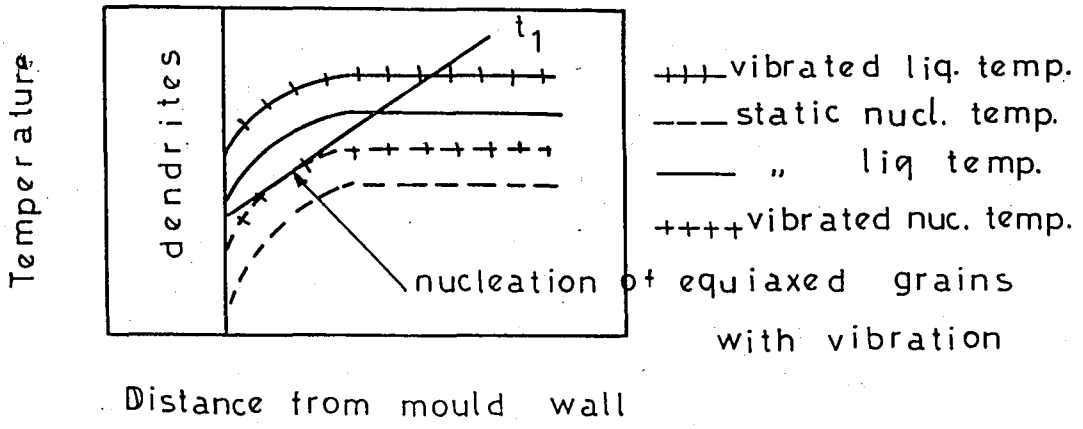

Figure 25- Influence of vibration on liquidus and nucleation temperatures in a solid solution and nucleation of equiaxed grains(4)

E. THE EFFECT OF LOW-FREQUENCY VIBRATION ON EUTECTICS

The effect of vibration on the solidification of a eutectic alloy is significantly different than that of a solid solution or a pure metal. The hypothesis built about the solidification of eutectics under imposed vibration conditions will now be given.

A eutectic liquid experiences some difficulty in forming stable nuclei of the proper mixture of eutectic constituents, from which the solidification of the cells or grains of eutectic can proceed (Refer to Chapter II). It has been observed that liquid metal of a eutectic composition undercool considerably below the eutectic temperature because of the delay produced in forming stable nuclei of the proper composition. Stable cells will be nucleated after this appreciable undercooling. The growth of the eutectic cells and constituents will be very rapid due to the reserved high energy for phase change produced by undercooling. This undercooling and the rapid growth of the solid eutectic cells produces a structure that has fine eutectic constituents but few eutectic cells (Figure 26-a)(3).

Garlick and Wallace(4) claimed that the effect of vibration to the eutectic is similar to innoculation and predicted that the number of stable nucleus of the minor phase is increased and the undercooling is reduced. As a result the eutectic solidifies much more slowly than the static uninnoculated state, because the heat of fusion quickly overcomes the slight undercooling and solidification becomes dependent on the rate of heat removal from the ingot. Under these conditions, the eutectic constituents agglomerate into coarse phases with their reduced surface areas and low energy state. Also due to the induced nucleation more eutectic cells were formed to result in a finer cell structure (Figure 26-b)(3).

The increase in size of intergrain features, whose size is normally controlled by the rate of diffusion of solutes in liquid assesed by J.Champbell(13). Such features include the eutectic spacing and intermetallic particles, where these are actually the eutectic second phases. The reason for this coarsening explained as the effect of vibration on the motion of the liquid adjacent to the solidification front, the diffusion boundary layer was reduced in thickness so that the solute was transported more rapidly to the front by the bulk motion of the liquid.

Hunt(20) also predicted the coarsening of the eutectic constituents and suggested that coarsening may be a result of slower rate of growth of the interface as a consequence of the greater surface area of the increased number of grains.

On the other hand the coarsening of the eutectic constituents also explained by fragmentation theory, by Southin(4). The brittle constituents form within the liquid were not attached to a growing solid-liquid interface, therefore would not subject to bending stresses sufficient to cause fragmentation. They move out of their depleted zone and be able to grow to a larger size.

Also the reports on refined eutectic cell size is depending upon the fragmentation of the original nuclei in ways analogous

to those in which dendrites are fragmented. This fragmentation used by many others requires the precense of some solid, sufficient force to break solid (bending moments and detachment) and macroscopic fluid motion to transport those nuclei which act as nucleant agents.

Therefore the coarsening of the eutectic constituents and the formation of finer eutectic cells as a result of imposed vibration to the solidifying metal were obvious by many previous workers as stated above and explained either by theories anologous to dendrite-fragmantation or by induced nucleation due to the effect of vibration.

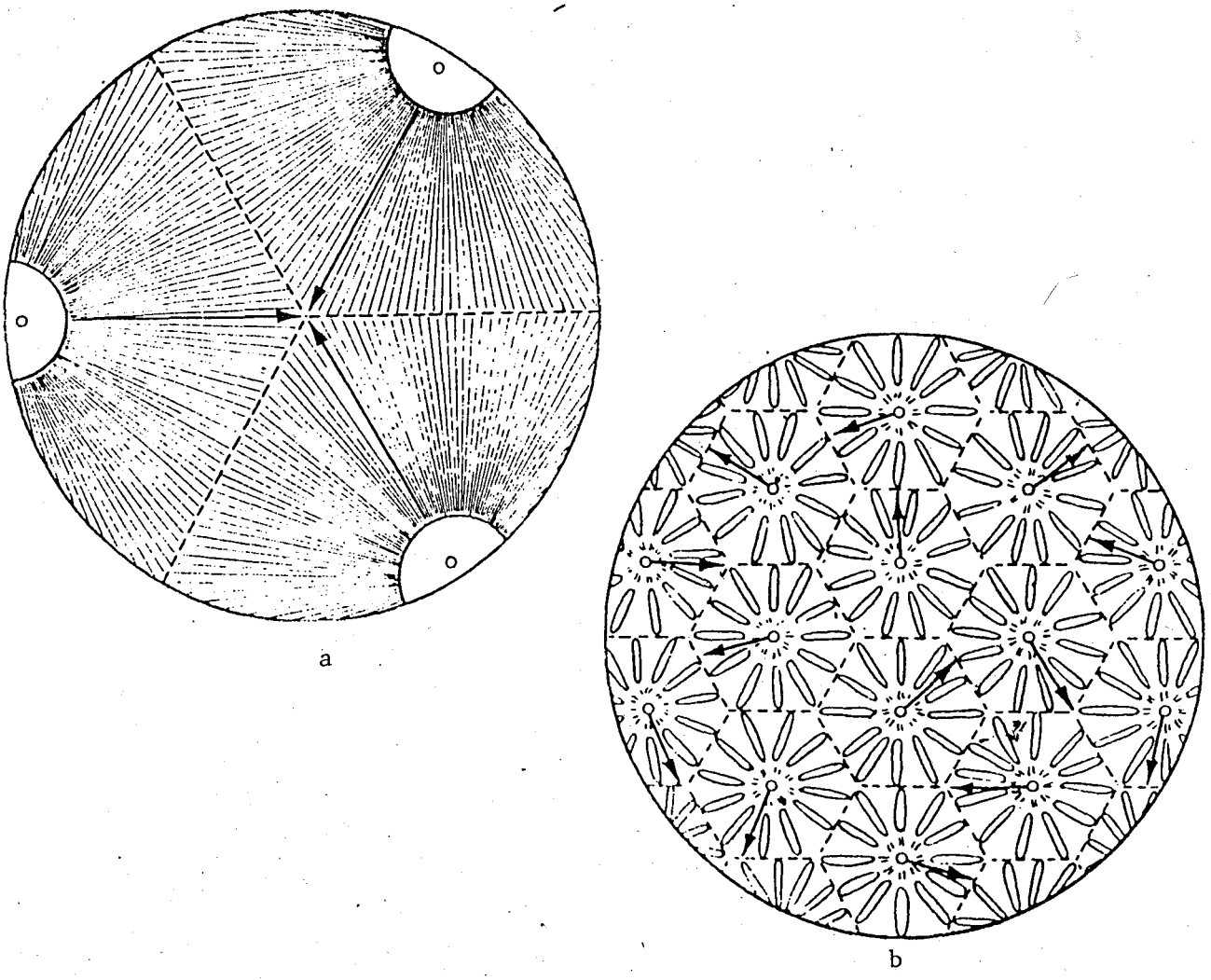

Figure 26- Schematic representation of coarsening effect produced by vibration of an eutectic alloy during solidification(3)

CHAPTER V

RESULT OBTAINED BY THE PREVIOUS WORKERS

A. METALLOGRAPHIC EXAMINATION

Macro and micro structures of the vibrated ingots studied repeatedly and some conclusions built on the formed structures and their former effect to other casting properties. Now some of those obtained results will be presented.

J.H.Gittus(17) Studied the steel and white iron castings with low-frequency vibration and stated that the conventional columnar structure of the austenite dendrites in steel and the primary carbides in hyper eutectic white-iron were largely eliminated by vibration. The former replaced by the equiaxed dendrites and, the latter by carbide platelets of random orientation.

Southgate(18) studied commercial purity aluminium and observed a grain refinement over most of the casting.

Eutectic Al-Si studied by A.Claro.F(16) and predicted the different appeareance in the micro-structure where as the Si plates were shorter, broader and random in orientation.

Also Freedman and Wallace(3) studied eutectic Al-Si and the vibrated ingots exhibited a finer cell structure but coarser eutectic constituents when compared with control ingots.

Beyond the obtained experimental results above, some workers studied the resultant effects produced by the micro structure. Lawson and Kerr(22) have investigated the yield and fracture properties of rapidly solidified Al-Al_3Ni structure, which were cellular and polycrystalline, and no precise trend in tensile or fracture data could be established to relate σ_y or σ_{UTS} with λ_1, lamellar spacings allthough a graphic is drawn.

Yield stress data on single crystal specimens of Al-Al_2Cu structure has obtained by Bertonello and Biloni(22) and it is observed that the yield stress decreases gradually as interlamellar spacing increases (Figure 27)(16).

Also from the studies of steen and Hellamel(19) it is understood that the coarse Si plates in Al-% 12.6 Si system which were thick and short, permits easy crack propagation and brittle fracture observed in the end.

On the other-hand hardness measurements on single crystal eutectic material, with Al-Al_2Cu strcture, is made by Davies and Hellawell(22) and Mc Kay(22). The results of these experiments in as grown, furnace cooled and quenched conditions are illustrated in figure 28(16) and the decrease in hardness with increasing lamellar thickness is predicted.

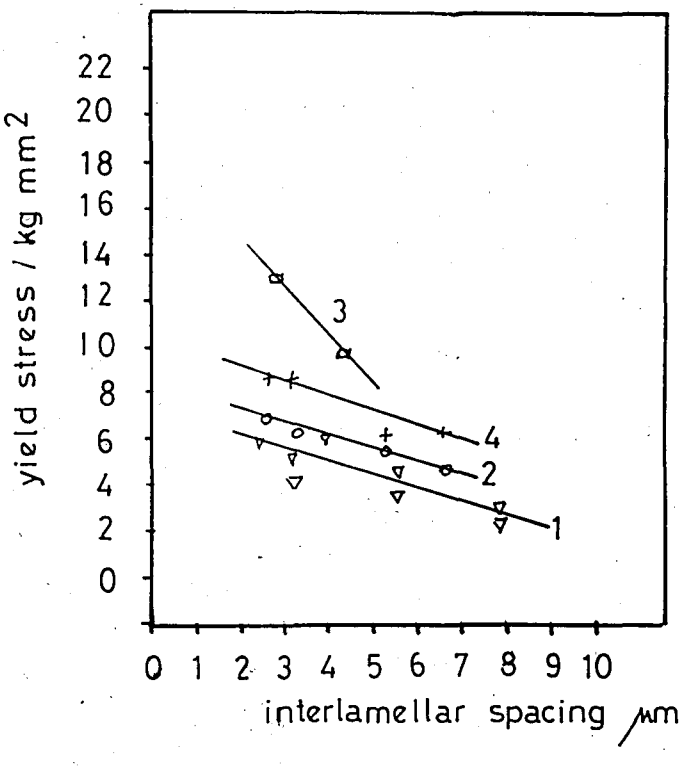

Figure 27- Yield stress data for Al-Al_2Cu eutectic crystals, ▽ as grown, Bertorello and Biloni; □ as grown Grossman et all;
o as grown Mc Kay; + water quenched from 783 °K, McKay(22)

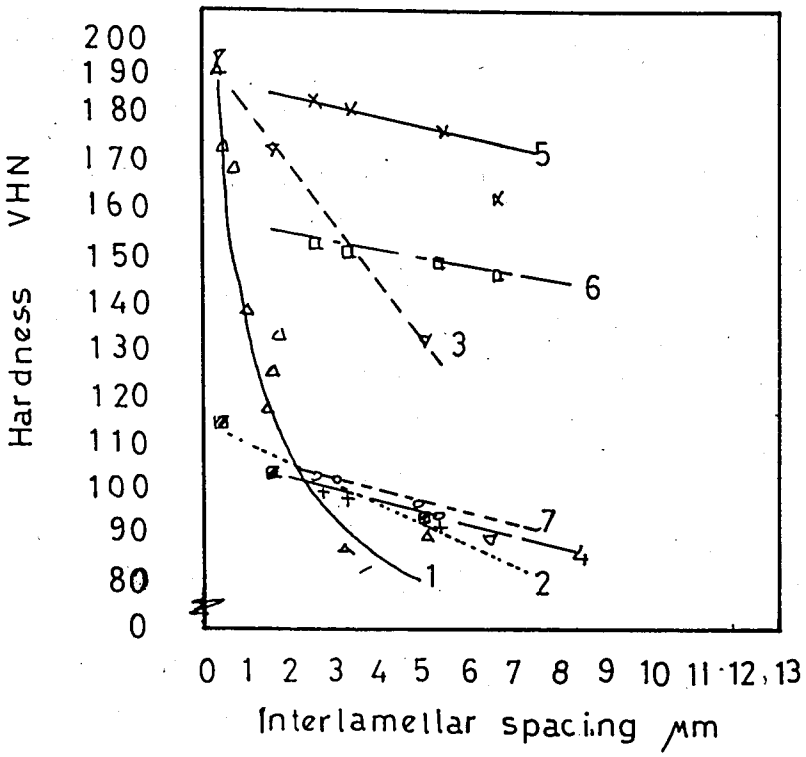

Figure 28- Hardness for Al-Al_2Cu eutectic crystal. ▲ as grown, ▼ quenched fron 798 °K, ■ furnace cooled, Davies and Hellawell; o as grown, + furnace cooled, quenched from 783 °K; x quenched from 813°K, McKay(20)

B. MECHANICAL PROPERTIES

Beyond the developed macro and micro structures of the casting alloys, the mechanical properties of the vibrated alloy castings were studied previously and some of those tension and hardness test results will be presented to understand the effects produced by vibration.

Al solid solution, Al-4.5 Cu and yellow brass has been studied by Freedman and Wallace(4) under imposed low-frequency vibration. By the tension tests performed a significant improvement, 24 %, for yellow brass and a less improvement, 9 %, for Al-% 4.5 Cu was predicted.

Fahy(20) studied the commercial purity aluminium and stated an increase in the tensile strength of the vibrated ingot.

Richards and Rostoker(6) also test the vibrated and unvibrated Alcoa-195 and specimens were solution treated and aged before machining. From the summarized data in figure 29(6) it seems to be that the increasing casting temperature has no systematic effect on tensile strength but a general superiority evidenced in the ductility of the vibrated ingots.

Also eutectic alloys were studied by some previous workers that, Southgate(18) predict a 10 % improvement in

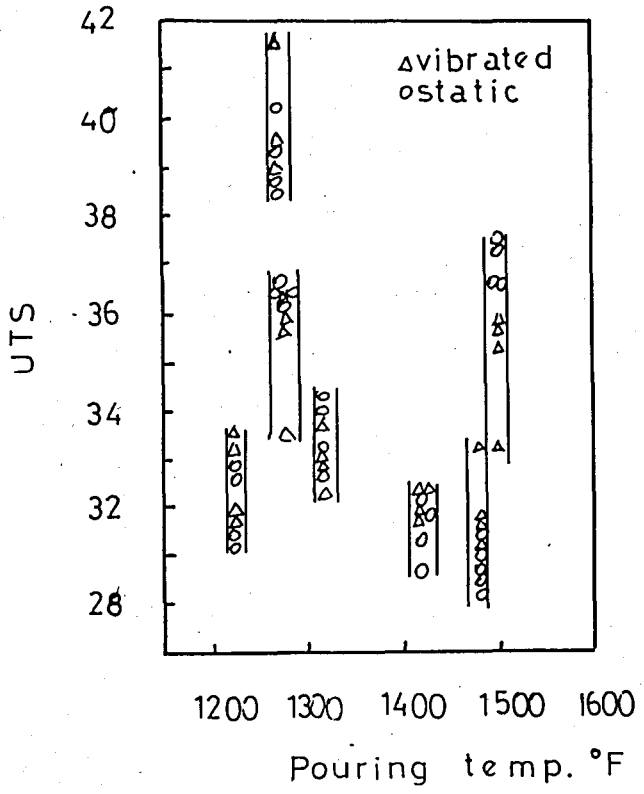

Figure 29- Summary of tensile data obtained by Richards and Rostoker(17)

tensile strength of Al-% 12.6 Si, where as any improvement could not be observed for Al-1.8 % Fe due to the strong anisotropy observed in tensile data arose from alloying centent. Southgate used high frequency vibration of 8 kHz and 25 μm.

T.P.Fisher(9) studied hypo and hyper eutectic Al-Si alloys and did not present any tensile data, but the attention was pulled to the coarsening observed in Si plates, which may be effective in tensile testings, and to the eutectic cell size Figure 30(7).

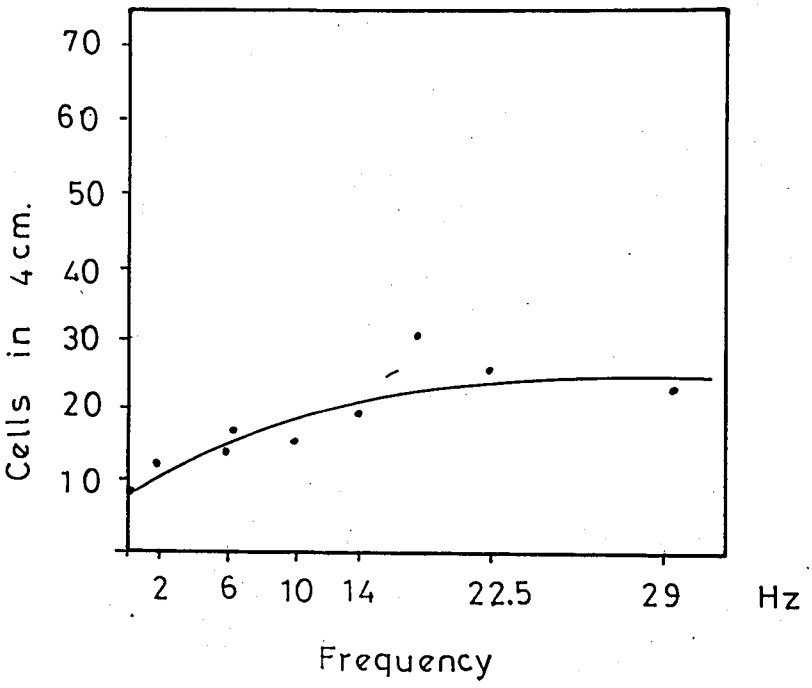

Figure 30- The increase in cell count for LM6 Ingots studied by T.P.Fisher(7).

R.R.Burbure(10) also studied aluminium eutectics with low-frequency vibration, where as in all cases tensile strength decreased by incerased mould temperature and Vibration amplitude (Figure 31)(6).

The behaviors of vibrated high alloy steels and cast iron were studied by Jagaciak(20) and Nicolaichik(20) respectively and it was stated that there was no any increase in VHN number but a uniform distribution of hardness observed.

Also the ternary system Al-4 Cu-4 Zn was studied by N.Erus lu(20) and from the investigation of the graphs given it is observed that the tensile strength of castings first increase to a maximum and decrease both with increasing mould and casting temperature.

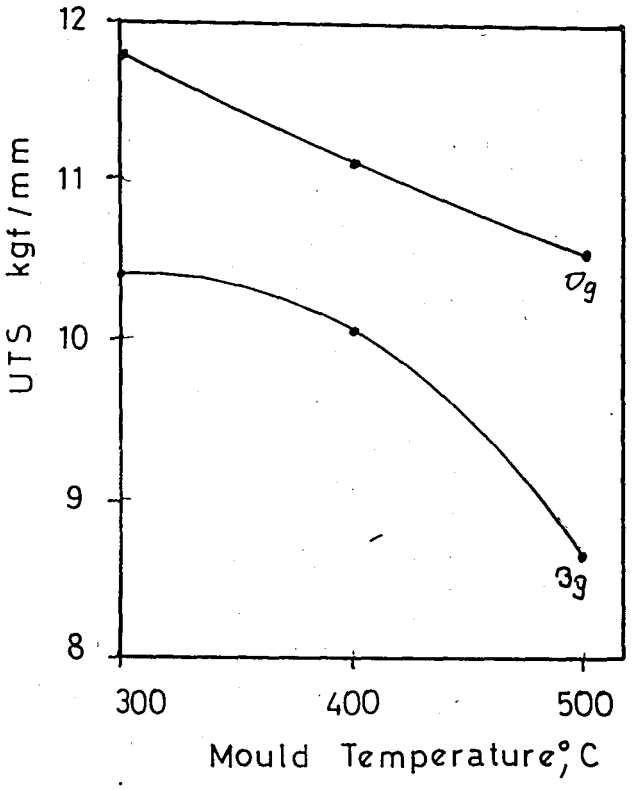

Figure 31- The effect of mould temperature to the tensile strength of Al-% 33 Cu, by R.R.Burbure(10)

CHAPTER VI
EXPERIMENTAL WORK

In order to study the effects of low-frequency vibration on aluminium eutectics, Al-% 33 Cu, Al-12.6 % Si and Al-% 5.7 Ni, two groups of castings were performed. In the first group the static control ingots were casted, where as the rate of solidification is changed either by increasing mould temperature or by increasing casting temperature of the liquid metal. Beyond the variable mould and casting temperatures used during dynamic castings, variable amplitudes imposed to the solidifying alloys by a mechanical vibrator. The mechanical testing and microexamination of the structures were made after completing the decided castings.

A. APPARATUS

The low-frequency mechanical vibrator used during the dynamic casting of alloys is shown in figure 32. The system shown is composed of two parts, where one of them is the vibrating table and the other is the electronic feed-back sytem designed to supply constant frequency to the table mounted on springs.

1- The Vibrating and the Base Table

The rectilinear motion of the vibrating table, which is mounted on springs, was produced by a rotating unbalance, where as this unbalanceness supplied by mounted weights to the shaft of a direct current motor (Figure 32). The d.c motor and the tachogenerator, apparatus of feed-back system, were bolted seperately to the vibrating table and the linkage between them was made with an elastic segment (Figure 33). The journals which were made of grinded steel, screwed to the vibrating table, work in journal bearings placed inside the base table and the length of the bearings used, that were made from phosphor-bronze, were designed as 100 mm by purpose, to reduce

the lateral motion of the table originated from the working tolerances of the shaft and the bearing. The tolerances H7 and f6 were choosen, for hole and shaft respectively, to provide the "precision-running" of the shaft inside the hole.

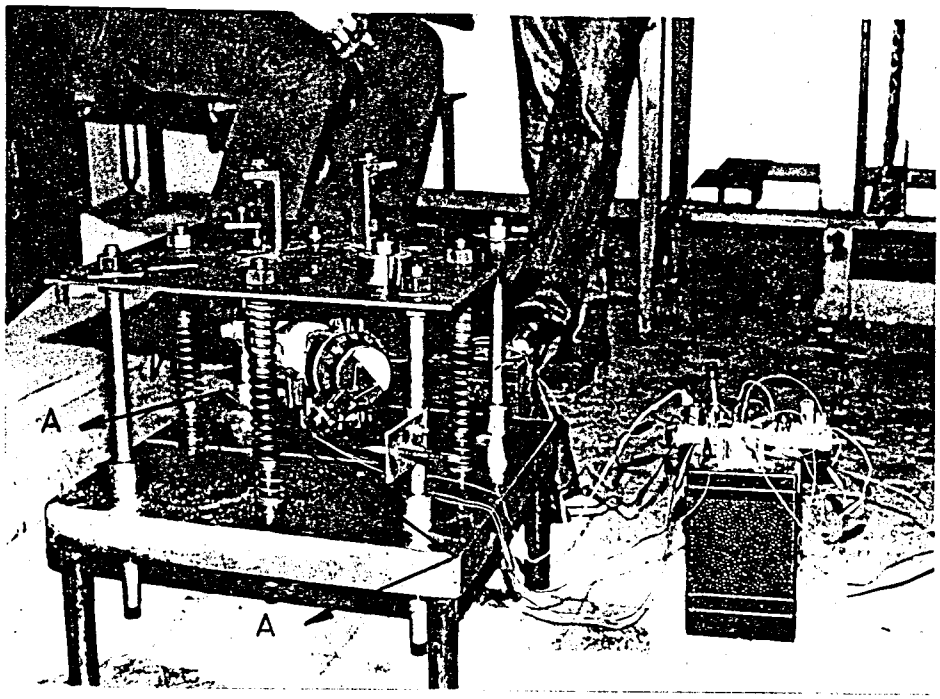

Figure 32- Vibrating table and the frequency control unit

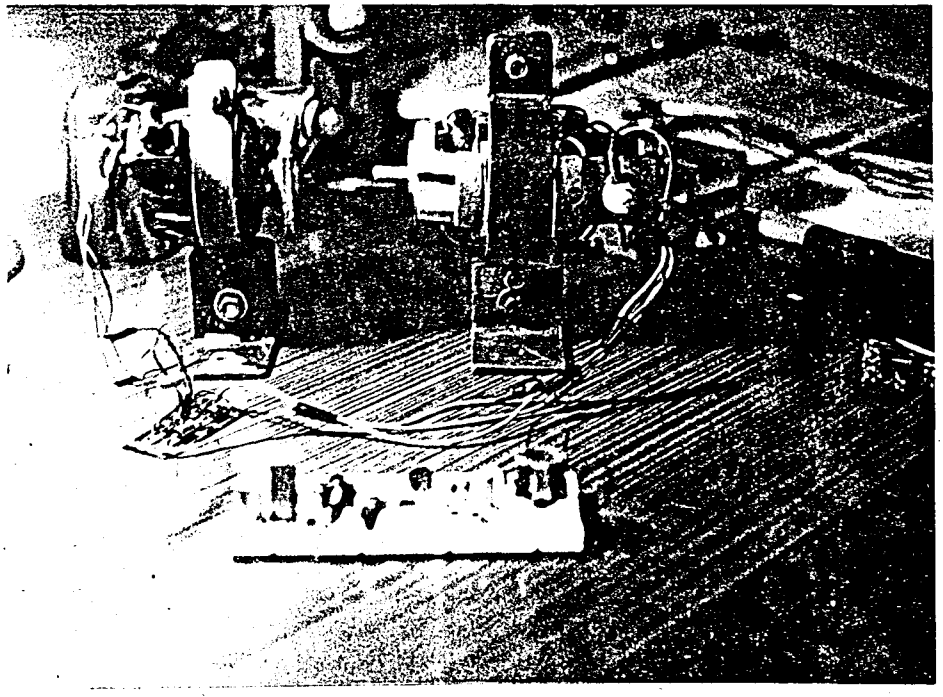

Figure 33- Seperate handlings of d.c motor and the tachogenerator

On the other hand the calculations and the design of the compression helical springs made from circular section wire used was made according to the TS 3077 standart and first quality steel were wires used during production of springs.

The base table was specially choosen large, 50x475x475 mm, in orderto prevent the decay of vibration that will originate from the vertical motion of it. The upper surface of the wrought iron table was milled and the holes, where bearings were placed, were bored to provide the parallel placing of the bearings.

The measurement of the vibration amplitude is made by using a recording pen and a scale where as the recording pen was bolted to the moving journal (Figure 32). The trace was recorded on a paper and measured with a scale. The scheme of the vibrating table is shown in figure 34.

2- Frequency Control Unit

The circuit prepared for frequency control of the vibrating system shown in figure 35. By the use of this control unit the frequency of the d.c motor, i.e the rotating unbalance, was hold at a desired constant value that any further increase in the applied load to the table could not effect the frequency of the vibration. The frequency control of the vibration is made with a potentiometer switched to the control unit and the frequency is held at 8-9 Hz during the experiments. The circuit diagram of the control unit is shown in figure 36.

3- Moulds Used During Experiments

The metals were melted in the standart 2 kg-Paco graphite crucibles and directly poured into an ingot-mold after alloying. Ingot mold used during static and dynamic castings was machined from extruded iron rod, with 100 mm outside diameter, 80 mm inside diameter and 65 mm deep mold cavity, where as the inside cavity is slightly tapered for

easy removal.

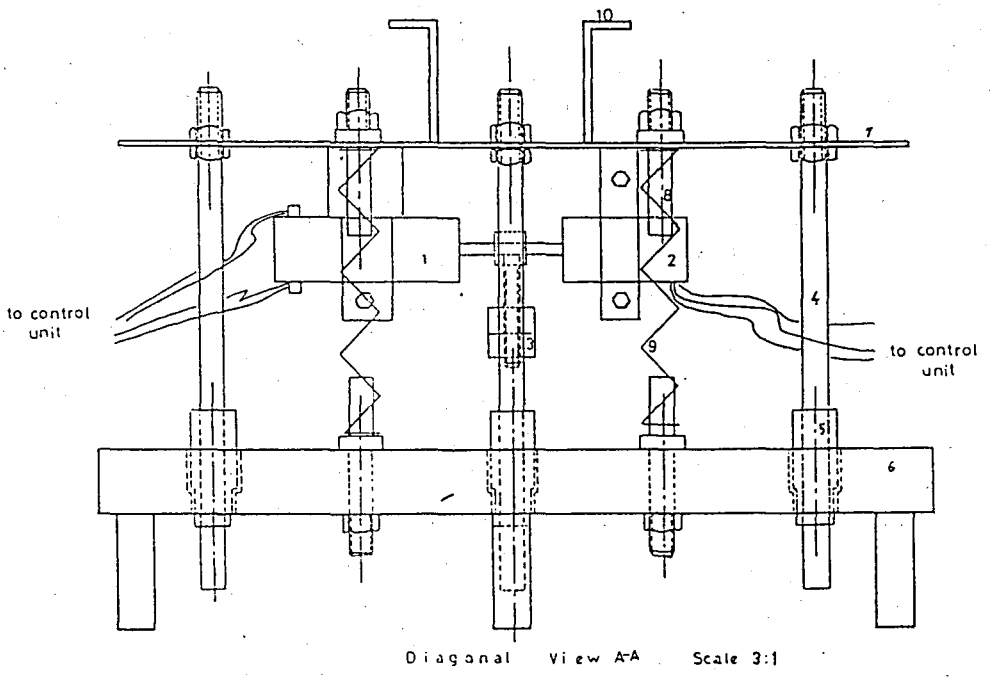

Figure 34- The scheme of vibrating table
Low-Frequency Vibrator:
1- D.C electric motor
2- Tachogenerator
3- Mounted unbalancess
4- Journal (shaft)
5- Journal bearing
6- Base table
7- Vibrating table
8- Spring-holder
9- Spring
10- Mould-holder

4- Character of Vibration

Low and medium frequencies up to 1 kHz are mostly provided by mechanical ways. The eccentric weights, coupled with d.c motor, used in this study to provide the simple sinusoidal motion to the vibrating table. This vertical motion of the mould and table together, is simpler and the amplitude can be precisely known. This kind of imposed vibration to the mould and liquid casting together is the most convinient way of influencing the solidification but the effectiveness is limited to relatively low frequencies and large amplitudes and

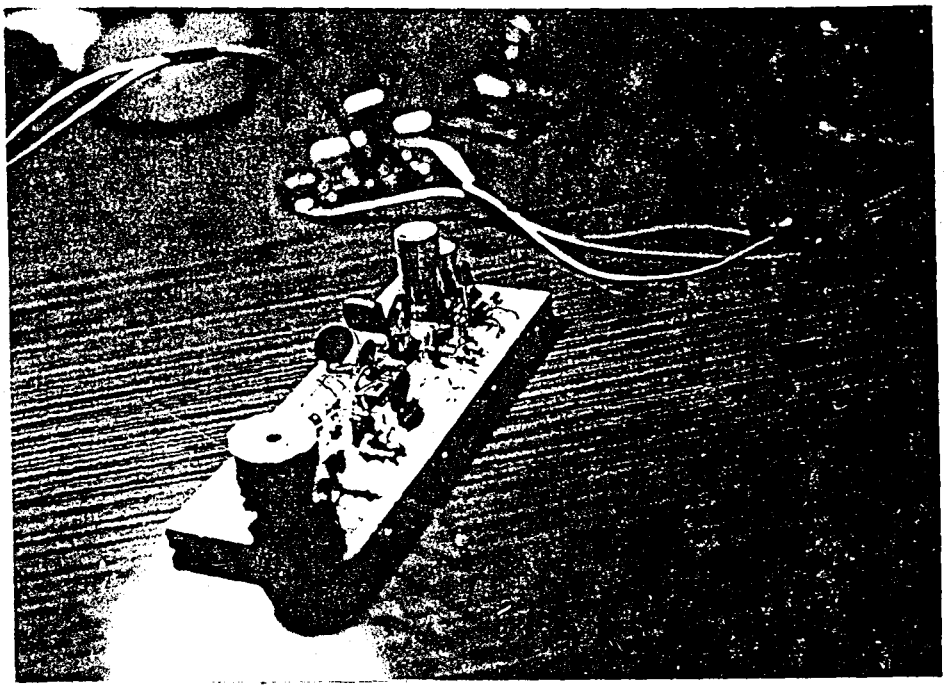

Figure 35- Frequency control unit

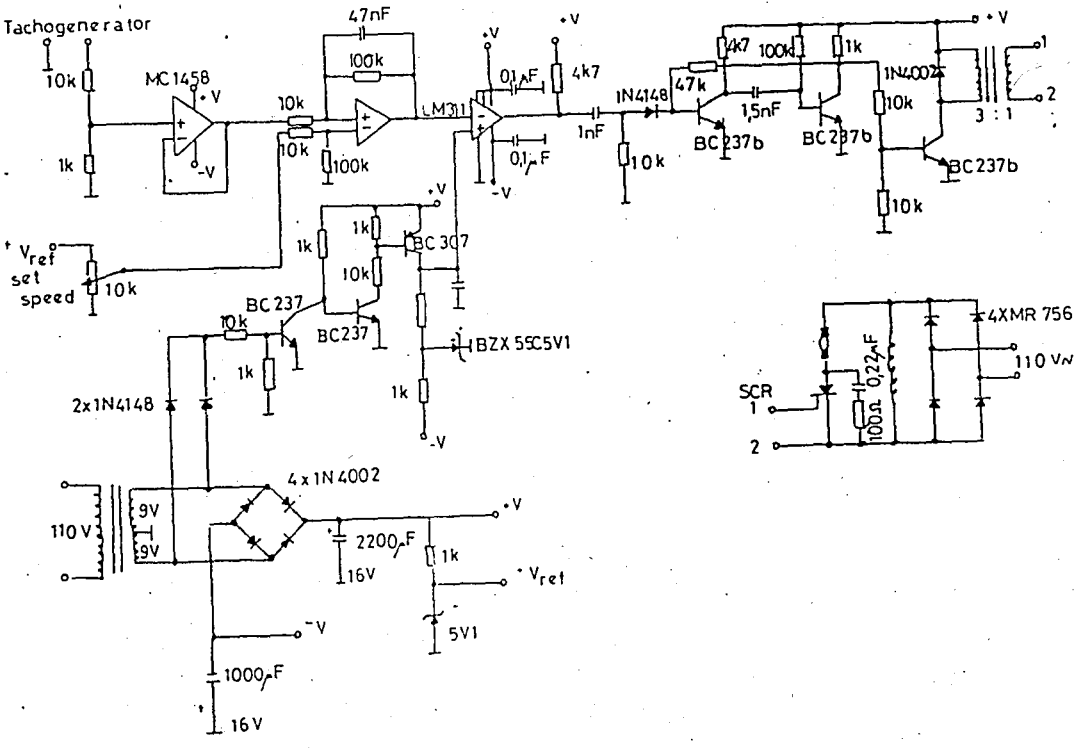

Figure 36- Scheme of frequency control unit

only metal molds can be used to prevent disintegration.

In figures 37 and 38 the studies of the previous workers and the present studies are shown in frequency-amplitude map for two different types of solidification. From the investigation of those studies it is revealed that the region where most of the workers studied is the low-frequency region with 10^{-4} to 10^{-2} m amplitudes.

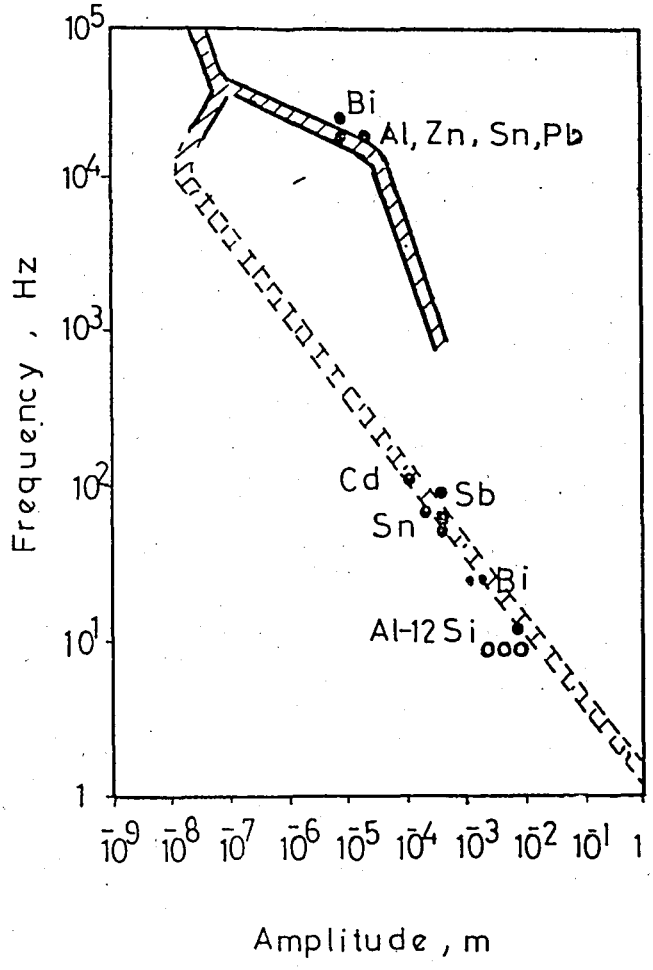

Figure 37- f-a map showing the previous studies made with planar or cellular front solidification and the data of present study. Continious lines denoting the successful refinement region studied by previous workers
• previous studies
o present study

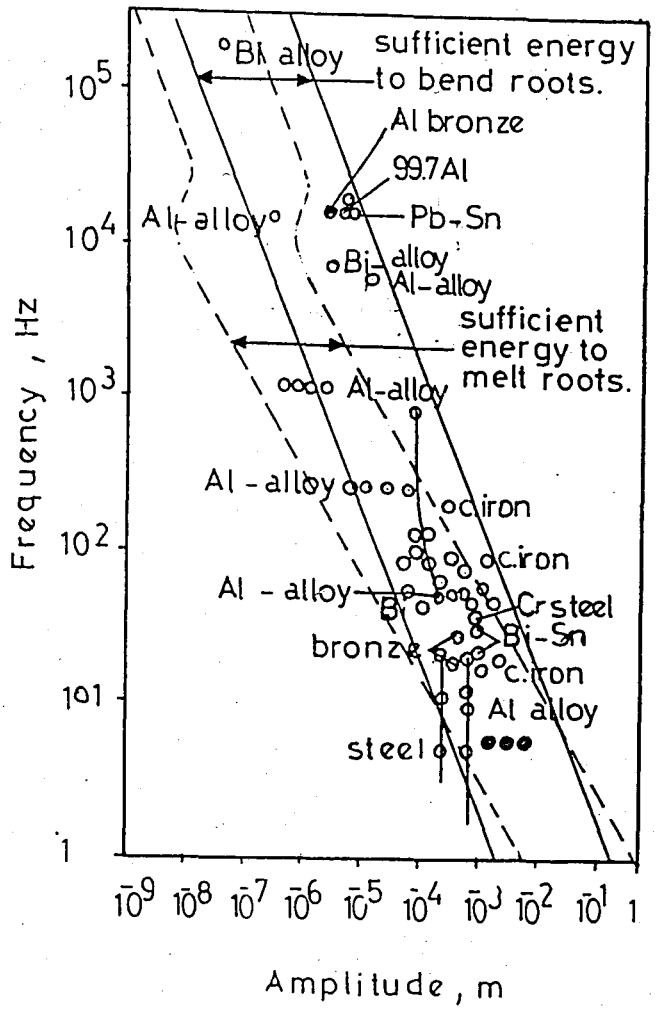

Figure 38- Experimental data from literature showing the f-a map of studies of the previous workers on dendritically freezing alloys together with the present study
o previous sucessful studies
• present study
- tails indicating unsucessful studies

B. EXPERIMENTAL TECHNIQUE

1- Alloy Preperation

The aluminium eutectic alloys, Al-% 33 Cu, Al-% 12.6 Si and Al-% 5.7 Ni, are prepared by using a commercial grade, 99.7 purity, aluminium supplied from Rabak. The phase diagrams of the eutectics are shown in figures 39, 40 and 41.

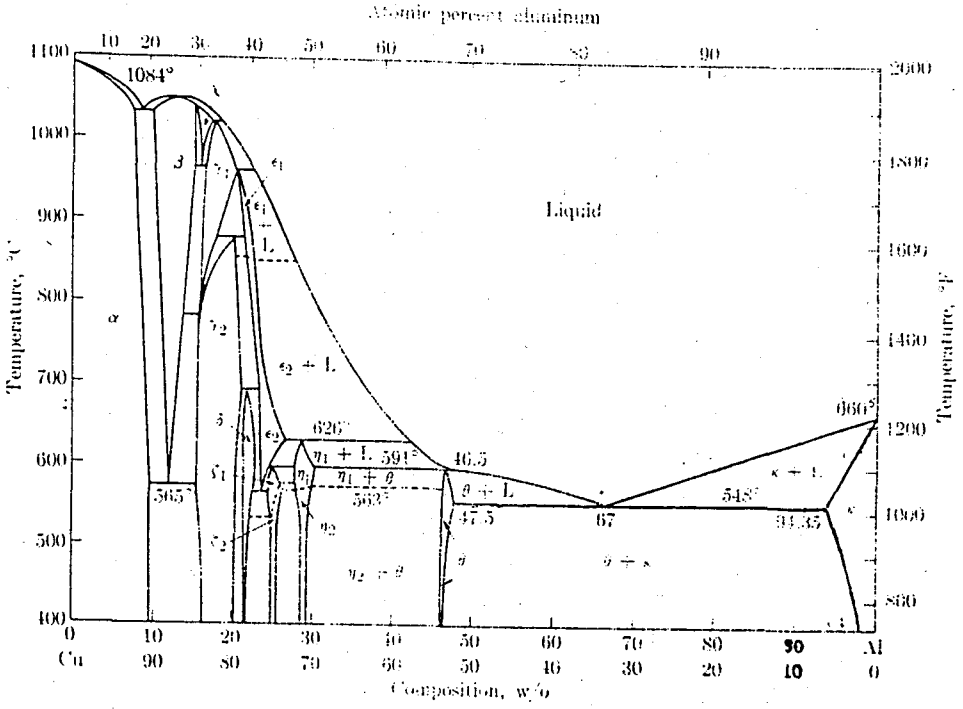

Figure 39- Al-Cu diagram, Adapted from metals Handbook, American Society for Metals

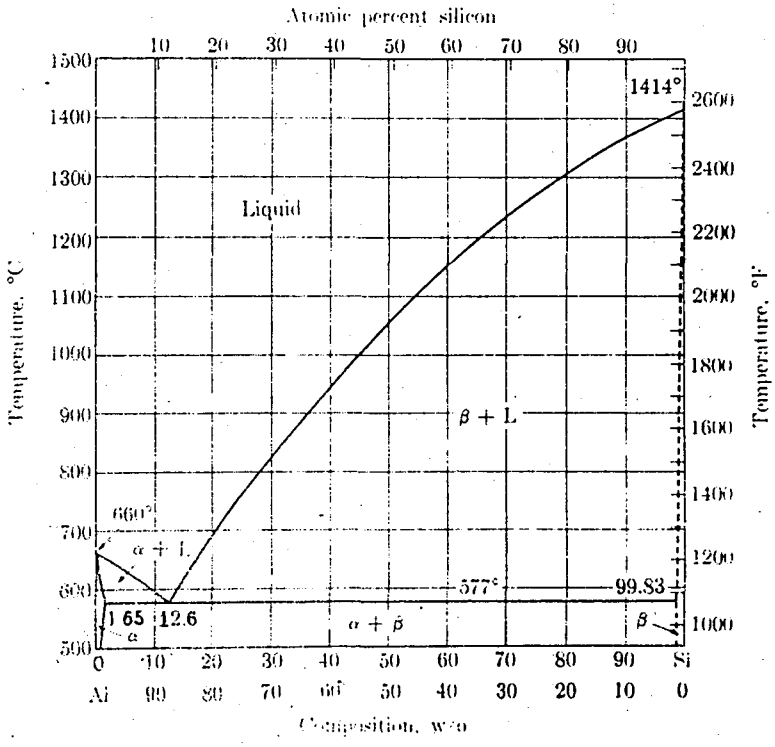

Figure 40- Al-Si diagram, adapted from metals Hand Book, American Society for Metals

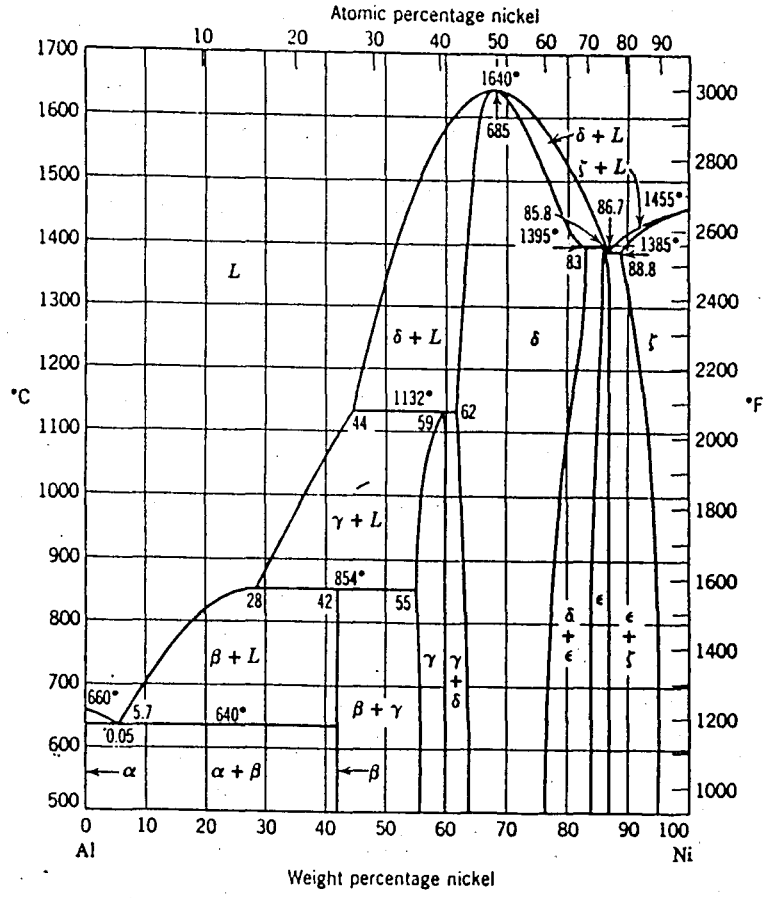

Figure 41- Al-Ni diagram, adapted from Metals Handbook, American Society for Metals

Carefully weighed amounts of aluminium were melted in graphite crucibles by the use of an electric resistance heating furnace and than the needed amount of Cu, Si or Ni were added into the molten metal. After wards the prepared alloys were stirred with graphite rod to provide the complite solubility of solute and also stirred with graphite plunger to homogenize the melt composition.

2- Melting and Casting

The aluminium eutectics, which were carefully alloyed inside the graphite crucibles were heated to the casting temperatures inside the heating furnace. Due to the interaction of the aluminium alloys with the surrounding atmosphere,

aluminium oxides were formed on the top surface of the crucible. No degassing, or fluxing treatment was made and no grain refiners were added to the molten metal.

The temperature of the molten metal measured with Ni/NiCr thermocouple and the value read from the potentiometer. When casting temperature was reached, slag cleared from the top surface and metal poured into the initially heated ingot moulds, in which the inside cavity was coated with graphite, either the moulds were vibrated or unvibrated.

The ingot mold together with casting was vibrated for 5 to 15 minutes during solidification depending on the alloy and casting or mould temperatures. When higher mould temperatures and casting temperatures wereused, the solidification rate of the liquid is lowered that longer vibration treatment time is choosen. Also those choosen times for vibration treatment is longer from the solidification time of the alloys, as revealed from the casting of the control ingots. On the other hand, the choosen time interval is over the limits offered by N.Eruslu(28) for solidification of the ternary aluminium alloys.

During the performed static castings, first the casting temperature was kept constant and four different mould temperatures, 300°C, 425°C, 550°C and 600°C, were used. Subsequently, the mould temperature was kept constant, 300°C, to cast four ingots for different casting temperatures, depending on the alloy used. When the castings were performed under dynamic conditions, ingots casted with constant casting temperature were repeated for 1, 2.5 and 4 mm amplitudes. On the other hand ingots casted with constant mould temperature, repeated for only 2.5 mm amplitude. Therefore eight unvibrated and sixteen vibrated ingots were casted for each group of alloys. The casting temperatures used for different alloys can be listed as follows:

i 575°C, 600°C, 650°C and 700°C for Al-% 33 Cu

ii 600°C, 650°C, 700°C and 725°C for Al-% 12.6 Si and

iii $700^{o}C$, $725^{o}C$, $750^{o}C$ and $775^{o}C$ for Al-% 5.7 Ni.

In order to obtain proper results from the casted ingots, the parameters tried to keep constant other than the controlled ones, such as mold, casting temperatures and vibrating amplitude and frequency, can also be listed.

i the experiments performed at room temperature, $21^{o}C$
ii both static and dynamic castings were solidified in still air, as the metal mould hang
iii the liquid metal is heated to a temperature at most $50^{o}C$ above the casting temperature and the liquid metal rested in the furnace prior to casting until the temperature droped to the casting temperature.

C. METALLOGRAPHIE EXAMINATION

1- Specimen Preperation

The microstructures of the eutectic alloy, either vibrated or unvibrated, were investigated in detail under microscope after carefull polishing was performed. The specimens used for hardness tests (Figure 52-b) polished down to 500 grade emery paper. After wards in the final stage of polishing, Struers DAP-5 polishing machine and alumina polishing paste used to gether to reveal the micro-structure of the specimen. Subsequently the specimens were cleaned in ultrasonic cleaner, Struers Metason-120, and blown dried with alcohol just after rinsing under running water.

An Olympus microscope was used during the performed microscopic examination of the specimens and the photographs were taken by using on Olympus Camera attachment.

2- Experimental Results

The microstructure of Al-% 33 Cu alloy exhibits the colony type growth, the colonies growing parrallel to the

direction of heat flow at the mould wall. The eutectic phases are arranged in a lamellar pattern within the colonies, where as the lamellar growth direction is random. From the examination of the micro-structure of Al-% 33 Cu the following observations are made.

i The length and width of the colonies at the mold wall decreases as mould temperature increases (Figure 42

ii The lamellar structure within the colonies coarsen as mould, casting temperature increases (Figure 43, a, b,).

iii The sizes of the equiaxed colonies formed at the mid ingot increased as mould and casting temperature increases (Figure 44 a, b).

iv The coarse equiaxed formed in the mid ingot is more striking at 2.5 mm amplitude (Figure 45).

In the micro-structure of the Al-5.7 Ni the degenerated lamellar structure is observed, where as the independently nucleated Al_3Ni, second eutectic phase, forms the boundaries of the eutectic cells. By examination the following results are obtained:

i Al_3Ni plates become very long and thick in static ingots as mould temperature increases and in vibrated ingots as casting temperature increases (Figure 46 a, b).

ii Eutectic second phase Al_3Ni, became thicker and longer as mould temperature increases (Figure 47)

iii The fine and dispersed eutectic cells formed in the mid ingot become coarser as mould temperature increase (Figure 48).

iv Eutectic cell size is increased as casting temperature increases (Figure 49)

Si in Al-Si alloys normally appears as irregular interconnected silicon plates. The behaviors of these observed plates are summarized as following:

i Si plates become coarser as mould temperature increases and amplitude increases the coarsening mostly striking at 2.5 mm amplitude (Figure 50 a, b).

ii The primary dendrites of Al are refined in vibrated ingots (Figure 51-b)

iii The Si plates become coarser after primary refinement as casting temperature increases in vibrated ingots (Figure 51-a)

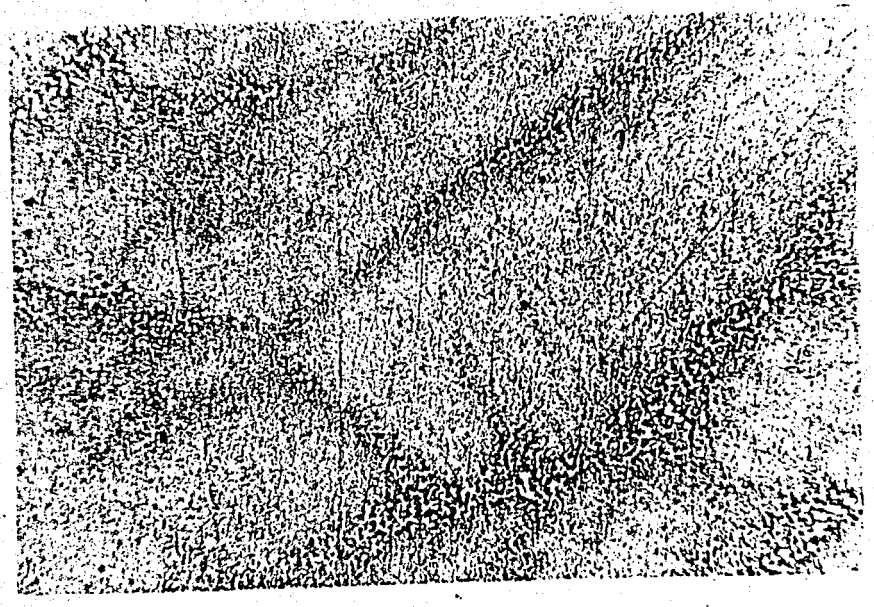

300°C mould Temperature

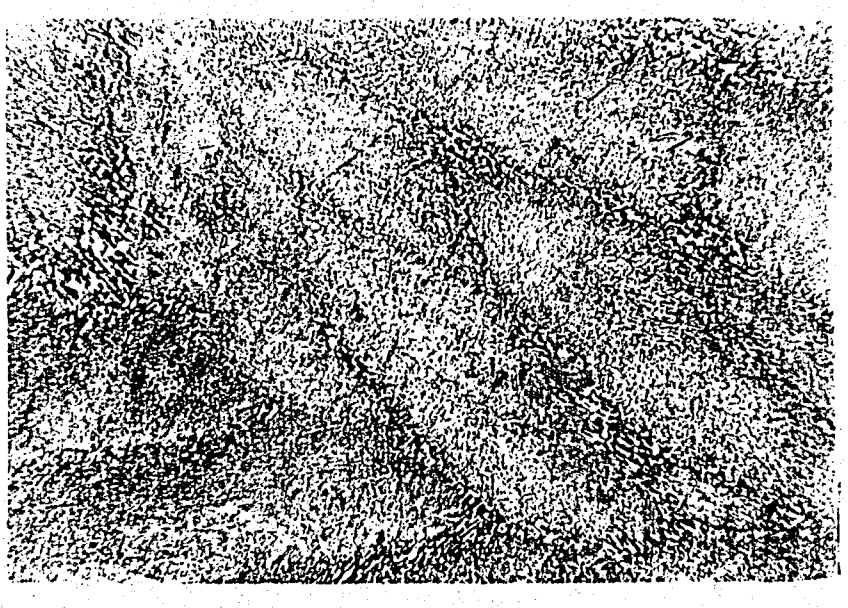

425°C mould temperature

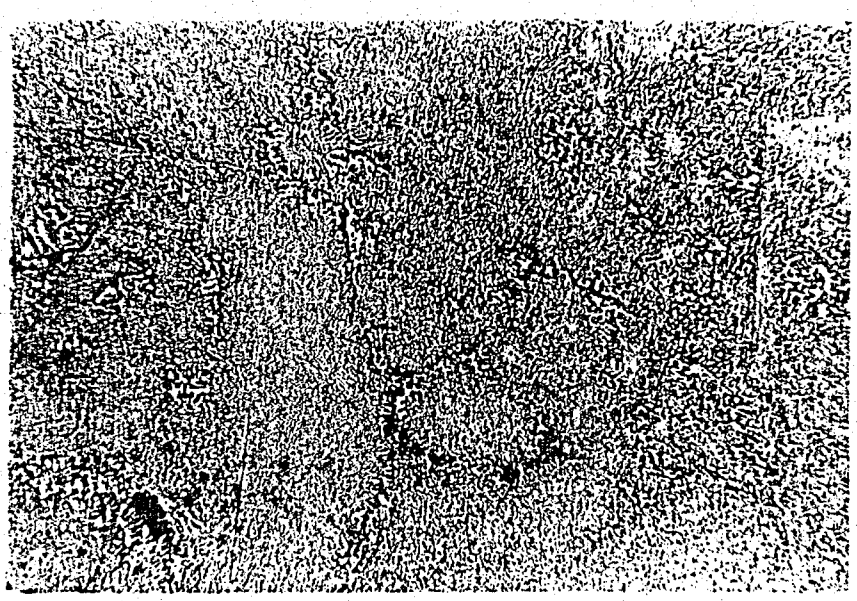

550°C mould temperature

Figure 42- Al-% 33 Cu, the decreased cell size at the wall, by increasing mould temperature, loops observed are representing the eutectic cells. Low magnification 40.5X. Black holes observed representing the porosity formed in side the casting

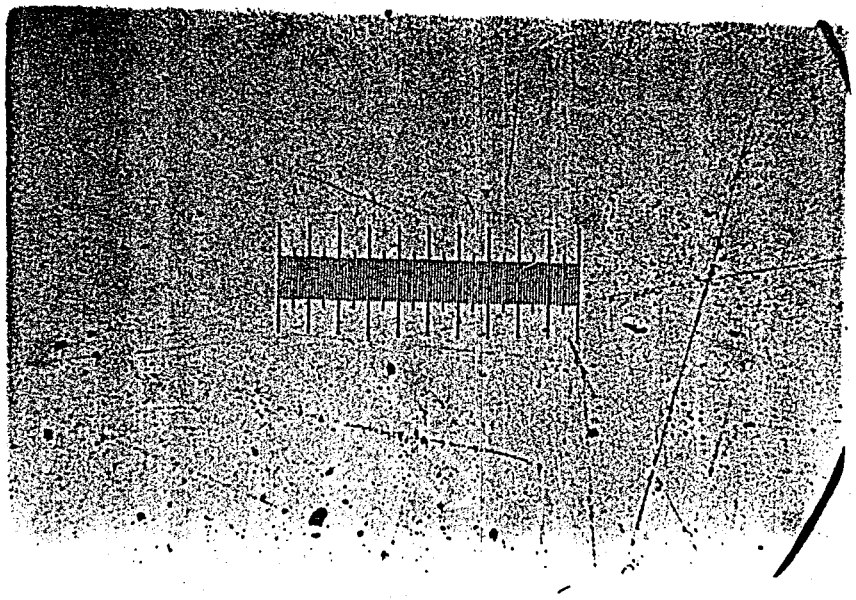

40.5X

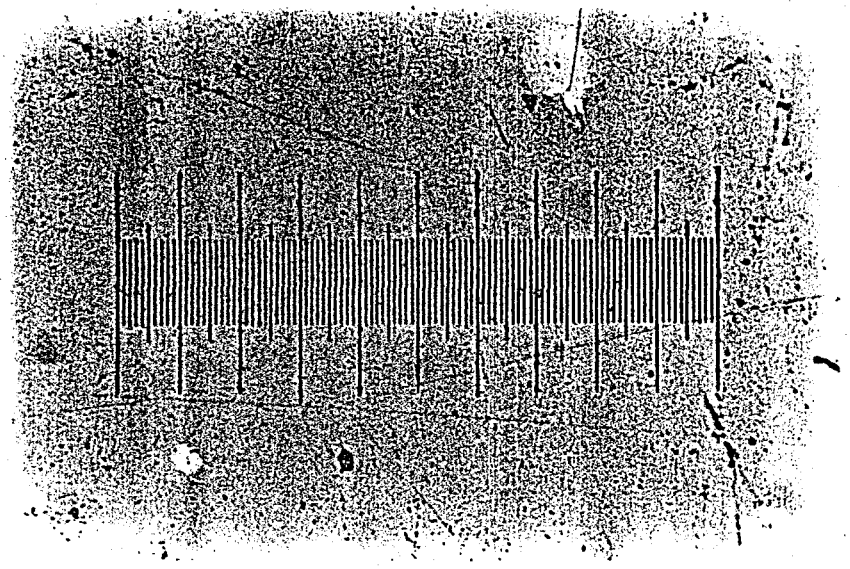

81X

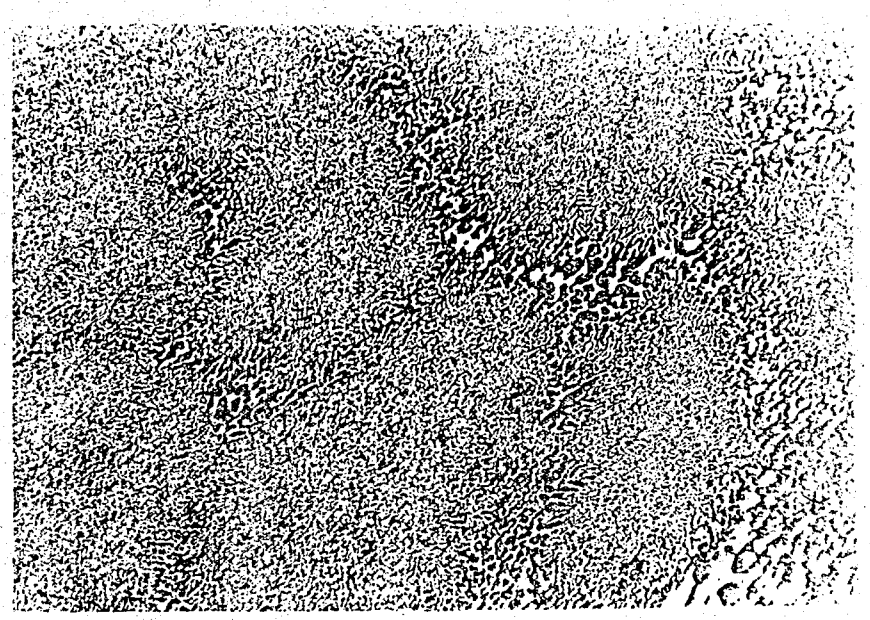

300°C mould temperature

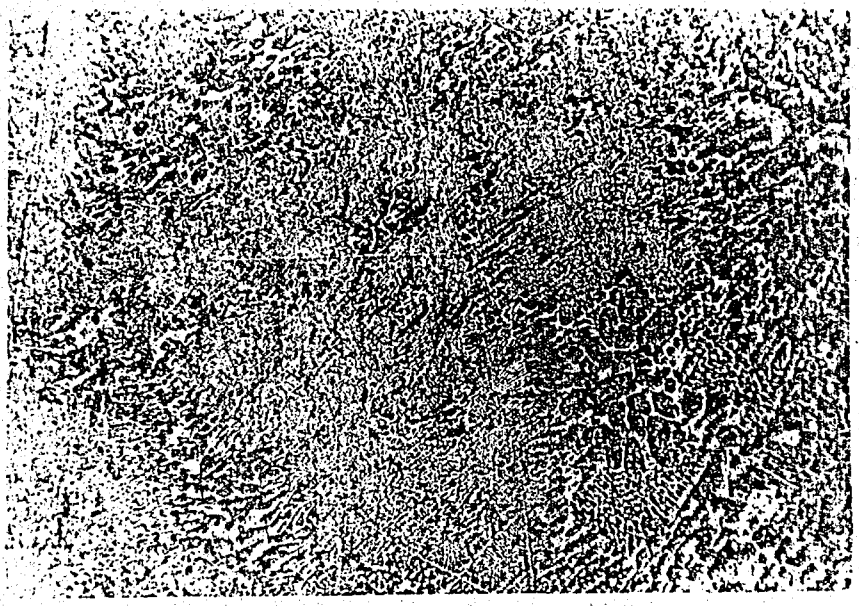

425°C mould temperature

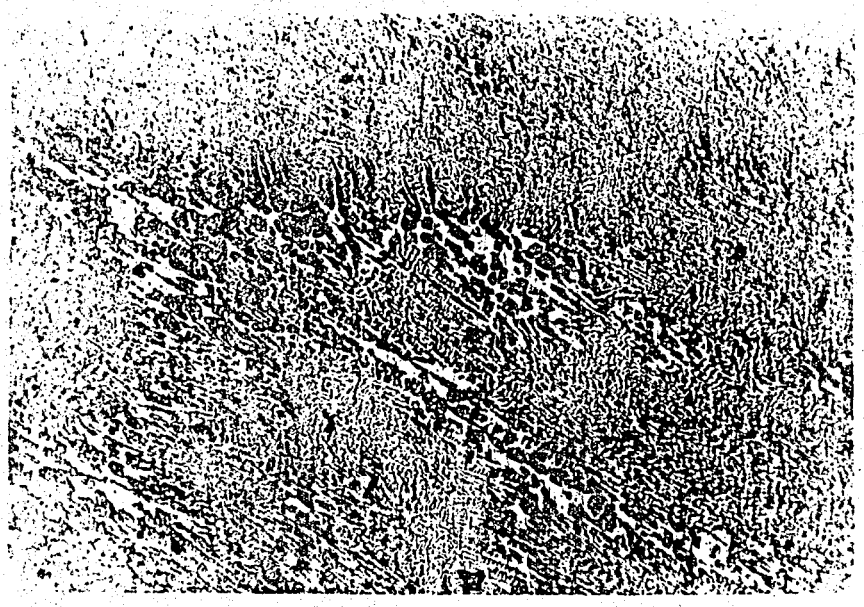

550°C mould temperature

Figure 43- a) Al-% 33 Cu, the coarsening of eutectic constituents with increasing mould temperature, primary aluminium crystals are black and Al_2Cu form a white envelope round primarses, high magnification, 83X, black holes representing the porosity.

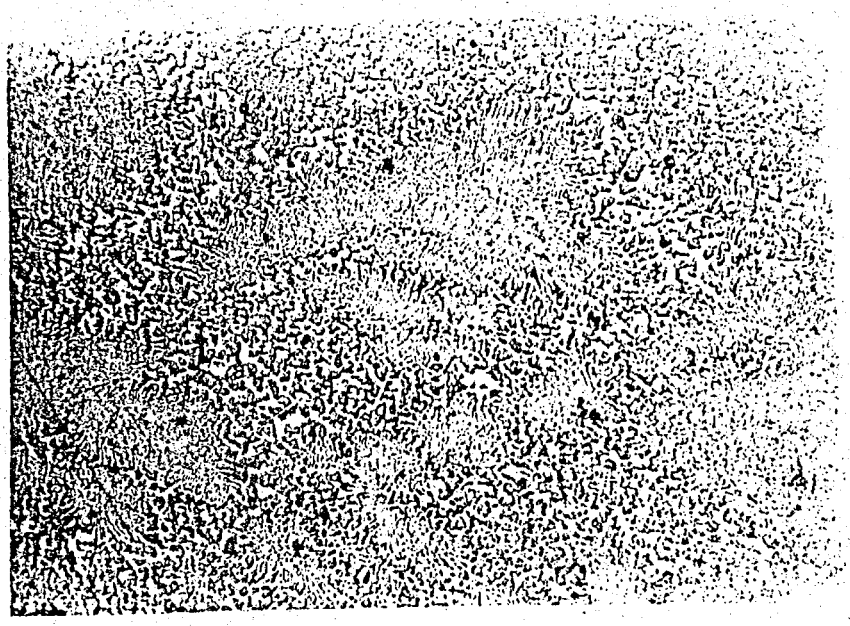

575°C casting temperature

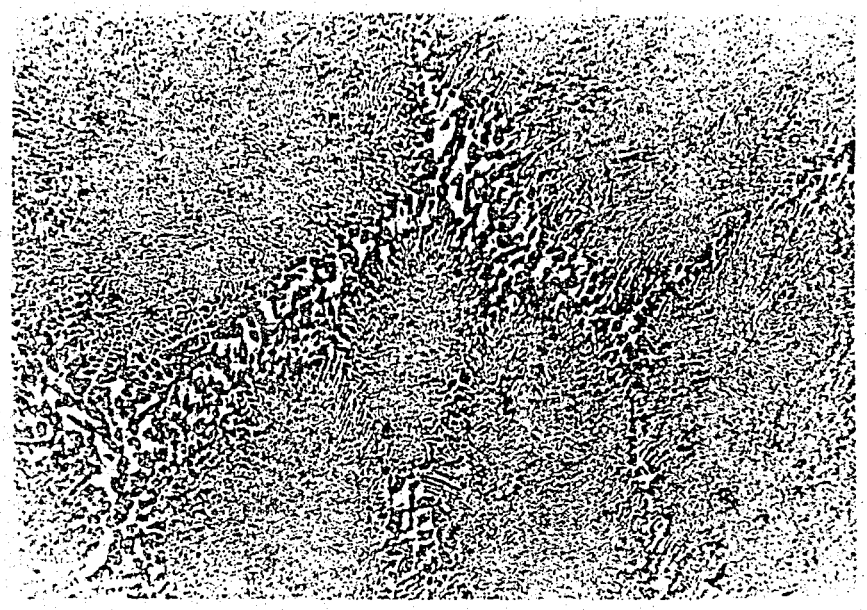

600°C casting temperature

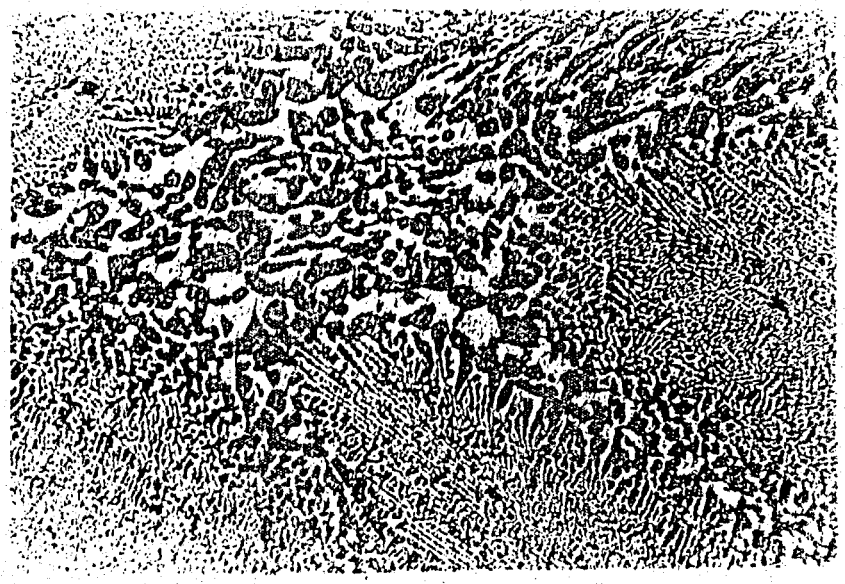

700°C casting temperature

Figure 43- b) Al-% 33 Cu, the coarsening of eutectic constituents with increasing casting temperature, primary aluminium crystals are black and Al_2-Cu form a white envelope round the primaries high magnification 81X, blackholes representing the porosity

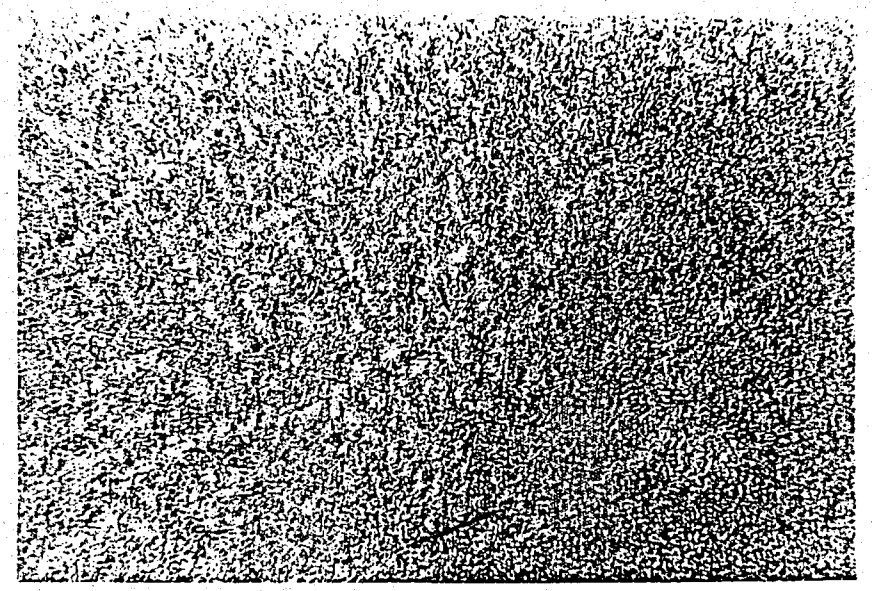

300°C mould temperature

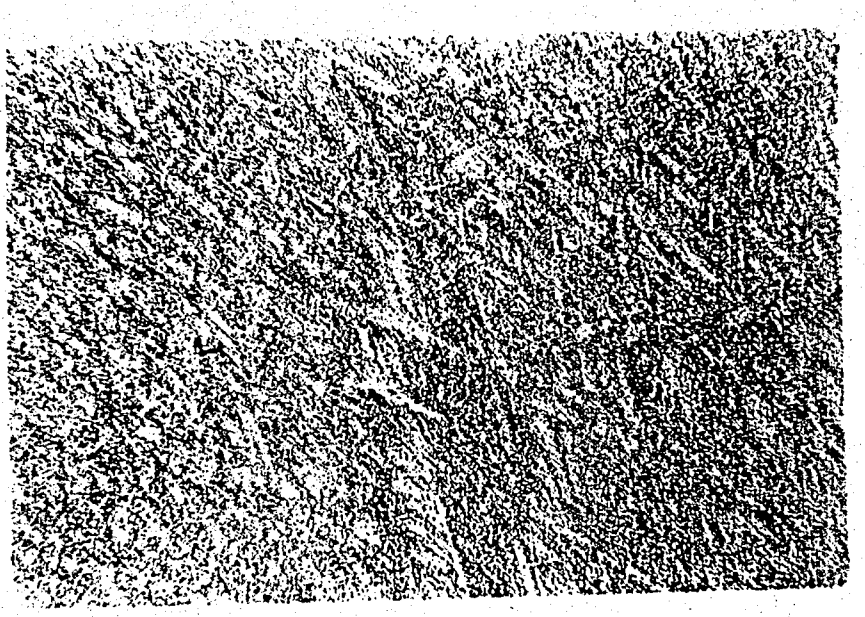

425°C mould temperature

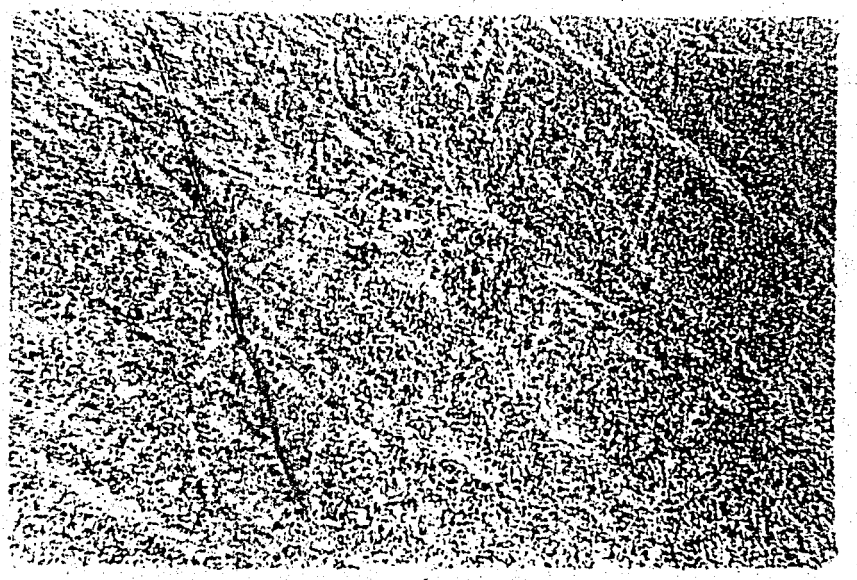

550°C mould temperature

Figure 44- a) Al-% 33 Cu, the coarsening of the eutectic cell size at the mid ingot with increasing mould temperature, gray loops representing the inside of cells and dark gray lines are cell boundaries, low magnification, 40.5X, black holes representin, the porosity in mid ingot

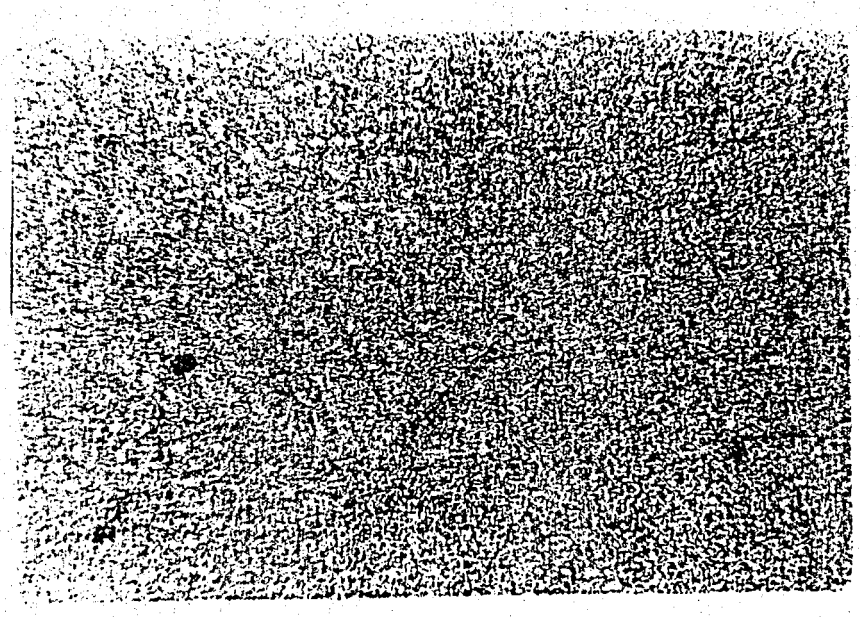

575°C casting temperature

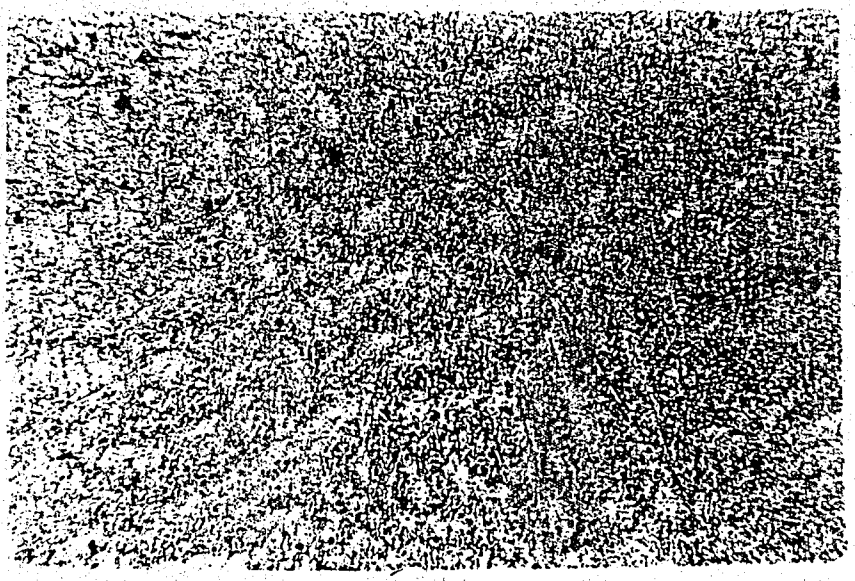

600°C castin temperature

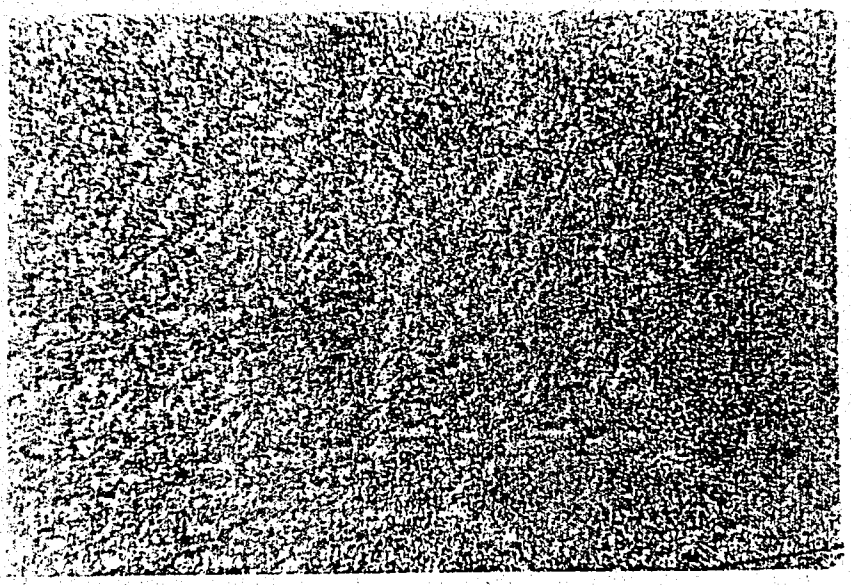

650°C casting temperature

Figure 44- b) Al-Cu % 33, the coarsening of eutectic cells formed in the mid ingot with increasing casting temperature, gray loops representing the inside of the cells and dark gray lines round the loops are eutectic cell boundaries, Low magnification, 40.5X, black holes representing the porosity

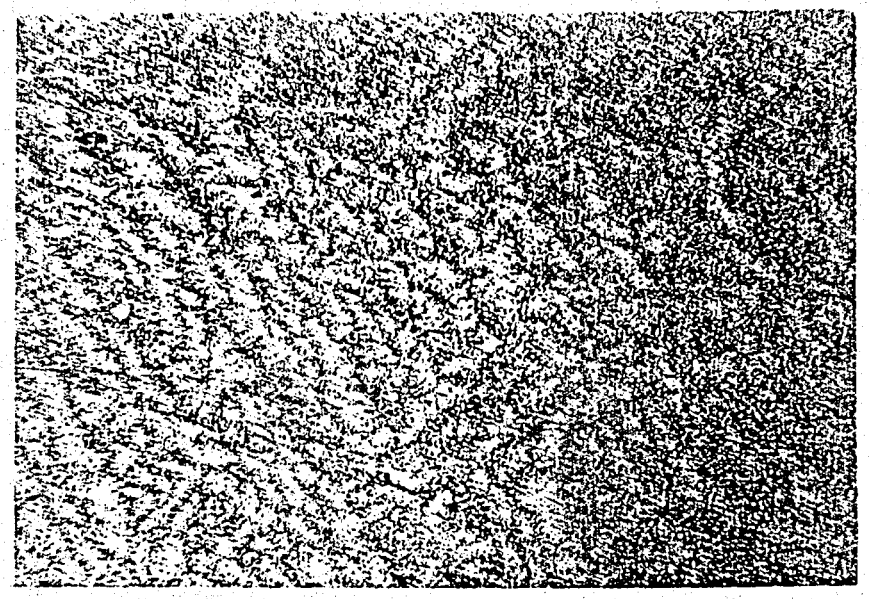

1 mm amplitude

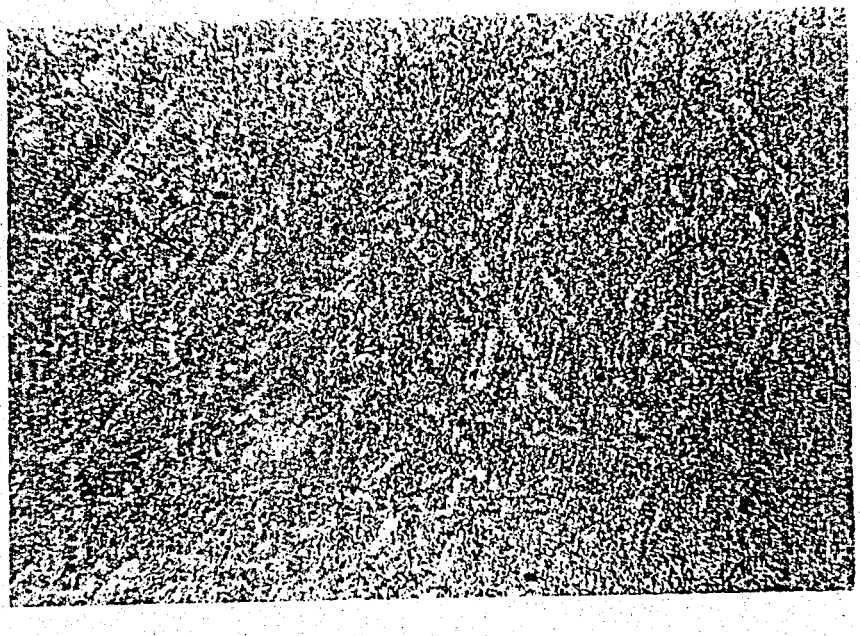

2.5 mm amplitude

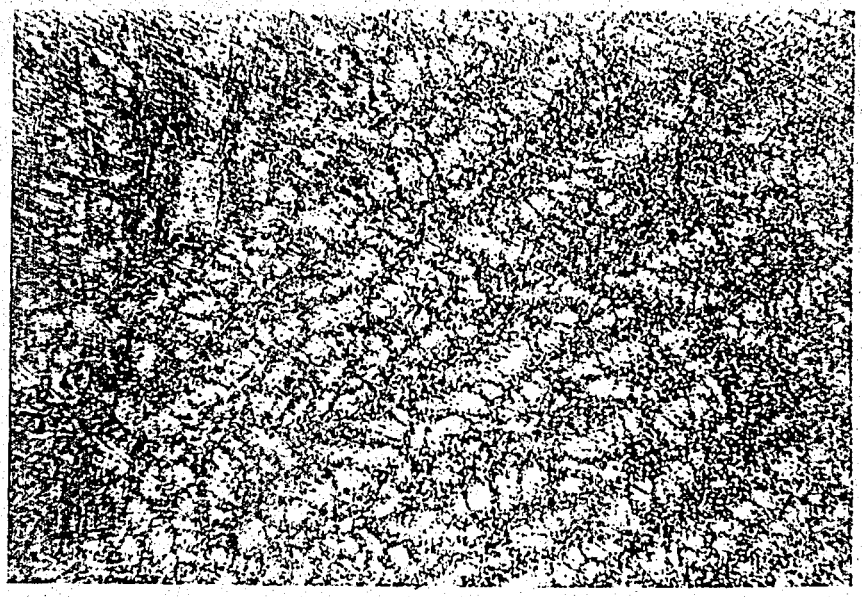

4 mm amplitude

Figure 45- Al-% 33 Cu, coarsening of the eutectic cell formed at the mid ingot at 2.5 mm amplitude, gray loops re-presenting the eutectic cell sizes and dark gray lines formed round the loops are eutectic cell boundaries, Low magnification, 40.5X, black holes representing the porosity

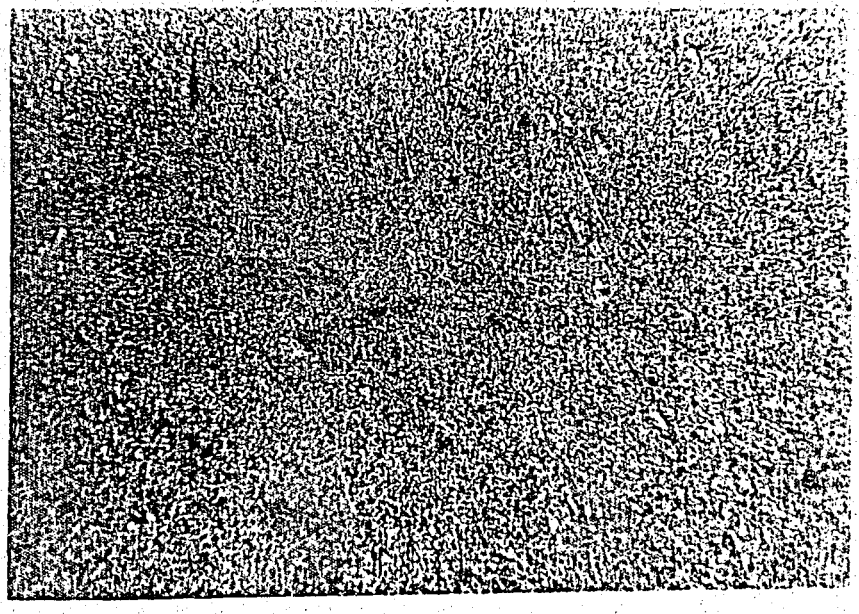

300°C mould temperature

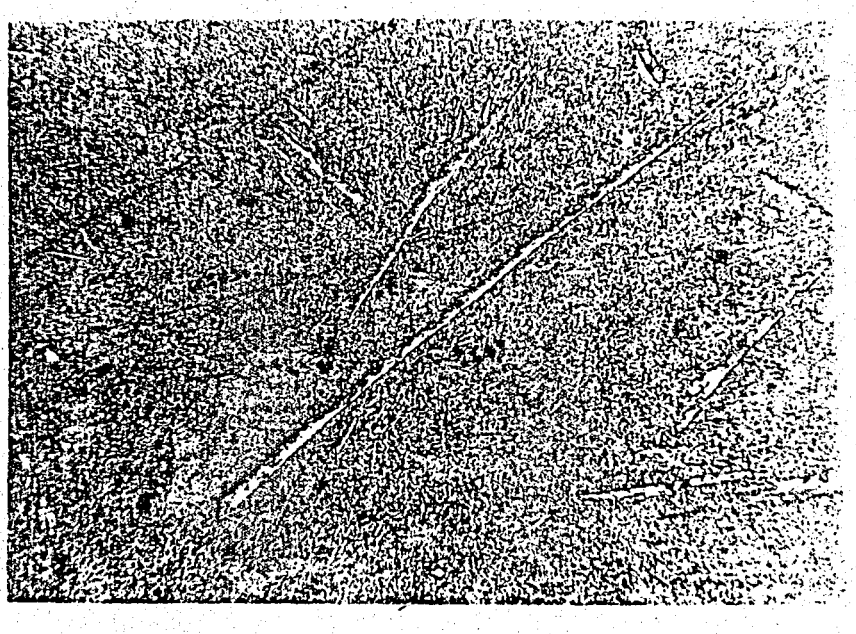

425°C mould temperature

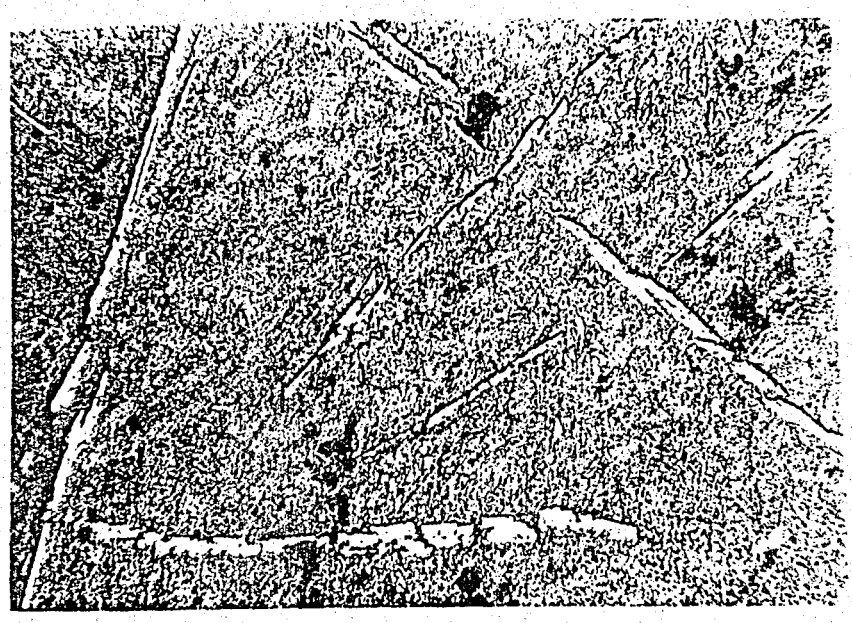

550°C mould temperature

Figure 46- a) Al-5.7 % Ni, the extremely coarsed eutectic constituents as mould temperature increases in static ingots, white plates representing Al_3Ni, Low magnification, 40.5X

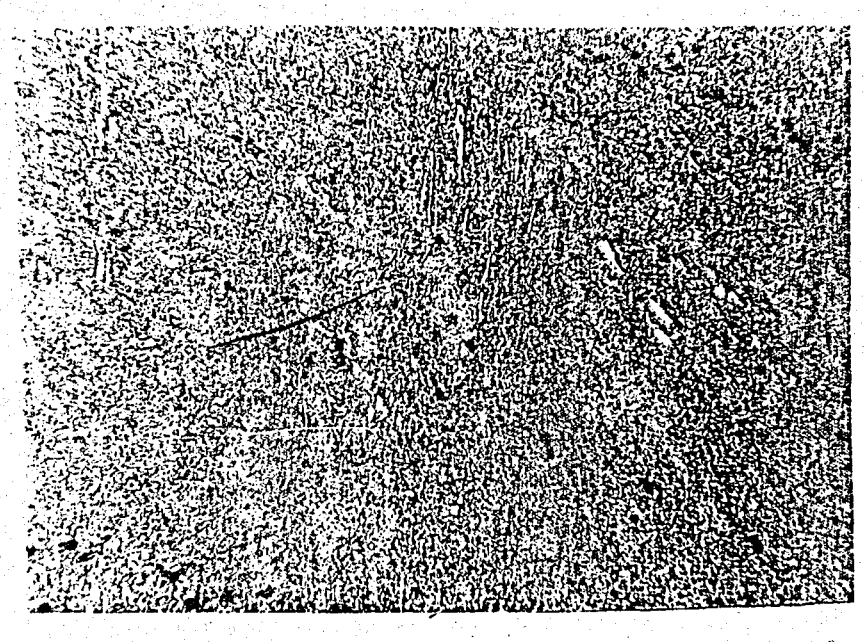

700°C casting temperature

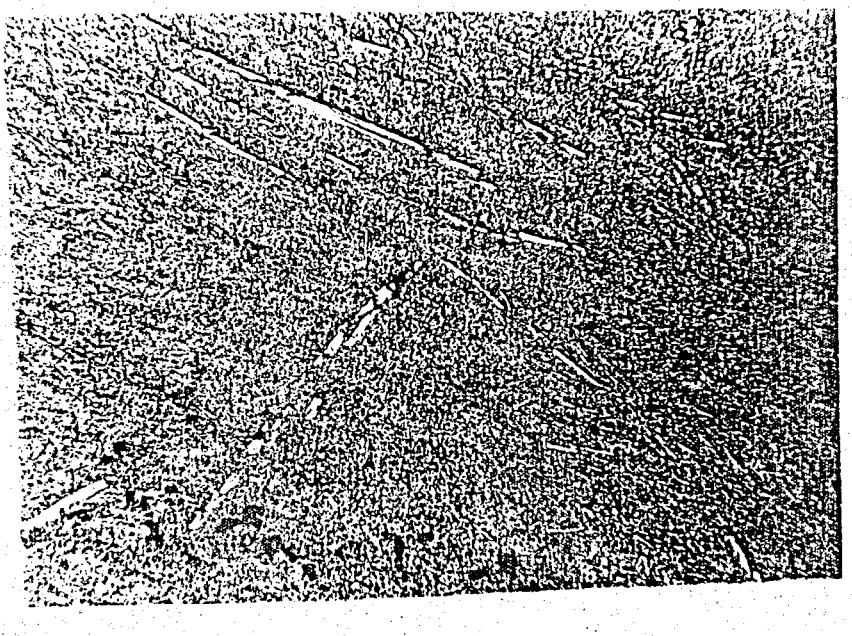

750°C casting temperature

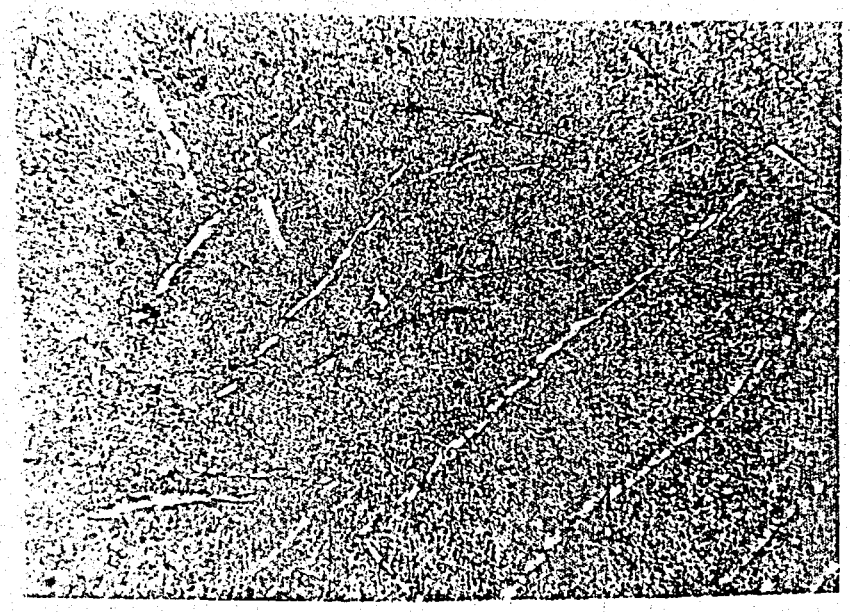

775°C casting temperature

Figure 46- b) Al-% 5.7 Ni, eutectic constituent coarsening as casting temperature increases in vibrated ingots, white plates are Al_3Ni which were formed on the matrix of eutectic cells, low magnification, 40.5X

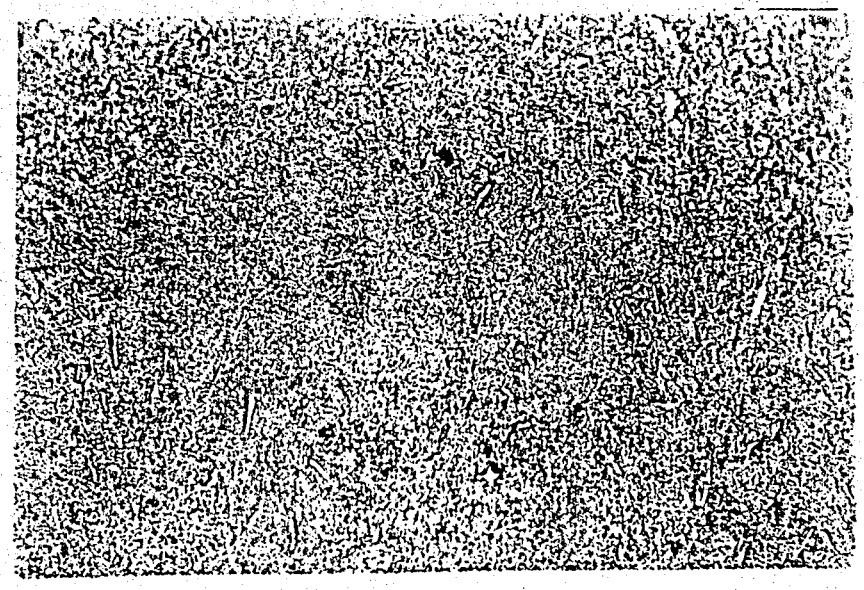

300°C mould temperature

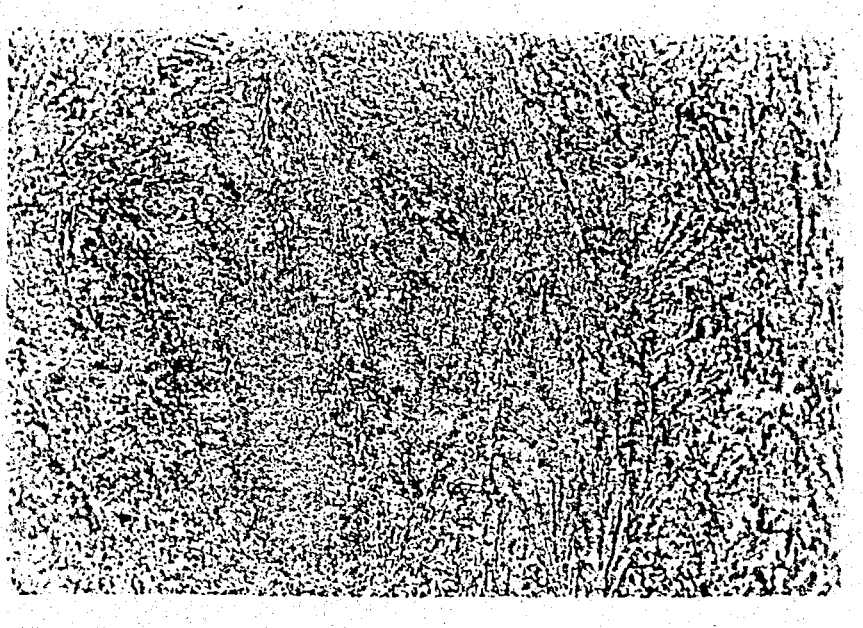

425°C mould temperature

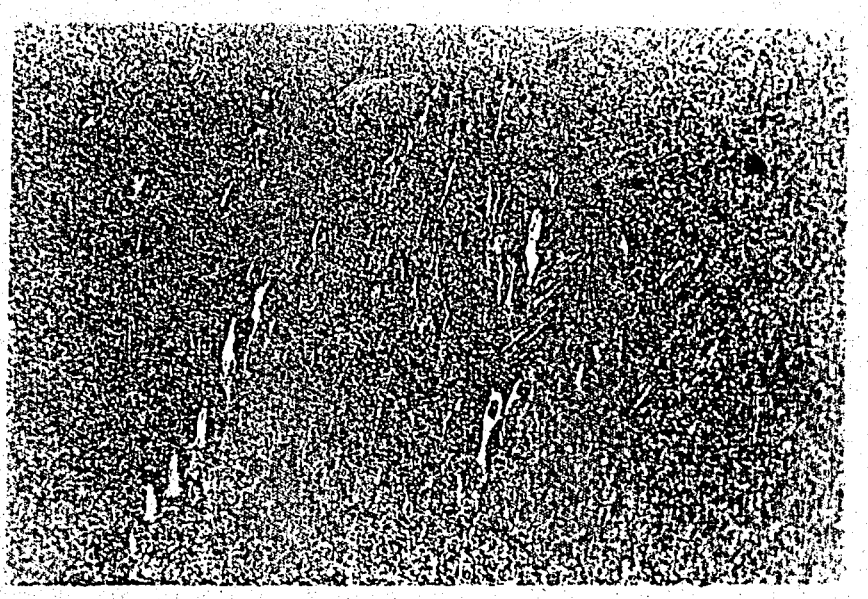

550°C mould temperature

Figure 47- Al-% 5.7 Ni, coarsening of eutectic constituents as mould temperature increases, white needles are Al_3Ni on the matrix, high-magnification, 405X, black holes representing the porosity formed in ingot

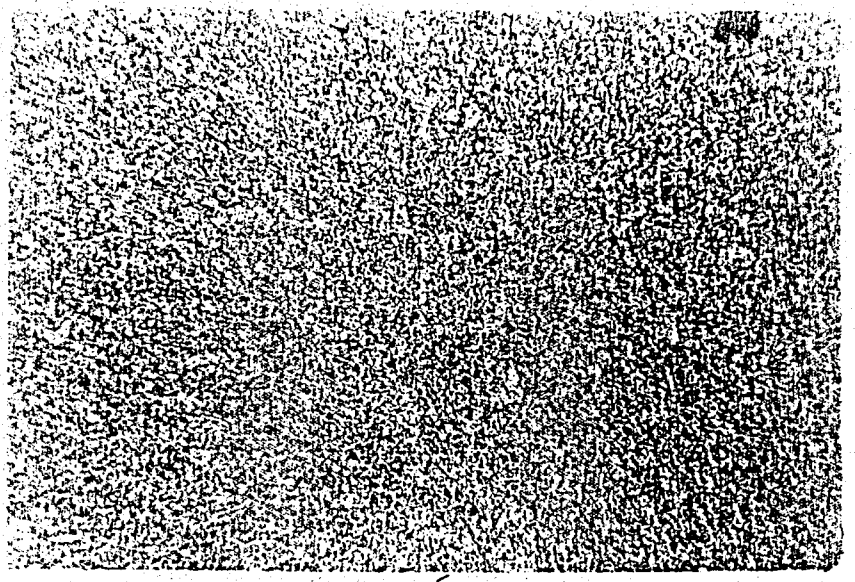

300°C mould temperature

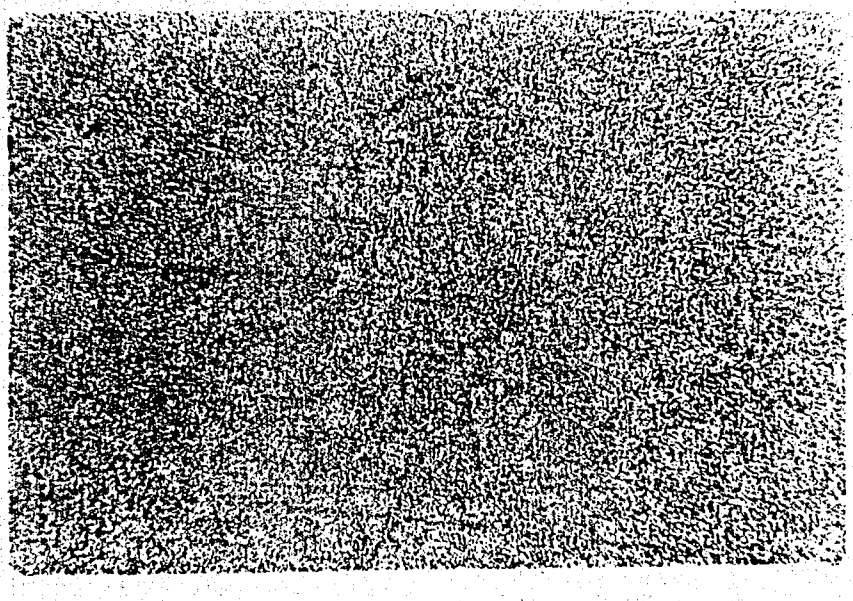

425°C mould temperature

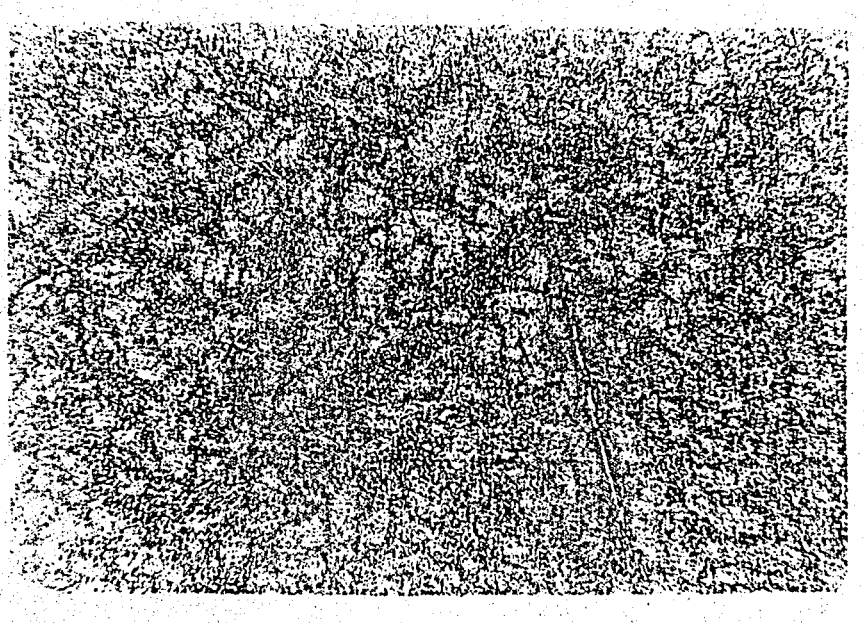

550°C mould temperature

Figure 48- Al-% 5.7 Ni, coarsening of the eutectic cells formed at the mid ingot as mould temperature increases, light gray loops are the inside of the eutectic cells and dark gray is representing the boundary formed round the cells, low-magnification, 40.5X

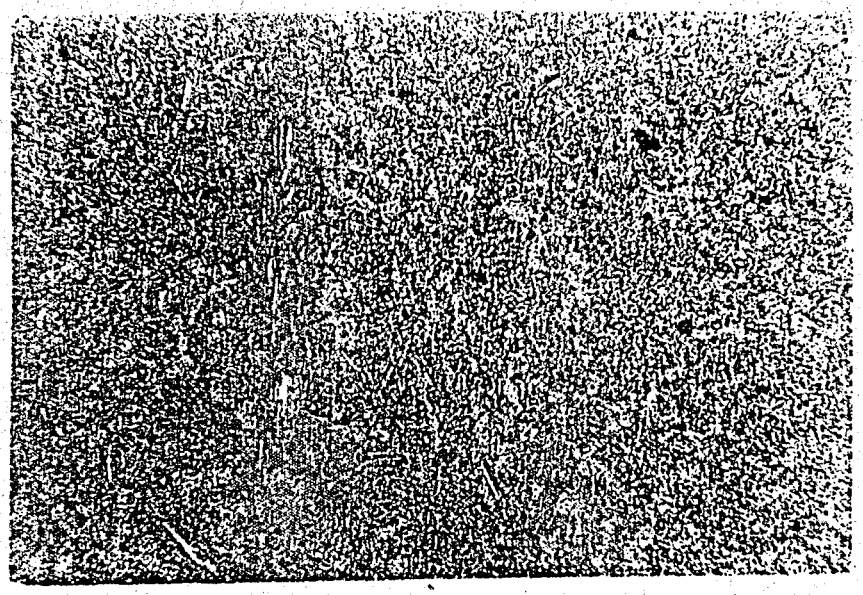

700°C casting temperature

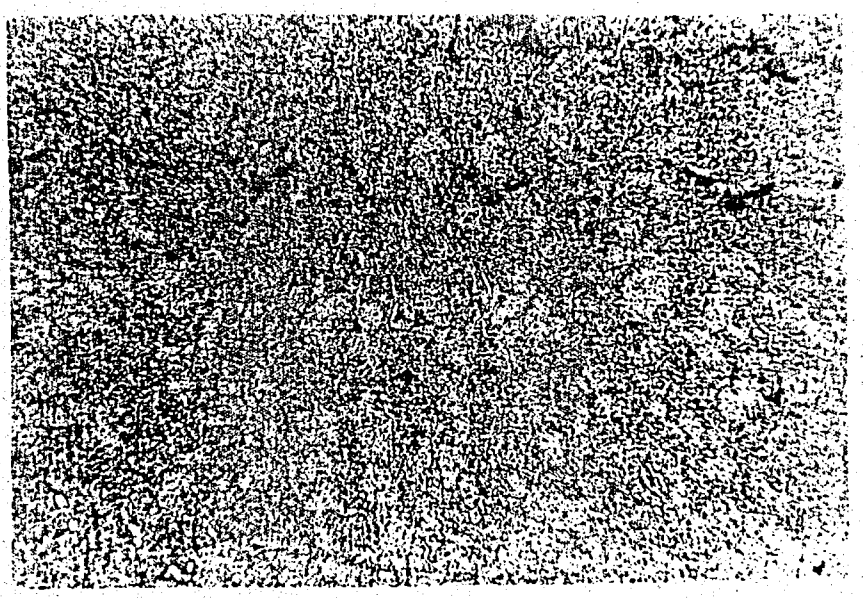

725°C casting temperature

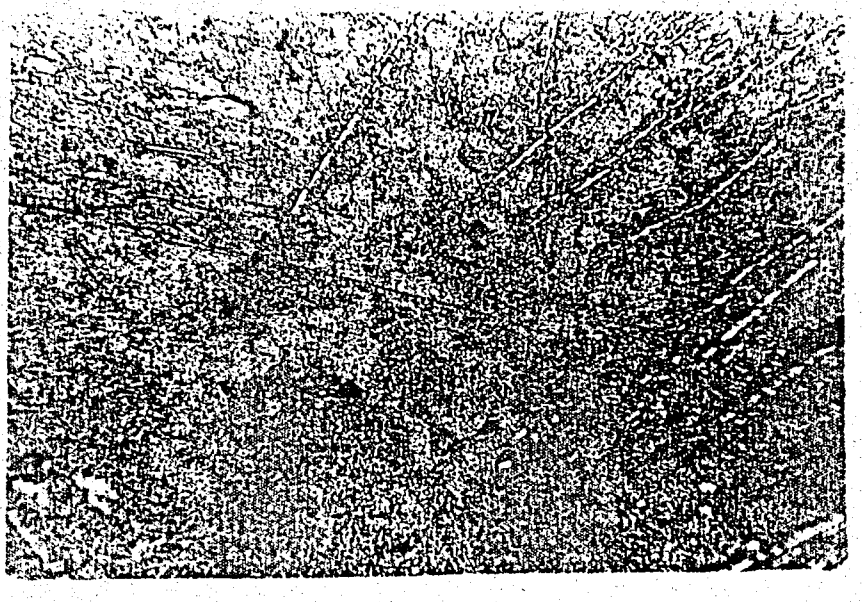

775°C casting temperature

Figure 49- Al-% 5.7 Ni, coarsening of eutectic cell size by increased casting temperature, light-gray loops is representing the inside cell and the dark-gray is representing the cell boundary formed round the cells, low magnification, 40.5X

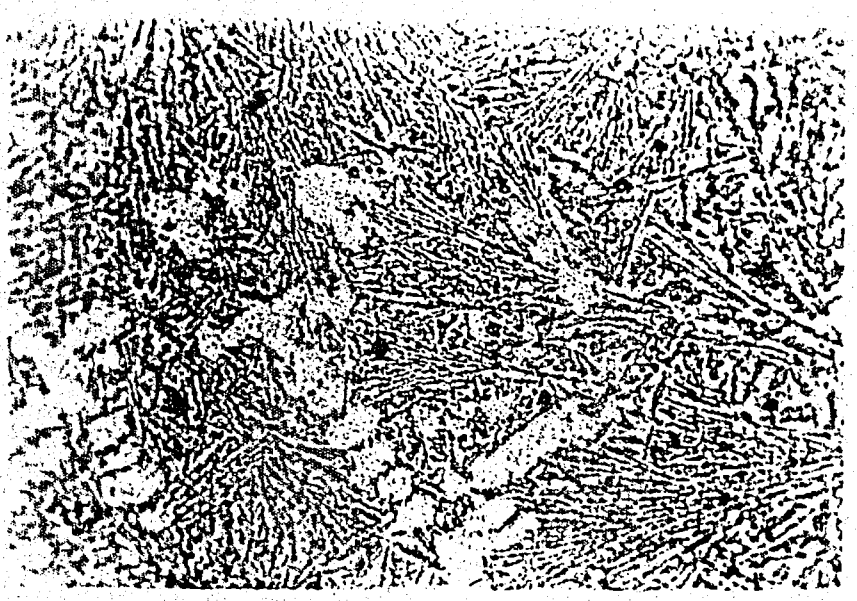

300°C mould temperature

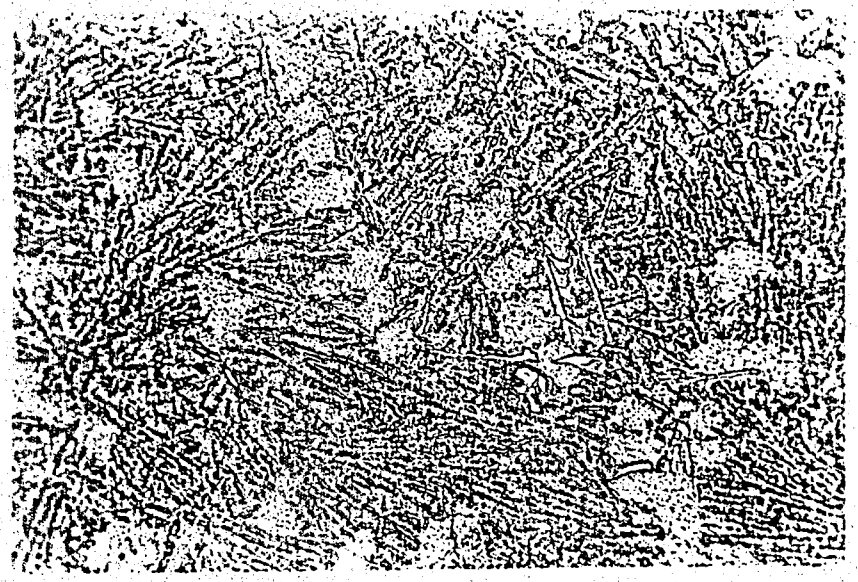

425°C mould temperature

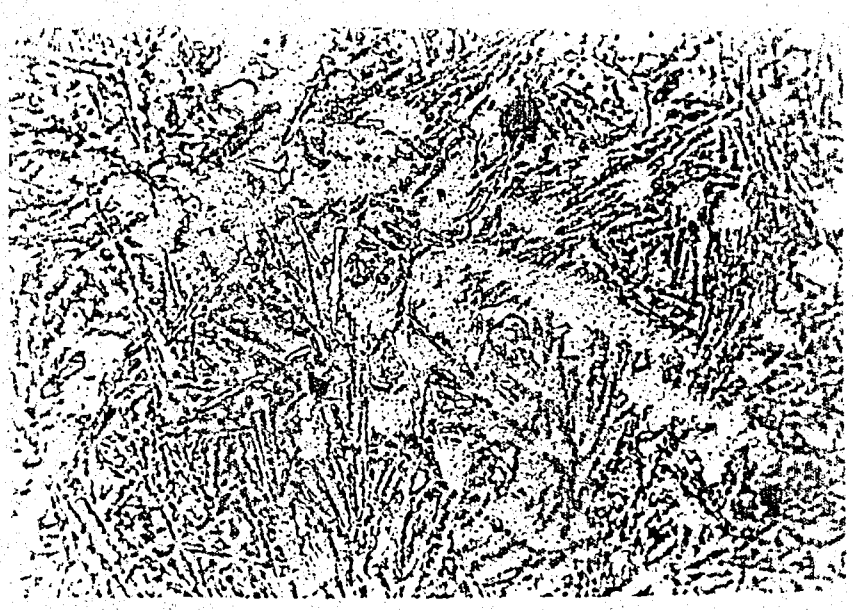

550°C mould temperature

Figure 50- a) Al-12.6 % Si, coarsening of Si plates as mould temperature increases, needles observed on the matrix are Si plates, high-magnification, 84 X, black holes representing the porosity formed m ingot

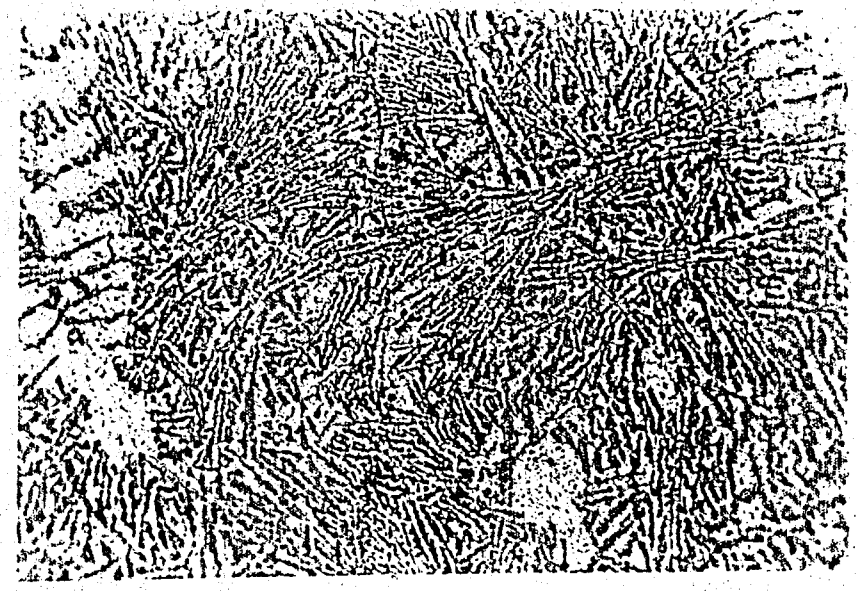

0 mm amplitude, unvibrated

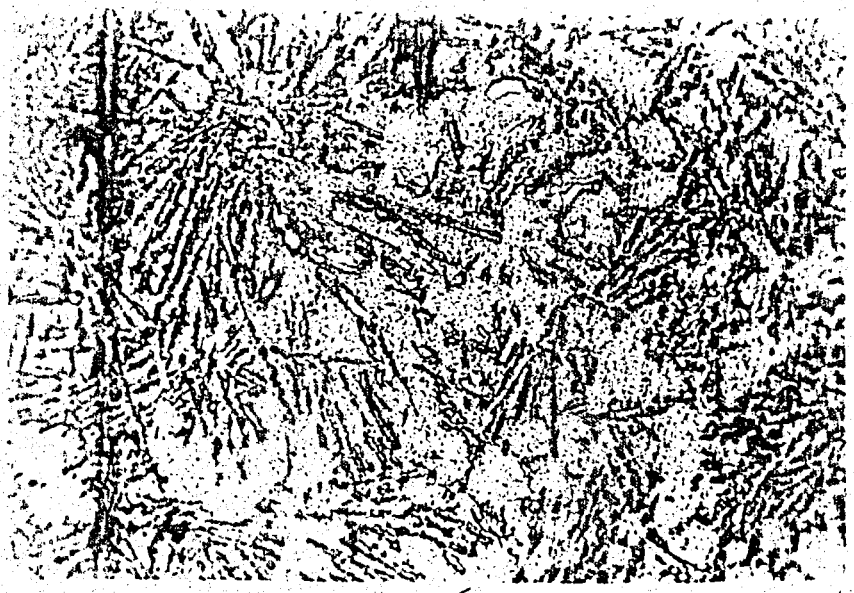

2.5 mm amplitude

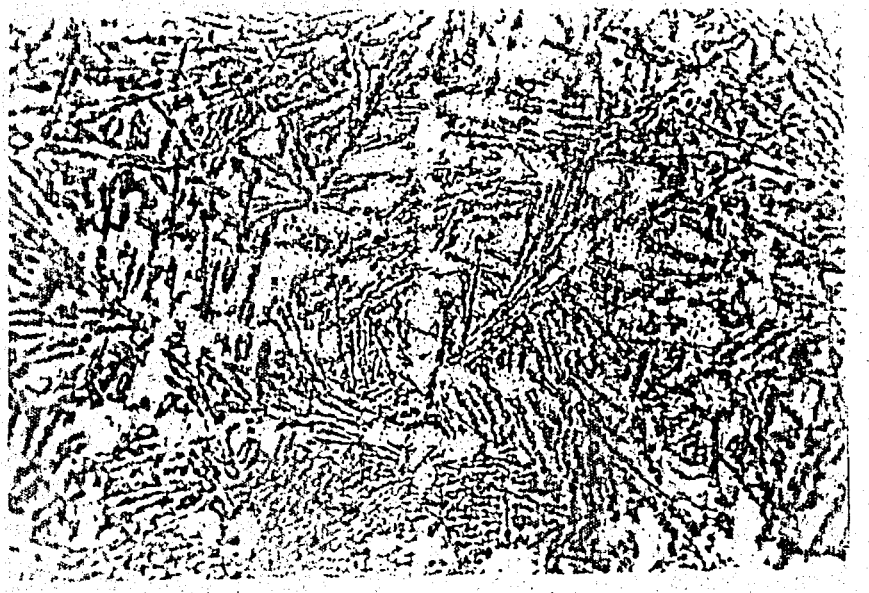

4 mm amplitedu: The light gray loops representing the dendrite arms

Figure 50- b) Al-% 12.6 Si coarsening of Si plates at 2.5 mm vibration amplitude, the needles representing the Si plates, high magnification. 83X, black holes representing the porosity formed in ingot

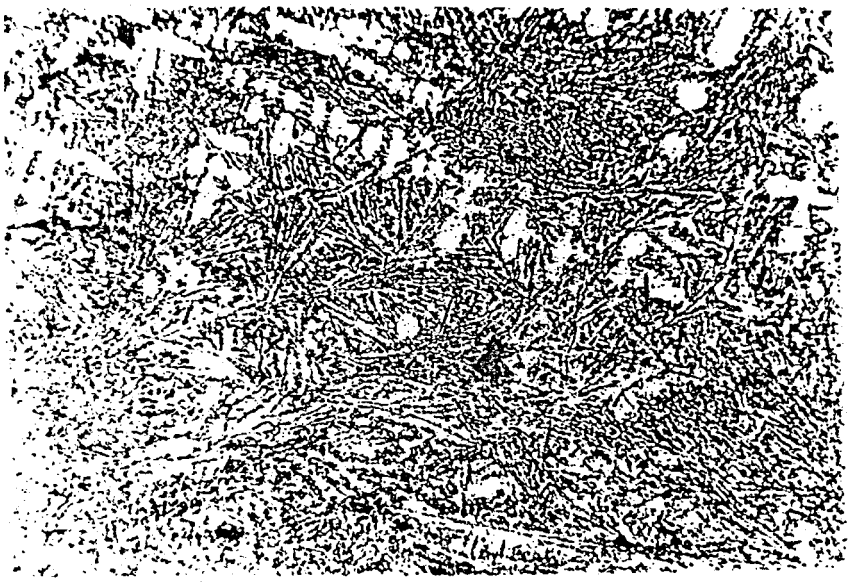

600°C Casting Temperature

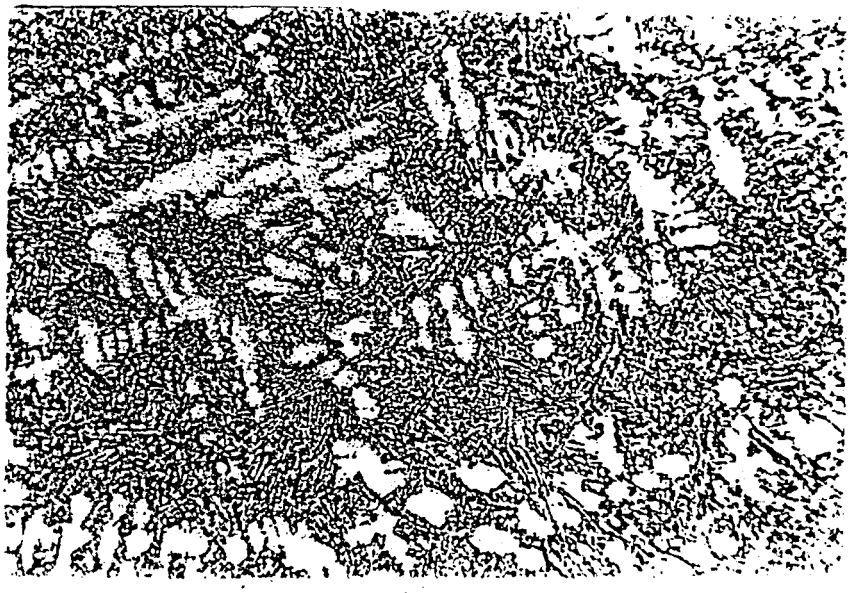

650°C Casting Temperature

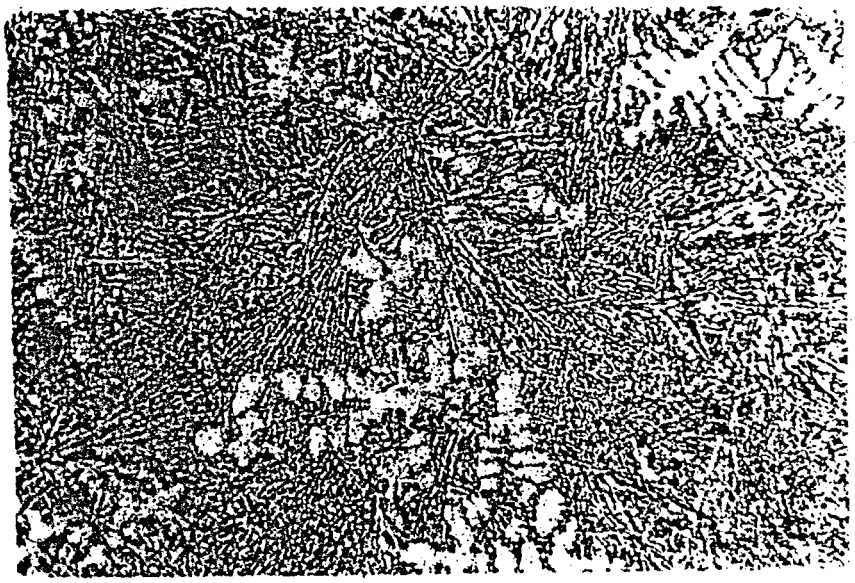

700°C Casting Temperature

Figure 51-a: Al-% 12.6 Si, Effect of increasing casting temperature on micro structure, needles represending the Si plates, and loops primary dendrite arms. Lo magnification 40.5 X

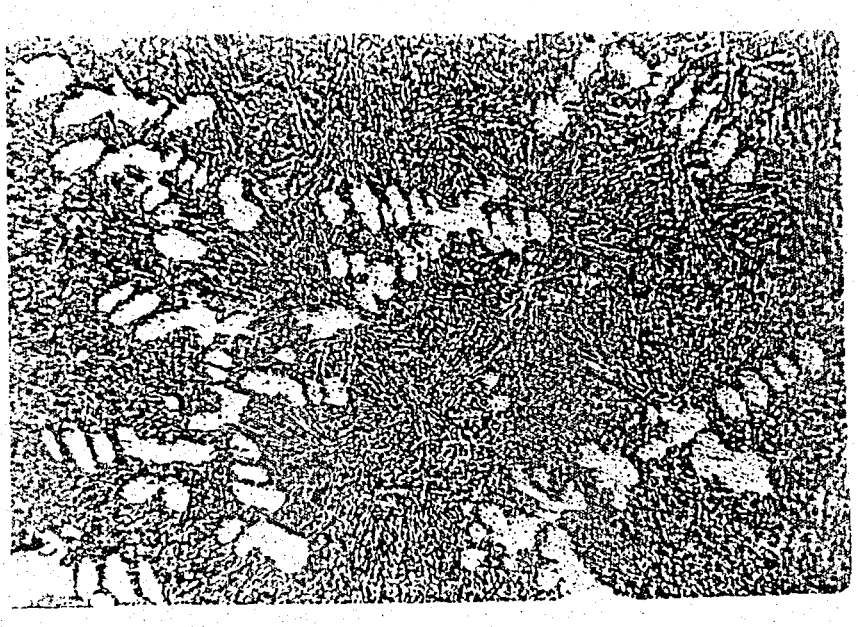

Unvibrated

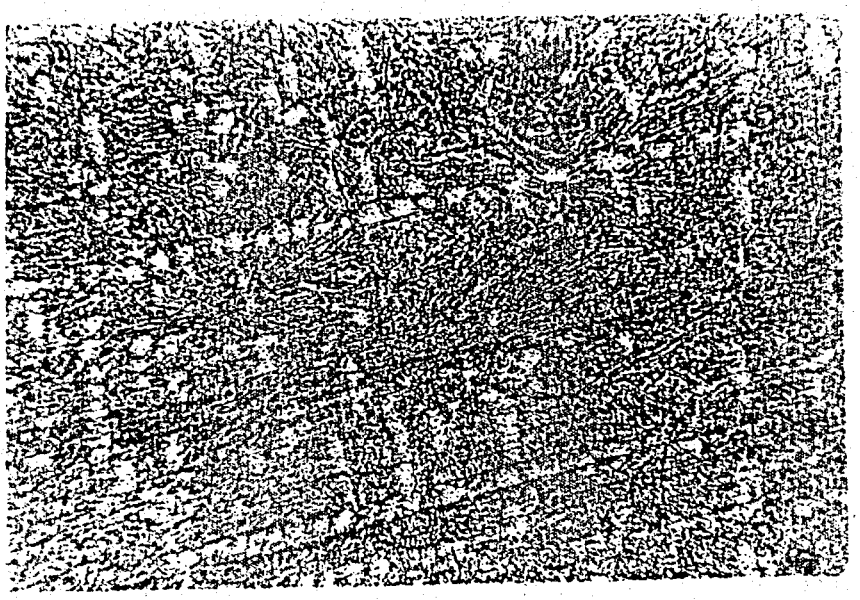

Vibrated 1 mm amplitude

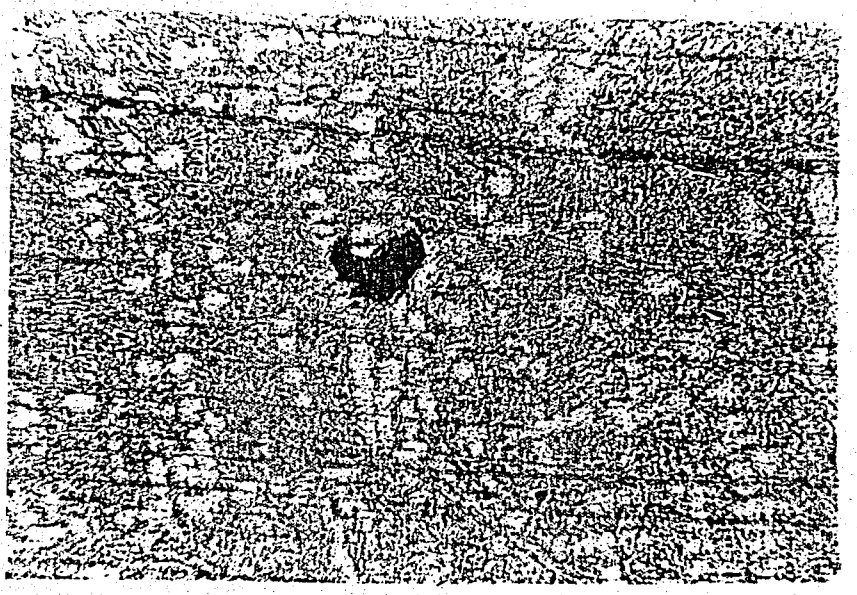

Vibrated, 4 mm amplitude

Figure 51- Al-% 12.6 Si, the reduced dendrite size in vibrated ingots, the light gray loops, representing dendite arms and needles representing Si plates, low magnification, 40.5X, black holes are representing the porosity formed in ingot

D. TENSION TESTS

1- Specimen Preperation

The test bars, which were removed from the mid slices provided by lateral sectioning of ingots, were machined down to the tension test specimens and subsequently polished to prevent the probable surface defects produced during machining (Figures 52 a and 52 b). Tension tests were performed at room temperature and tensile testing machine was used during tension tests. The dimensions of the test specimen illustrated in figure 53(29).

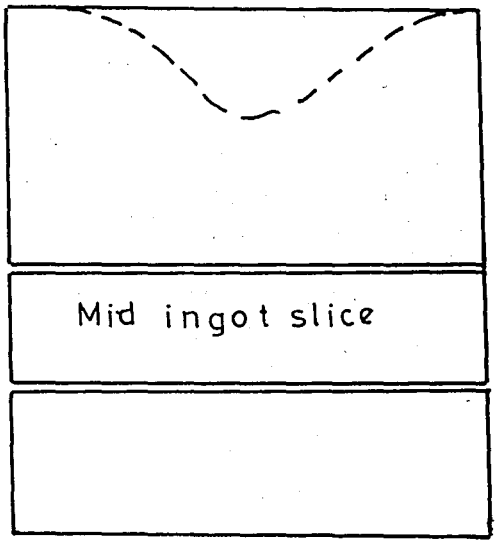

-a-

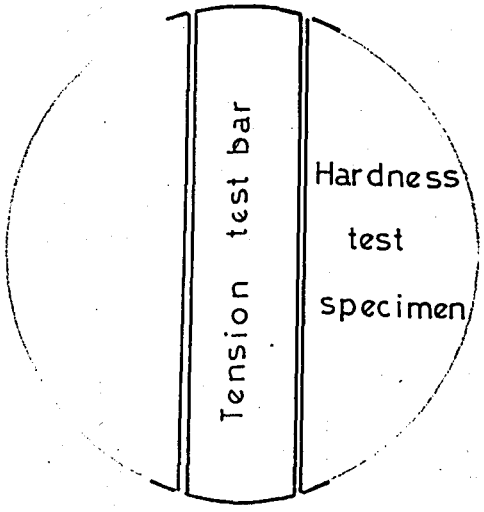

-b-

Figure 52- Obtaining test sepcimens from ingot casting

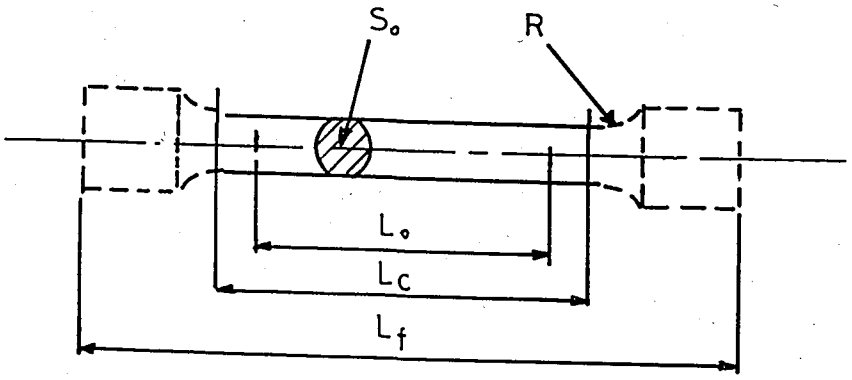

-a-

So mm.	d mm.	Lo mm.	Lc= 5.5d mm.	R wrought mm.	R casting mm.	diameter tolerance ± mm.
200	15,96	80	88	15	30	0,08
150	13,82	69	76	13	26	0,07
100	11,28	56	62	10	20	0,06
50	7,98	40	44	8	16	0,04
25	5,64	28	31	5	10	0,03
12,5	3,99	20	22	4	8	0,02

-b-

Figure 53- Dimensions of the circular section test specimens(21)

2- Experimental Results

Four each group of alloy twenty-four tests were performed by loading the specimen monotonically until failure. During loading, the load vs. displacement was recorded on a graphic and the results obtained from tension tests were illustrated in figures 54 a to 54 f.

3- Discussion of the Results

By the examination of the figures 54 a to 54 f and the experimental data the variation of the tensile strength due to the imposed vibration could be understood.

When the effect of increasing mould temperature to the Al-% 33 Cu ingot casting is considered, it is observed that at high mould temperatures, 550°C and 600°C, the maximum improvement 78 % and 135 % respectively, obtained in tensile strength at four milimeter vibration amplitude. At one and four milimeter amplitudes, the tensile data obtained from experiments follow the same trend that a sudden jump at 550°C is observed. By the way the worst tensile data obtained for the ingots vibrated with 2.5 mm amplitude, and for highest 600°C mould temperature 135 %, 114 % and 111 % improvements were predicted in the tensile strength of the vibrated ingots vibrated with, 4, 1 and 2.5 mm amplitudes respectively. On the other hand when the ingots casted with increasing casting temperature examined, the only improvement observed at 600°C casting temperature is 1.5 % which could be neglected.

In order to compare the results obtained for Al-% 33 Cu in this study, the graph illustrated in figure 55, is constructed. The obtained data for static ingots are superior than that of obtained by R.R.Burbure at low mould temperatures and the ingots vibrated with 1 mm amplitude present about % 20 improved data at all mould temperatures.

The tensile data obtained for the vibrated ingots of Al-% 5.7 Ni casted with 425°C, 550°C and 600°C mould temperatures show that, at all amplitudes, 1, 2.5 and 4 mm, improvement is predicted and the maximum improvements observed at above temperatures were 129 %, 670 % and 261 % respectively. The decreasing trend in tensile strength of the vibrated or unvibrated ingots with increasing mould temperature is observed to be mostly striking after 425°C. Any improvement is not obtained due to the imposed vibration when the effect of increasing casting temperature on tensile s trength is examined and the tensile strength of the vibrated ingots decreased with increasing temperature.

The tensile strength of vibrated Al-% 12.6 Si ingot castings do not show any improvement, when the ingots casted with increasing mould temperature is examined. The unvibrated and vibrated ingots, with 2.5 mm amplitude, show a decreasing trend in tensile strength by the increase of mould temperature and the vibrated ingots, of 1 and 4 mm amplitude, present a similar havior observed in Al-% 33 Cu that a sudden jump at 550°C is observed. When the variation of tensile data with the increase of casting temperature is examined, it is observed that the decrease in tensilestrength is striking after 650°C. Also the maximum improvement predicted in tensile strength, in the vibrated ingots casted with increasing casting temperature is 110 % for 650°C.

To compare the obtained tensile strength values for Al-% 12.6 Si, the permenant mould casting alloy, with trade number A132, is taken into consideration and solution or precipitation treated alloy samples exhibit 2317.45×10^5 N/m^2 minimum value, which is at least % 50 higher than the obtained experimental data.

The predicted decreasing trend in tensile strength of the above selected eutectic alloys, due to an increase in mould or casting temperature, may be related to the coarsening of the intermetallic eutectic constituents and eutectic partieles, as stated by G.A.Chadwick(16) and H.A.H.Steen(10),

and to the increase observed in size of the eutectic cells. The resultant effect of increasing cell size may be explained by adapting Hall-Petch equation to the eutectic cell size.

$$\sigma_F = \sigma_o + k\, d^{-1/2}$$

where as σ_F is the fracture stress, σ_o and k experimental constants and d is the grain size or cell size for our case.

4- Discussion of the Elongation Results

As the elongation data illustrated in figures 56 a to 56 f examined, the resemblance between the elongation data and tensile strength data could be observed.

It is predicted for Al-% 33 Cu that as mould temperature increases elongation exhibited a decreasing trend which is mostly striking after 425°C mould temperature. At high mould temperatures 550°C and 600°C, the vibrated ingots present a better elongation data when compared with the static ones and it is predicted that improvements observed are 100 % and 140 % respectively. Also the vibrated ingots casted with increasing casting temperature exhibit a better elongation with maximum improvement of 210 % at 650°C, where as elongation decreases as casting temperature increases.

The effect of increasing mould temperature to the elongation data obtained for Al-% 5.7 Ni, is to decrease it for vibrated, 1 and 2.5 mm amplitudes, and unvibrated ingot castings. It is observed that for 425°C, 550°C and 600°C mould temperatures all the vibrated ingot castings present a superior data and the maximum improvements obtained are 150 %, 600 % and 600 % respectively. There is no systematic effect produced by increasing casting temperature to the elongation but the static castings shaw a better elongation data.

The only improvement observed for vibrated ingots of Al-Si % 12.6 casted with increasing mould temperature, is at 600°C and 150 %. Also the vibrated and unvibrated ingot castings

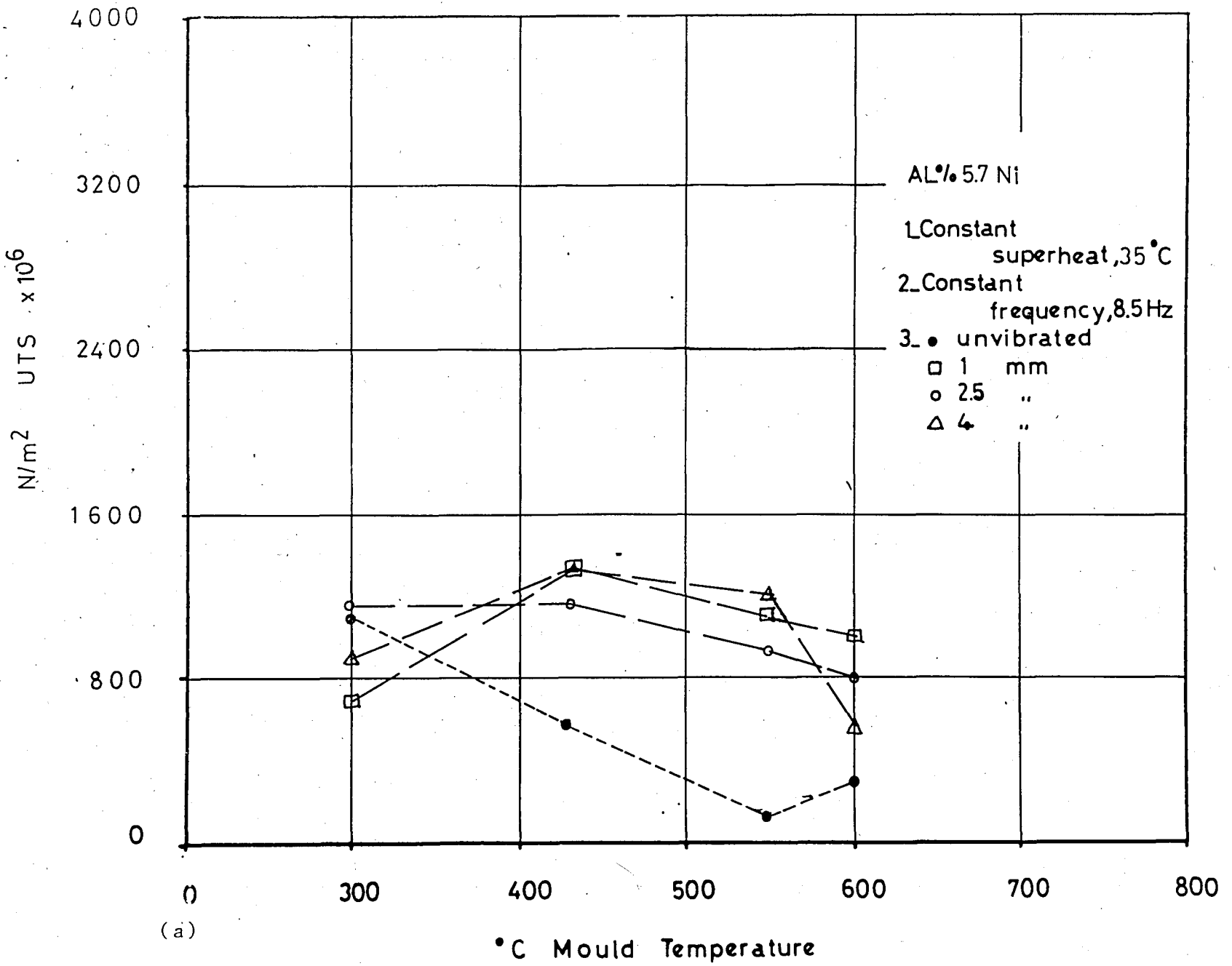

(a)

Figure 54- Results of tensile tests performed

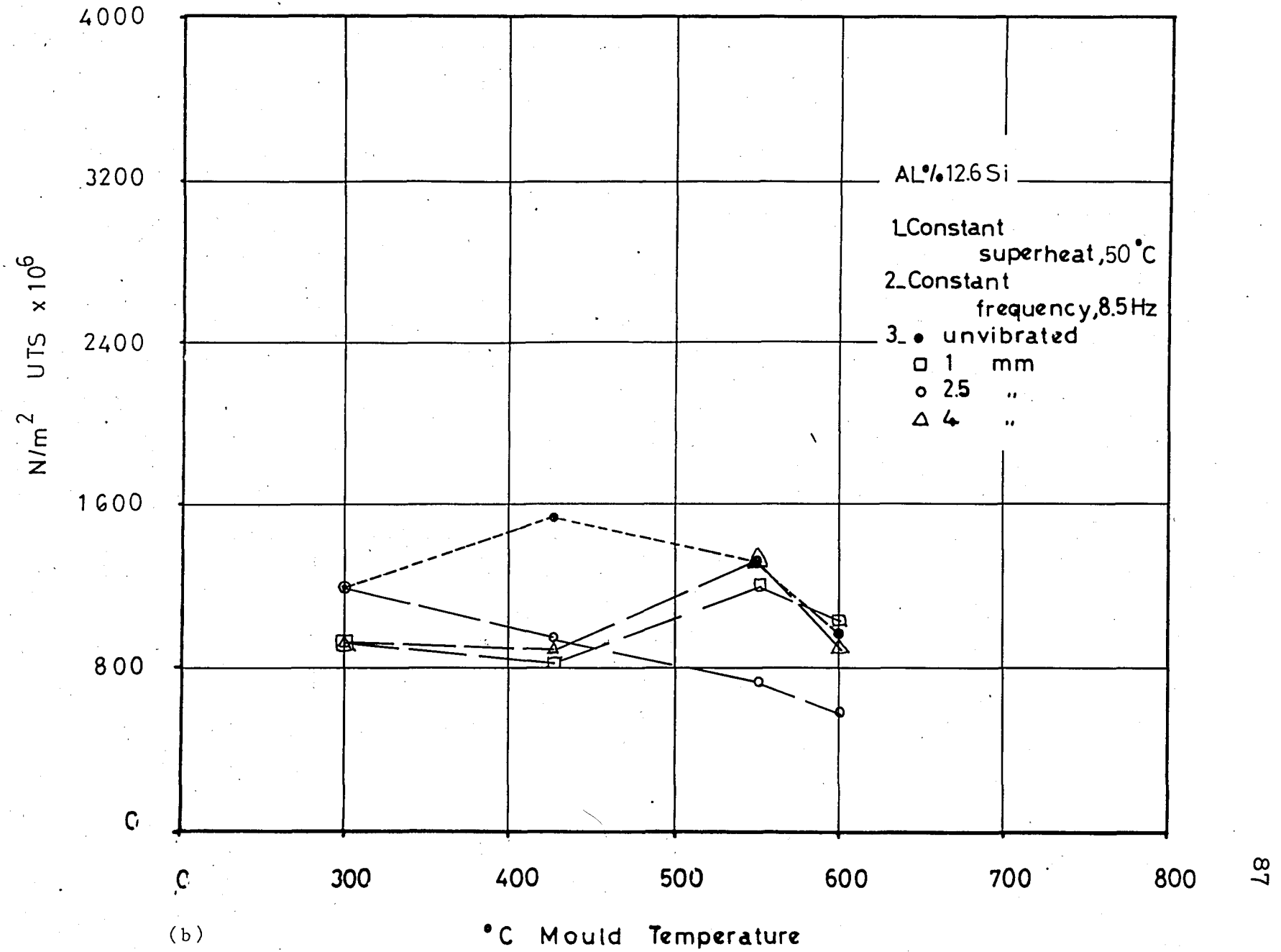
4000
3200
2400
1600
800
0
N/m² UTS x 10⁶
AL%12.6 Si
1 Constant superheat, 50 °C
2 Constant frequency, 8.5 Hz
3 ● unvibrated
□ 1 mm
○ 2.5 ,,
△ 4 ,,
0
300
400
500
600
700
800
°C Mould Temperature

(b)

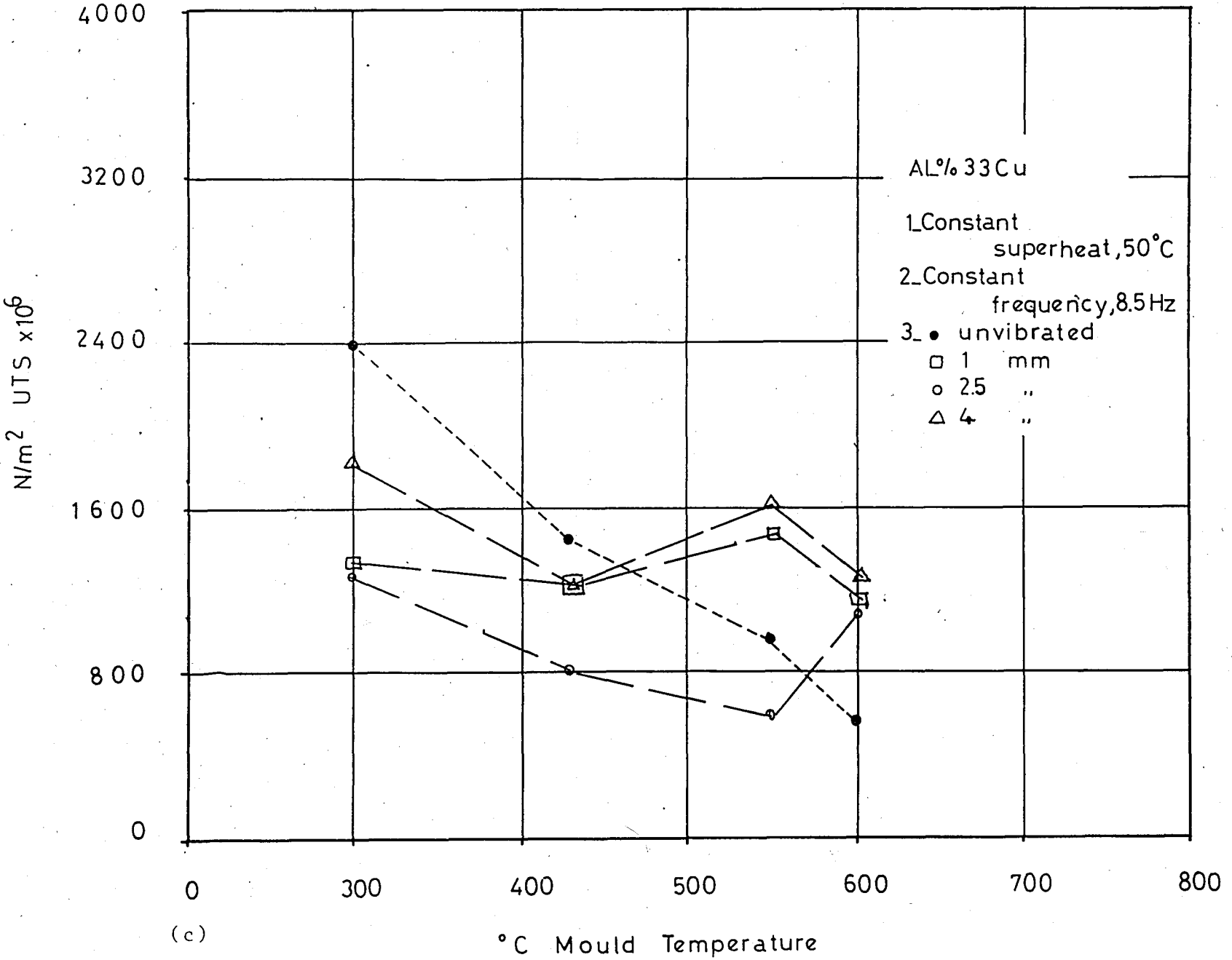
4000
3200
2400
1600
800
0
N/m² UTS x10⁶
0
300
400
500
600
700
800
°C Mould Temperature
AL% 33 Cu
1_Constant superheat, 50°C
2_Constant frequency, 8.5 Hz
3_ • unvibrated
□ 1 mm
○ 2.5 ,,
△ 4 ,,

(c)

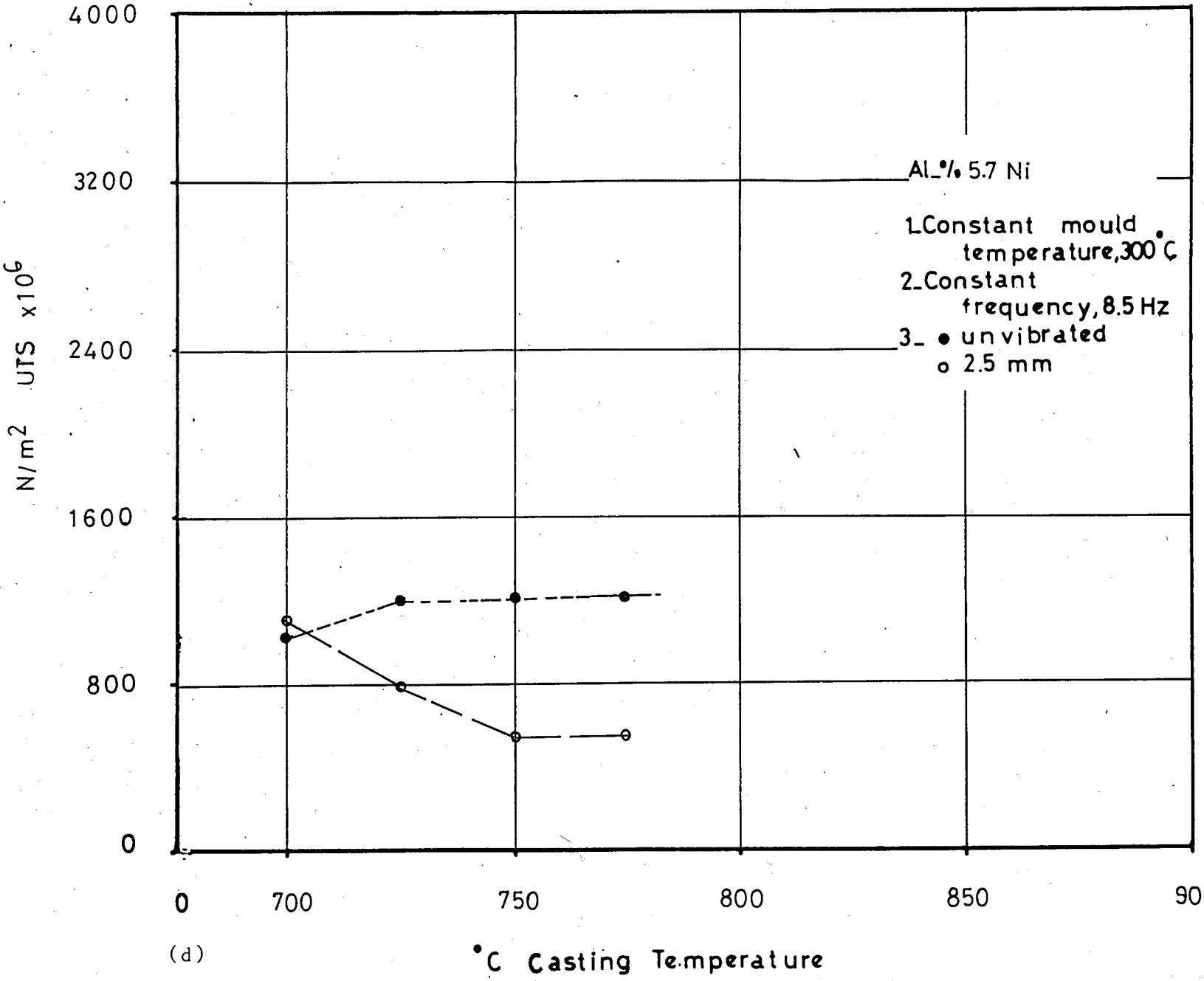
4000
3200
2400
1600
800
0
N/m² UTS x10⁶
Al-% 5.7 Ni
1.Constant mould temperature, 300°C
2.Constant frequency, 8.5 Hz
3. ● unvibrated
o 2.5 mm
0
700
750
800
850
900
°C Casting Temperature

(d)

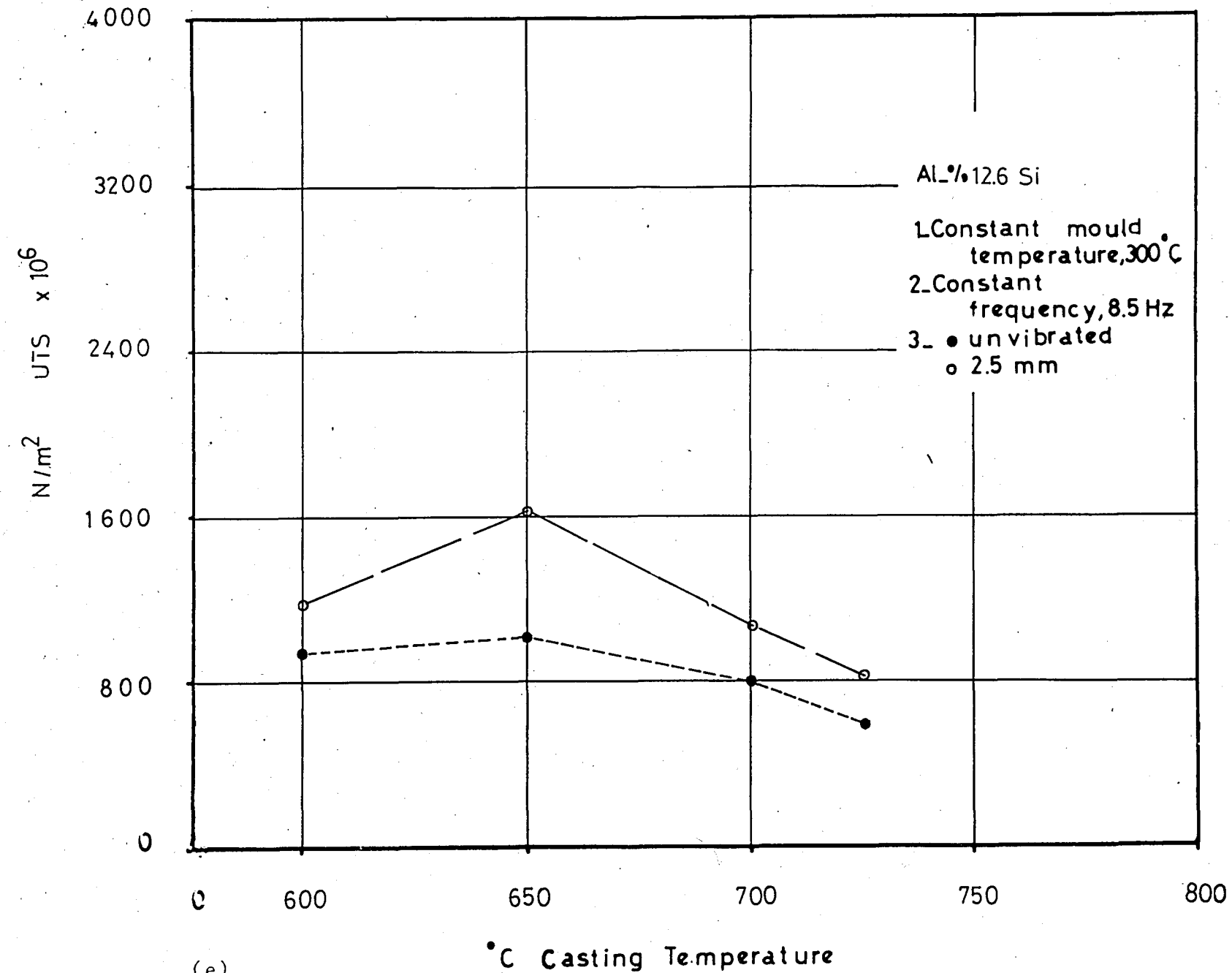
4000
3200
2400
1600
800
0
N/m² UTS x 10⁶
Al-%12.6 Si
1.Constant mould temperature,300°C
2.Constant frequency,8.5 Hz
3. • unvibrated
o 2.5 mm
0
600
650
700
750
800
°C Casting Temperature

(e)

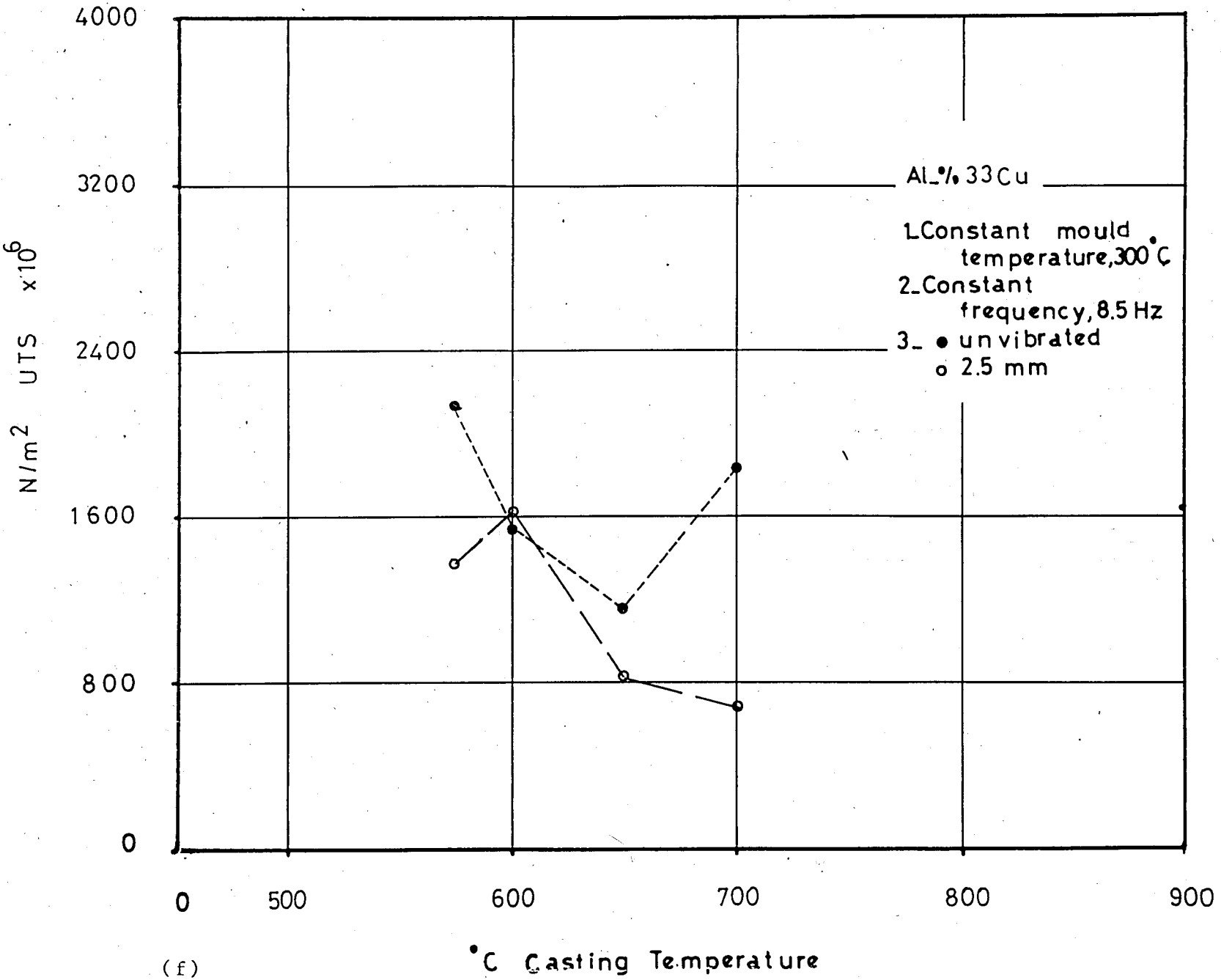
4000
3200
2400
1600
800
0
N/m² UTS x10⁶
Al-% 33 Cu
1. Constant mould temperature, 300 °C
2. Constant frequency, 8.5 Hz
3. ● unvibrated
o 2.5 mm
0
500
600
700
800
900
°C Casting Temperature

(f)

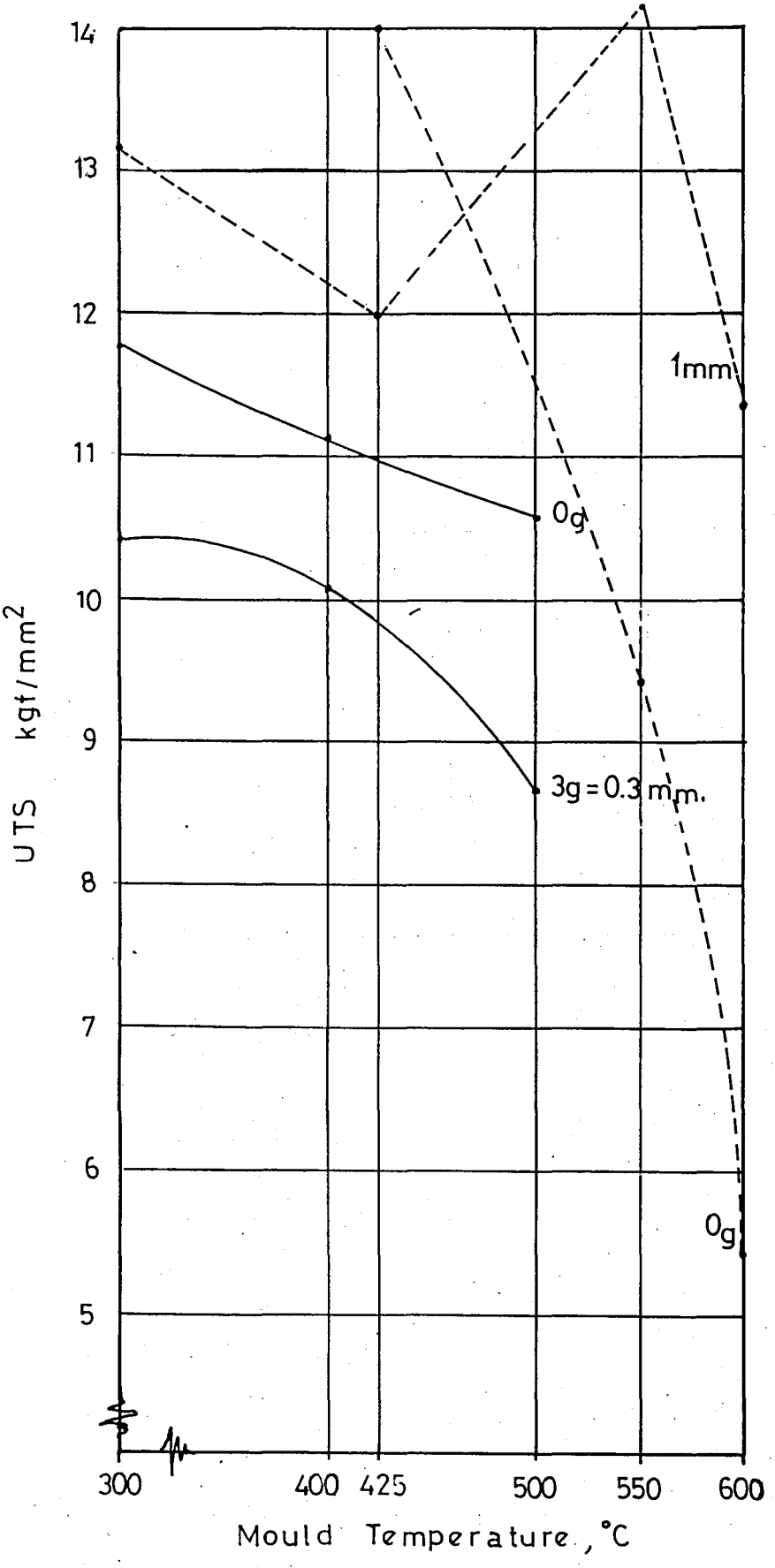

Figure 55- Tensile strength data for Al-% 33 Cu

— Results obtained by R.R.Burbure(10)

-- Results obtained in this study

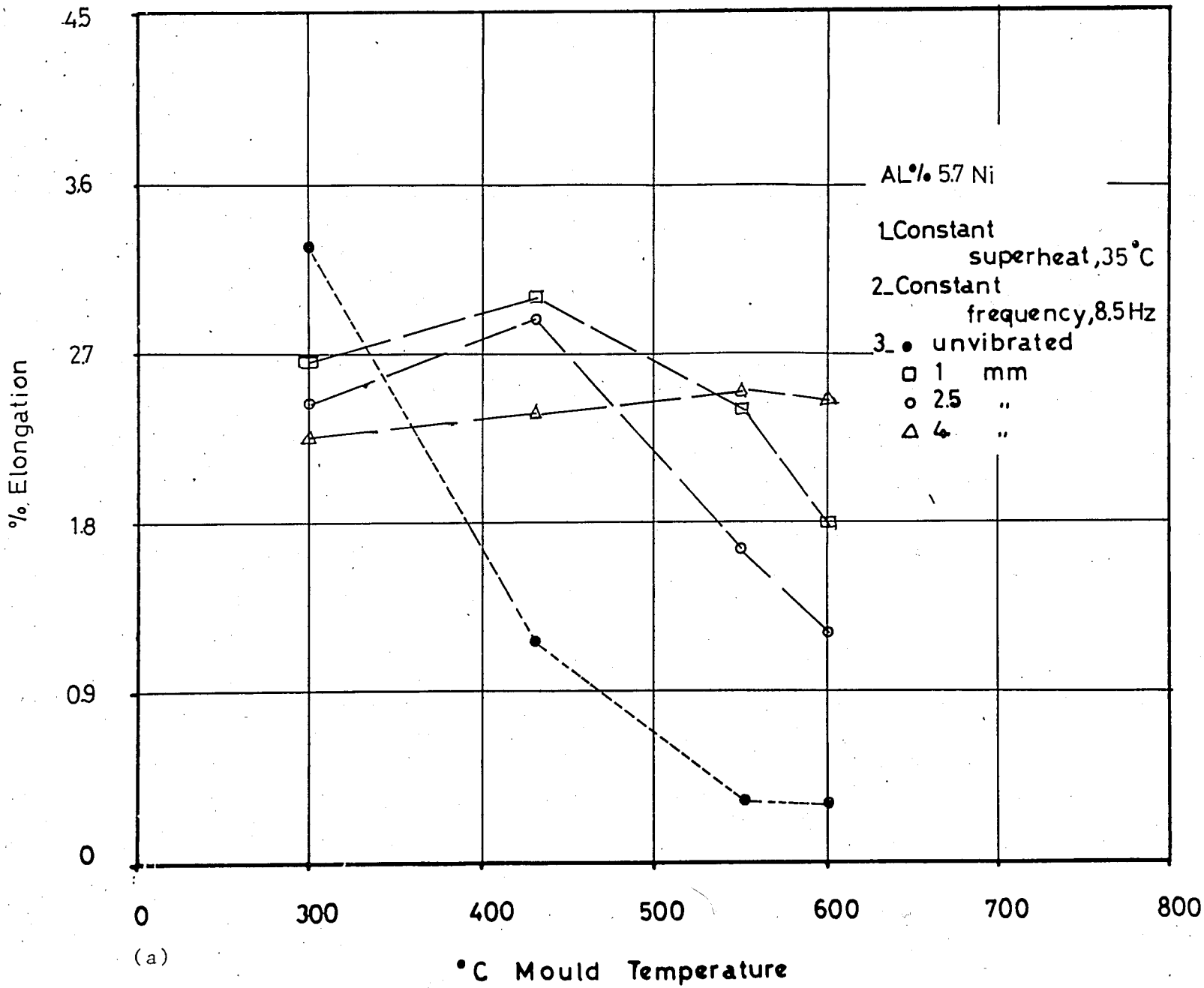

(a)

Figure 56- Results of the % elongation calculations

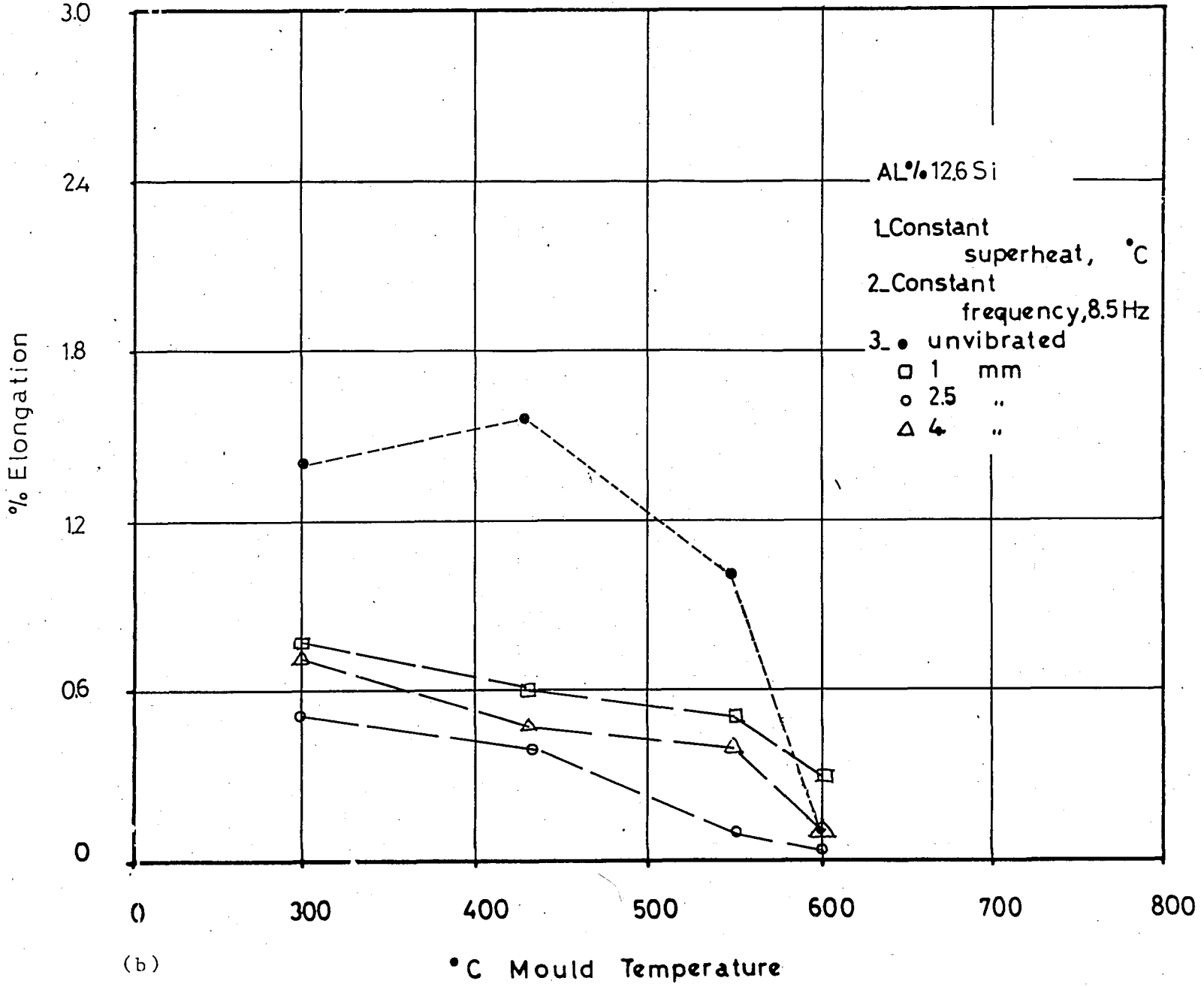
3.0
2.4
1.8
1.2
0.6
0
% Elongation
AL% 12.6 Si
1.Constant superheat, °C
2.Constant frequency, 8.5 Hz
3. ● unvibrated
□ 1 mm
○ 2.5 ,,
△ 4 ,,
0
300
400
500
600
700
800
°C Mould Temperature

(b)

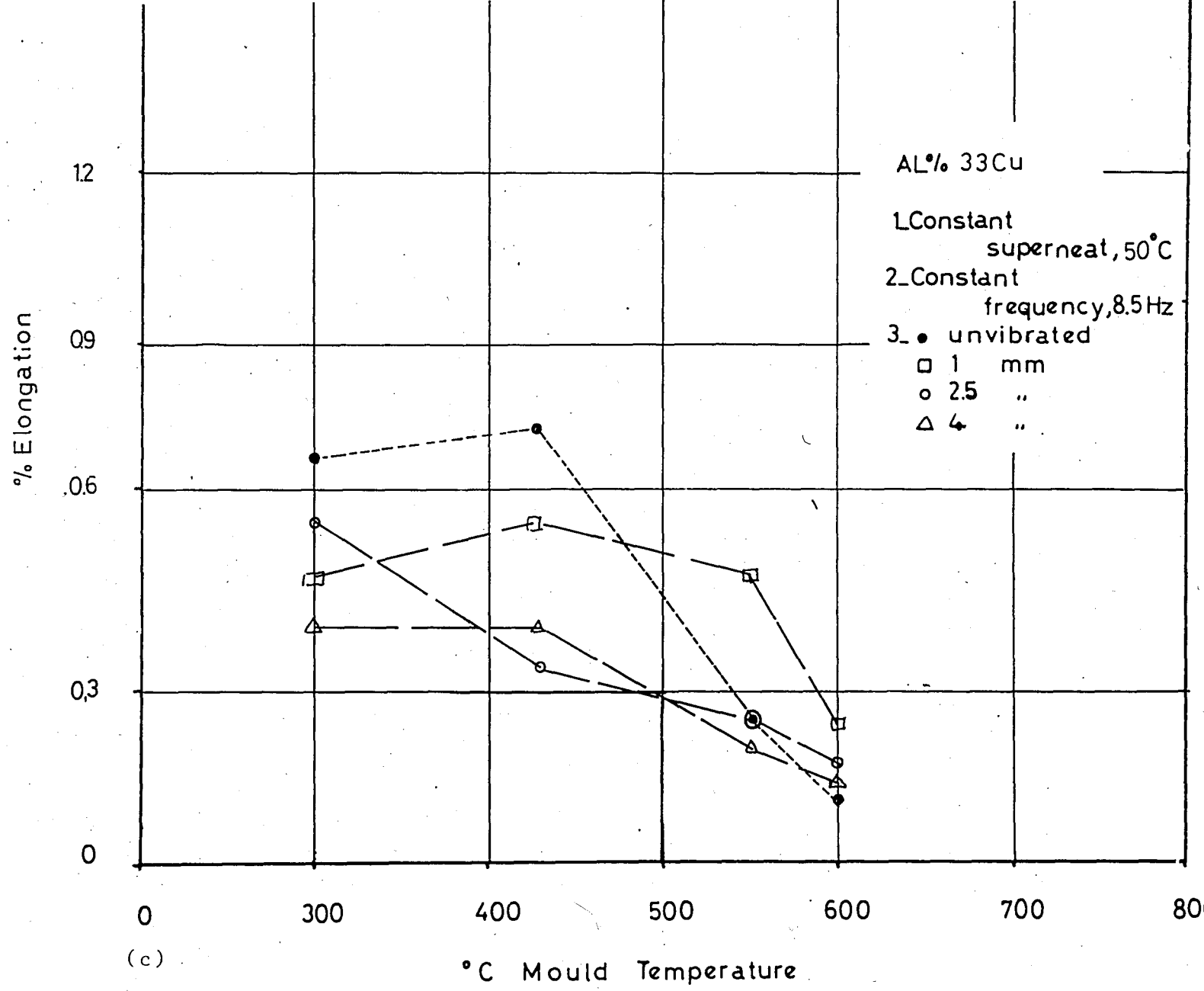
AL% 33Cu
1 Constant superneat, 50°C
2 Constant frequency, 8.5 Hz
3 ● unvibrated
□ 1 mm
○ 2.5 ,,
△ 4 ,,
% Elongation
1.2
0.9
0.6
0.3
0
0
300
400
500
600
700
800
°C Mould Temperature

(c)

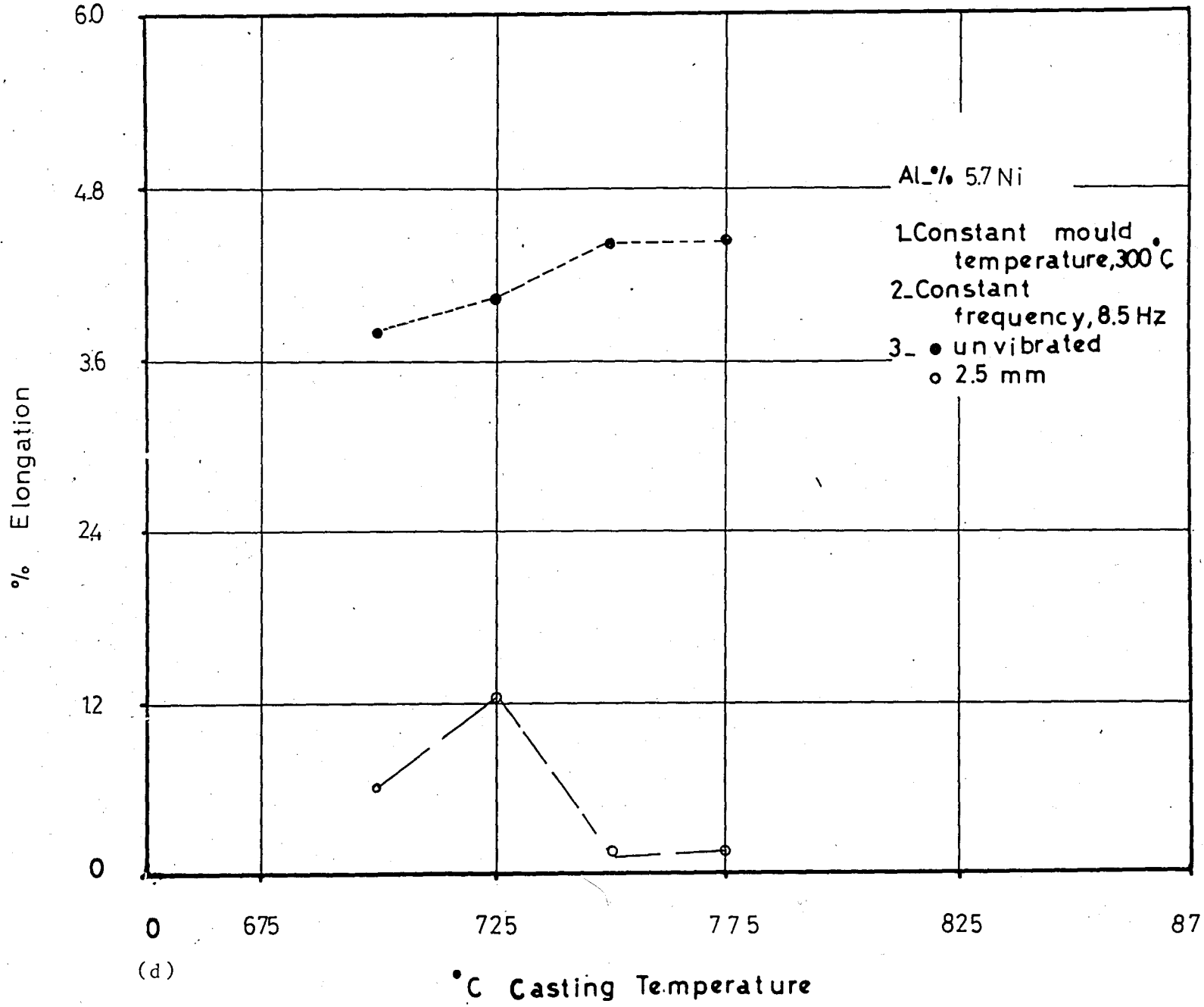
6.0
4.8
3.6
2.4
1.2
0
% Elongation
Al-% 5.7 Ni
1.Constant mould temperature, 300 °C
2.Constant frequency, 8.5 Hz
3. ● unvibrated
o 2.5 mm
0
675
725
775
825
875
°C Casting Temperature

(d)

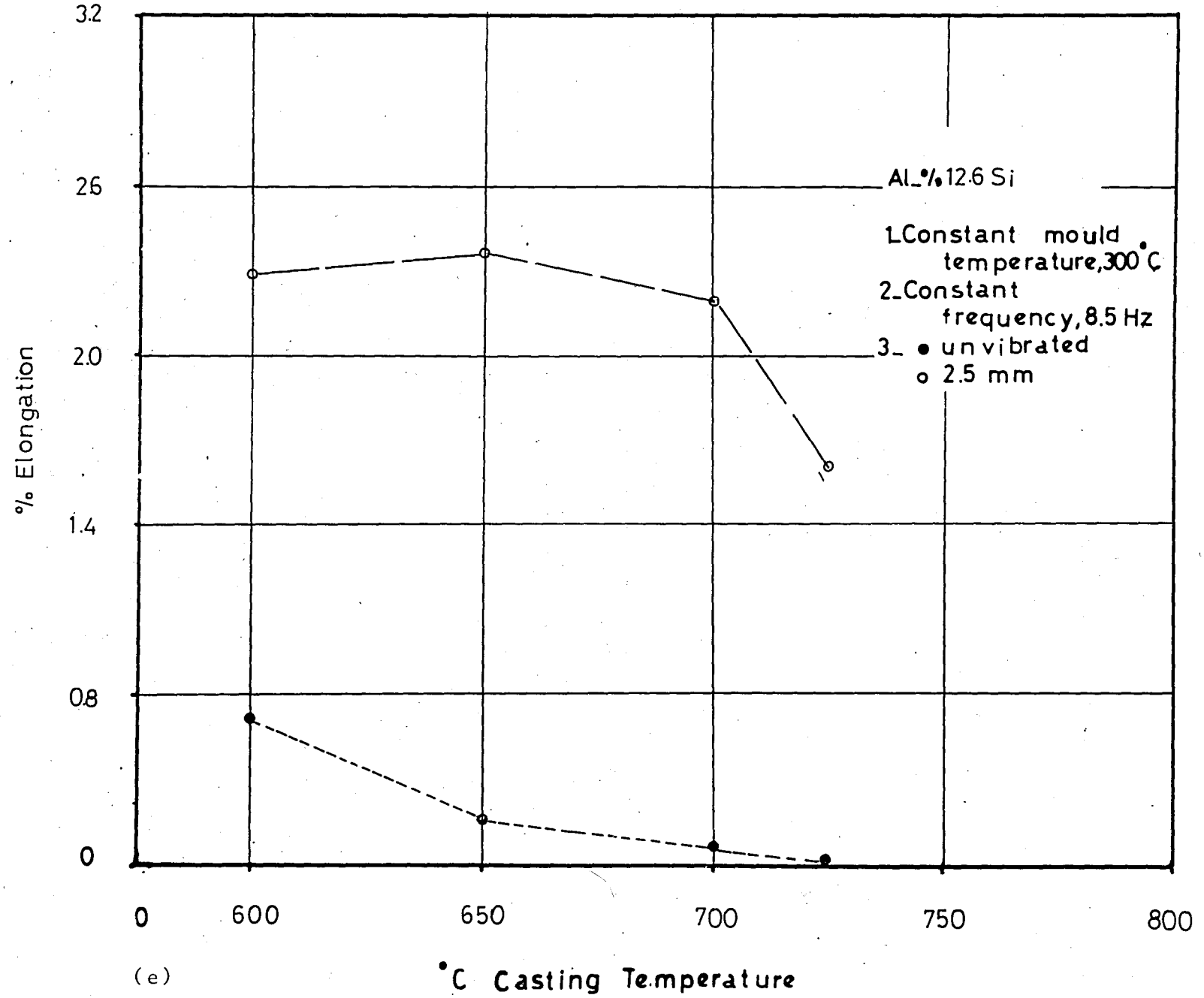
3.2
2.6
2.0
1.4
0.8
0
% Elongation
Al-% 12.6 Si
1. Constant mould temperature, 300 °C
2. Constant frequency, 8.5 Hz
3. • unvibrated
o 2.5 mm
0
600
650
700
750
800
°C Casting Temperature

(e)

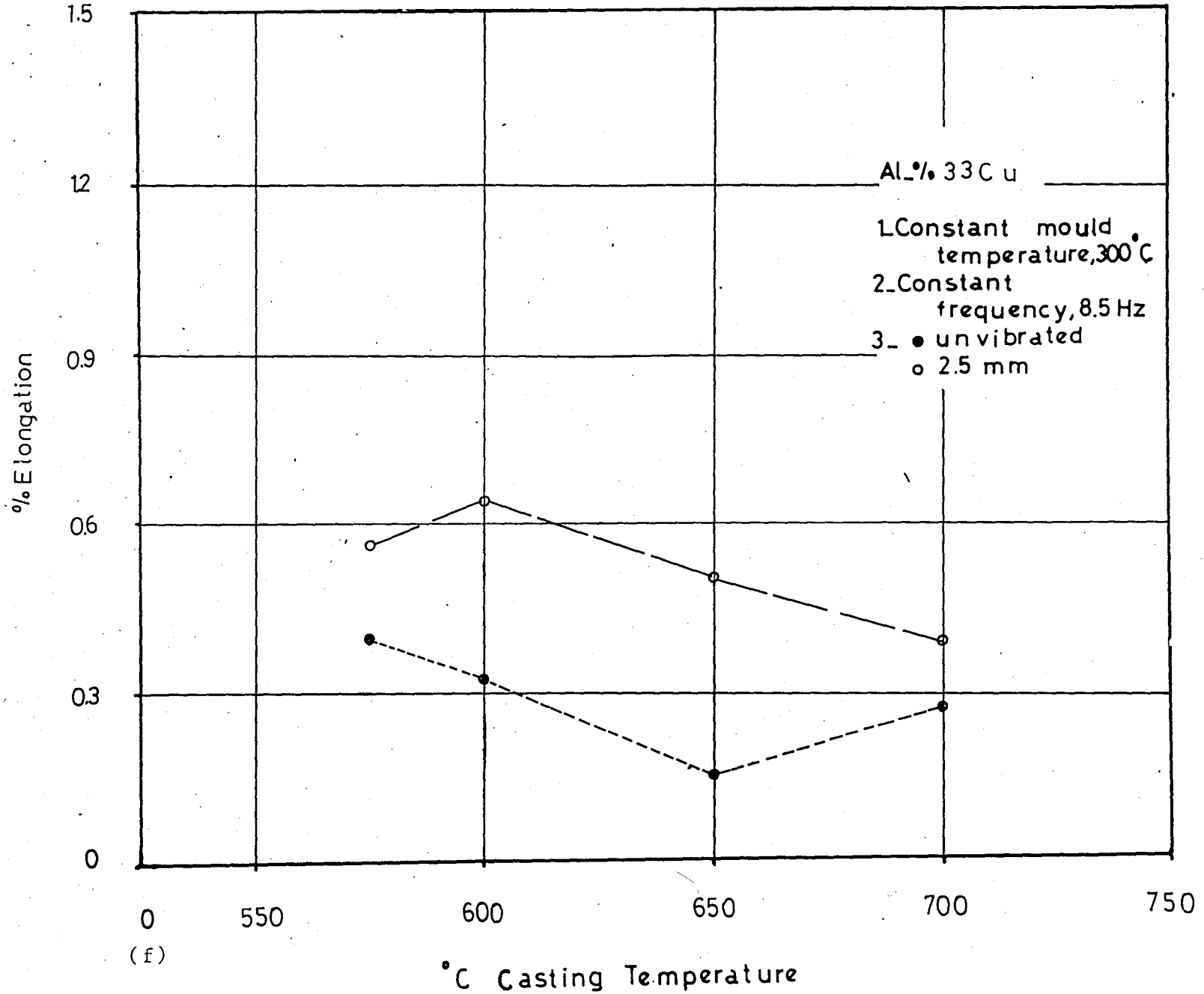
1.5
1.2
0.9
0.6
0.3
0
% Elongation
Al-% 33 Cu
1. Constant mould temperature, 300 °C
2. Constant frequency, 8.5 Hz
3. ● unvibrated
o 2.5 mm
0
550
600
650
700
750
°C Casting Temperature

(f)

present a decreasing elongation data as mould and casting temperatures increases, where as the maximum improvement obtained for vibrated ingots casted with increasing casting temperature is 630 % at 650^{o}C.

E. HARDNESS TESTS

1- Specimen Preperation

Vickers-Brinell hardness tester of Karl-Frank was used during tests. Different loads were employed for different alloys andspecimens of hardness tests were also obtained from the mid slices of the laterally sectioned ingots (Figure 52 a). The specimen surfaces were machined to provide parallel surfaces for correct testing.

Vickers Hardness tester uses a square base dimand pyramid as indenter and Vickers Hardnes Number (VHN) is defined as the lood divided by the surface area of the indentation which is calculated from microscopic measurements of the lengths of the diagonals of the impression.

$$VHN = 1.854\ P/L^2$$ where P = employed load, $L = (d_7 + d_8)/2$, d_7 = diagonal length, d_8 = second diagonal length.

2- Experimental Results

Twenty-four hardness tests were performed repeatedly for each group of alloys and different loads were employed for each group. On one test specimen, three different tests were made at different points, to obtain a correct mean hardness value. The hardness results are illustrated in figures 57 a to 57 f).

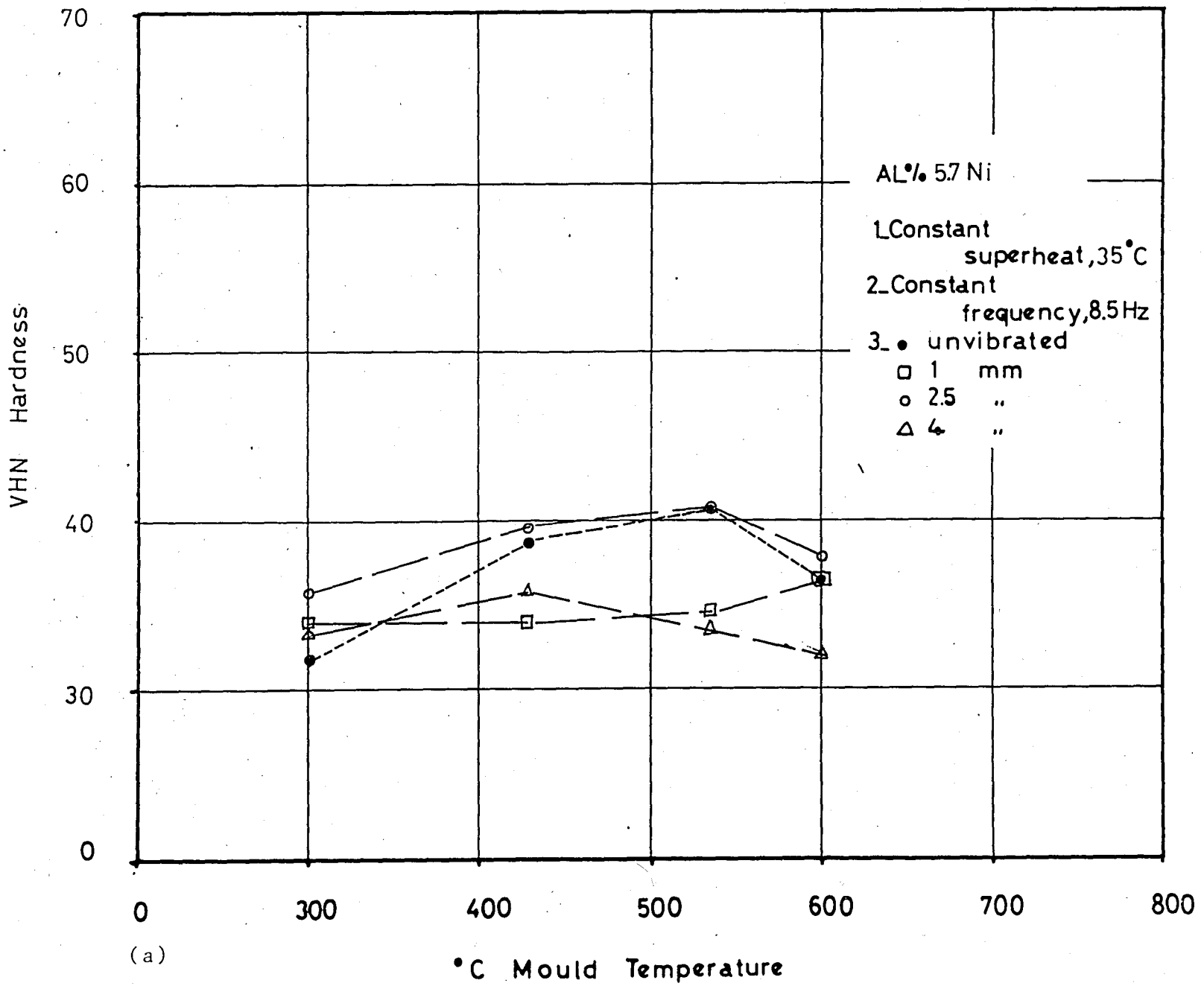

(a)

Figure 57- Results of the Hardness tests performed

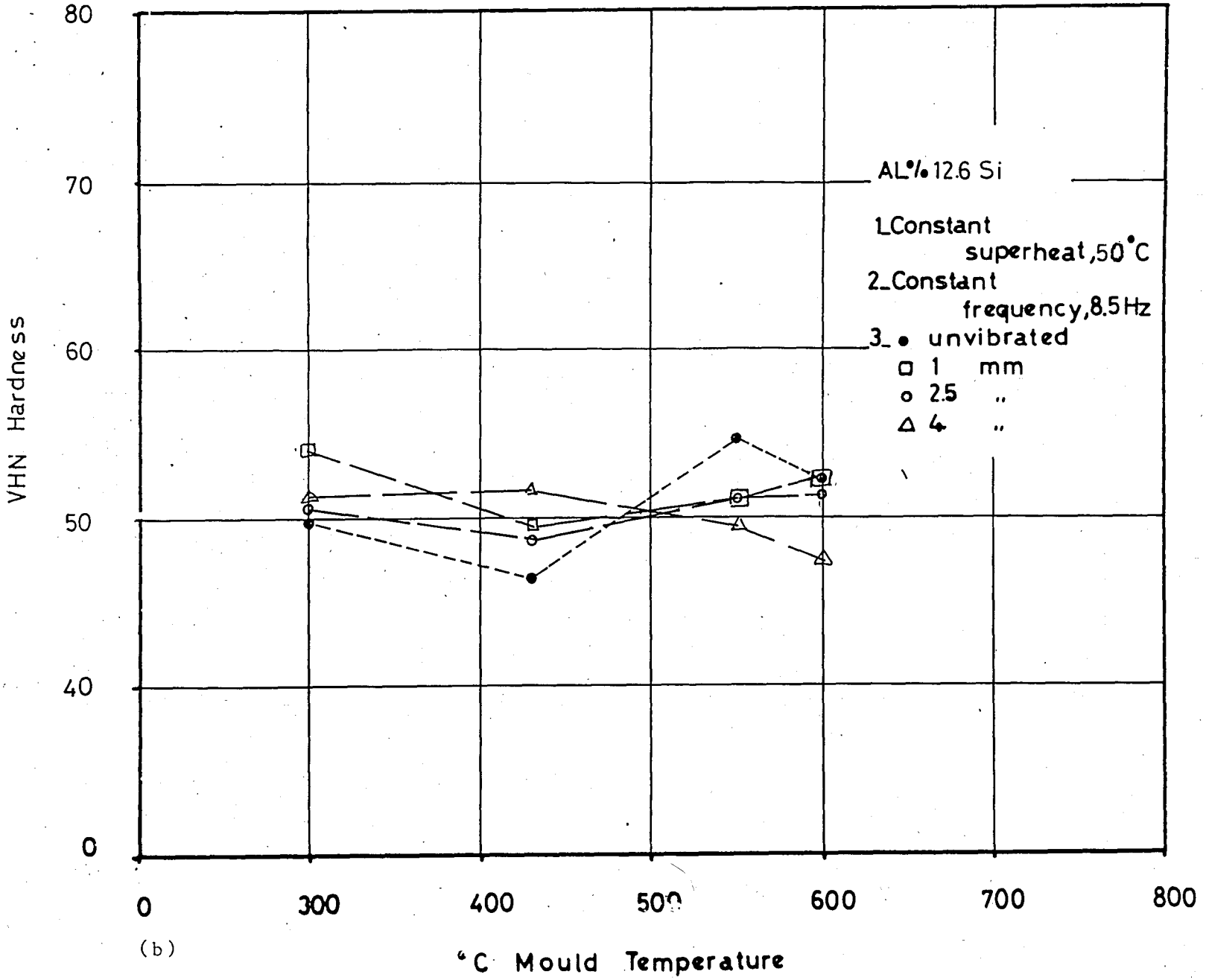
AL% 12.6 Si
1 Constant superheat, 50 °C
2 Constant frequency, 8.5 Hz
3 • unvibrated
□ 1 mm
o 2.5 ,,
△ 4 ,,
VHN Hardness
80
70
60
50
40
0
0
300
400
500
600
700
800
°C Mould Temperature

(b)

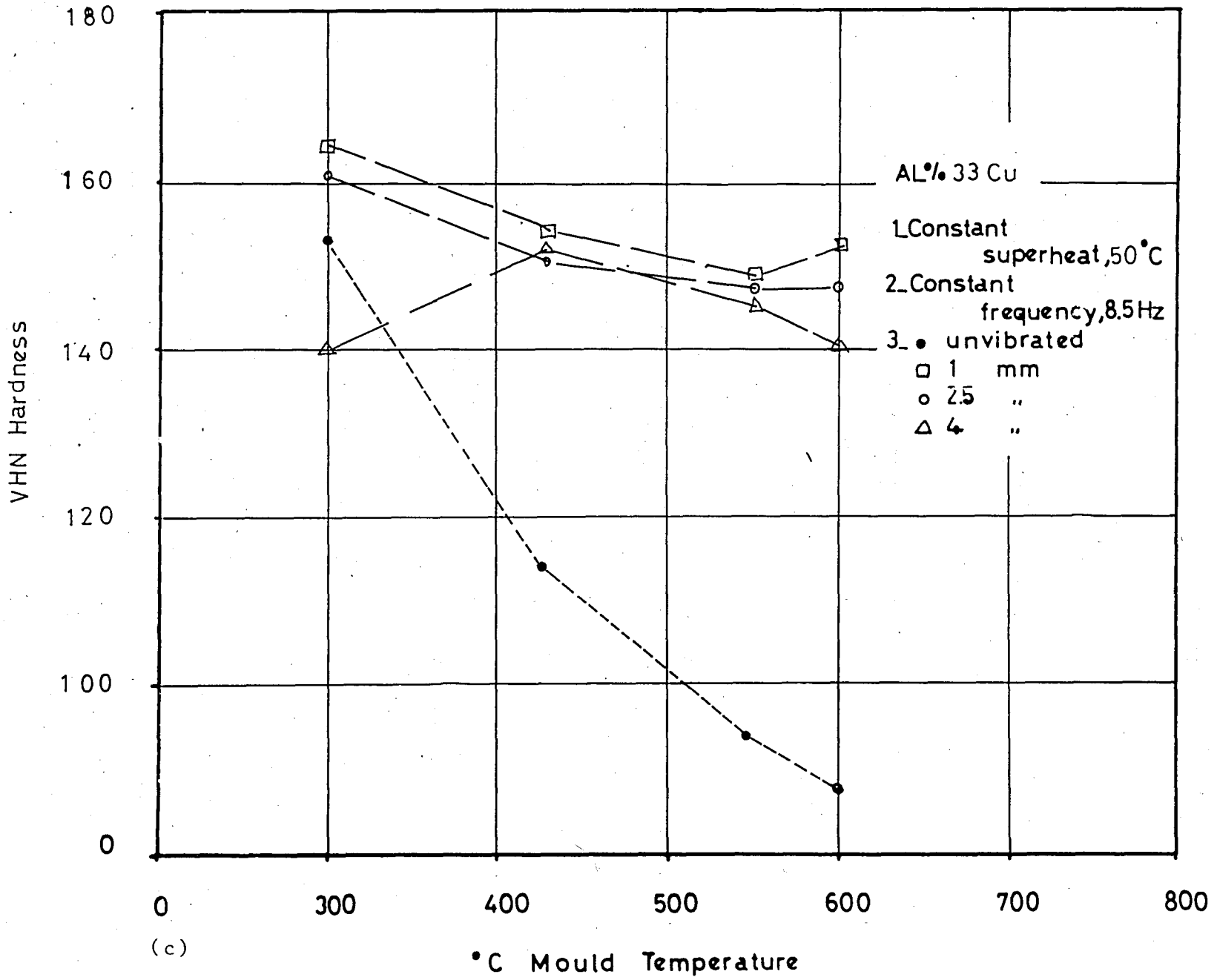
180
160
140
120
100
0
VHN Hardness
0
300
400
500
600
700
800
°C Mould Temperature
AL% 33 Cu
1 Constant superheat, 50°C
2 Constant frequency, 8.5 Hz
3 • unvibrated
□ 1 mm
○ 2.5 ,,
△ 4 ,,

(c)

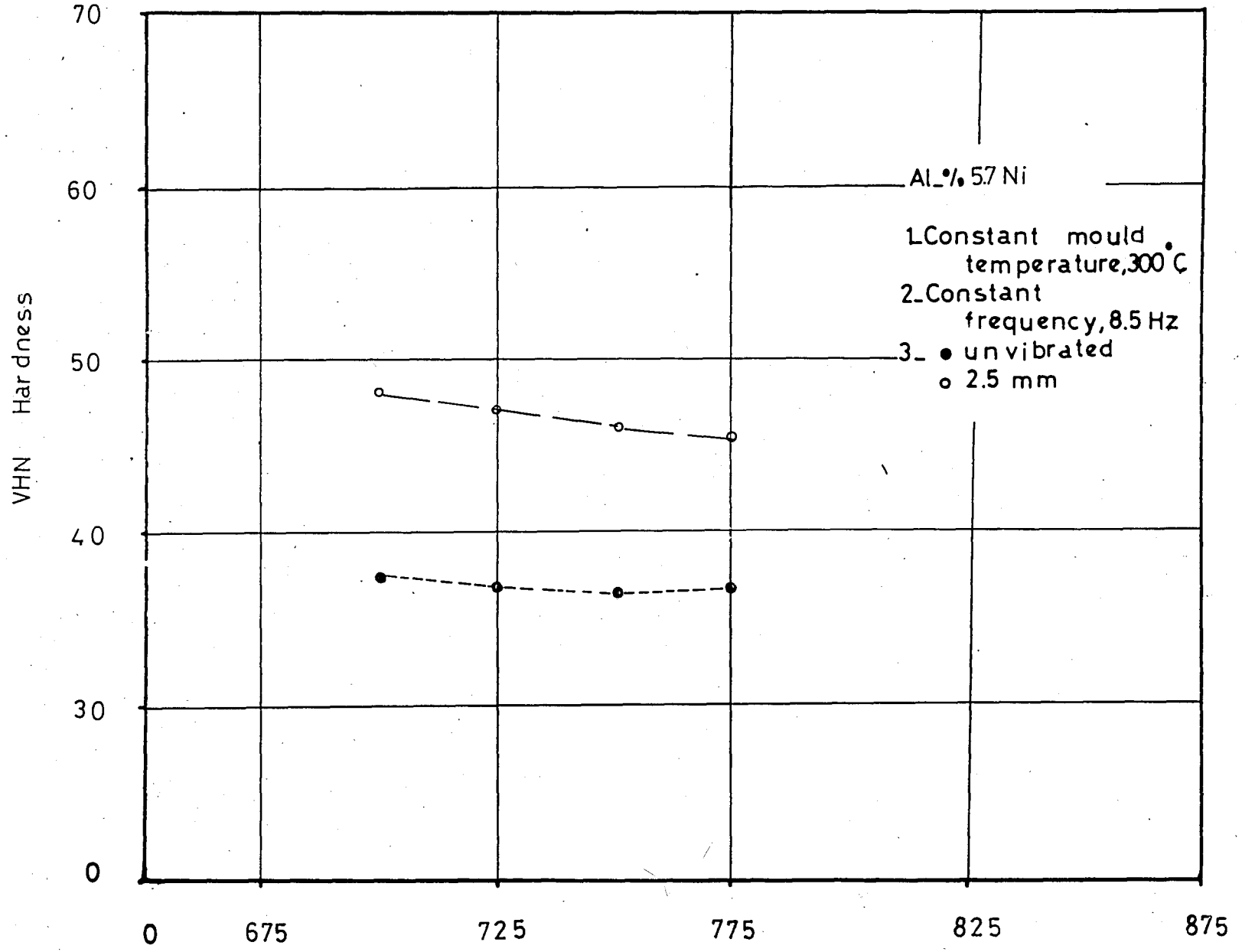
70
60
50
40
30
0
VHN Hardness
Al-% 5.7 Ni
1.Constant mould temperature, 300 °C
2.Constant frequency, 8.5 Hz
3. ● unvibrated
o 2.5 mm
0
675
725
775
825
875
°C Casting Temperature

(d)

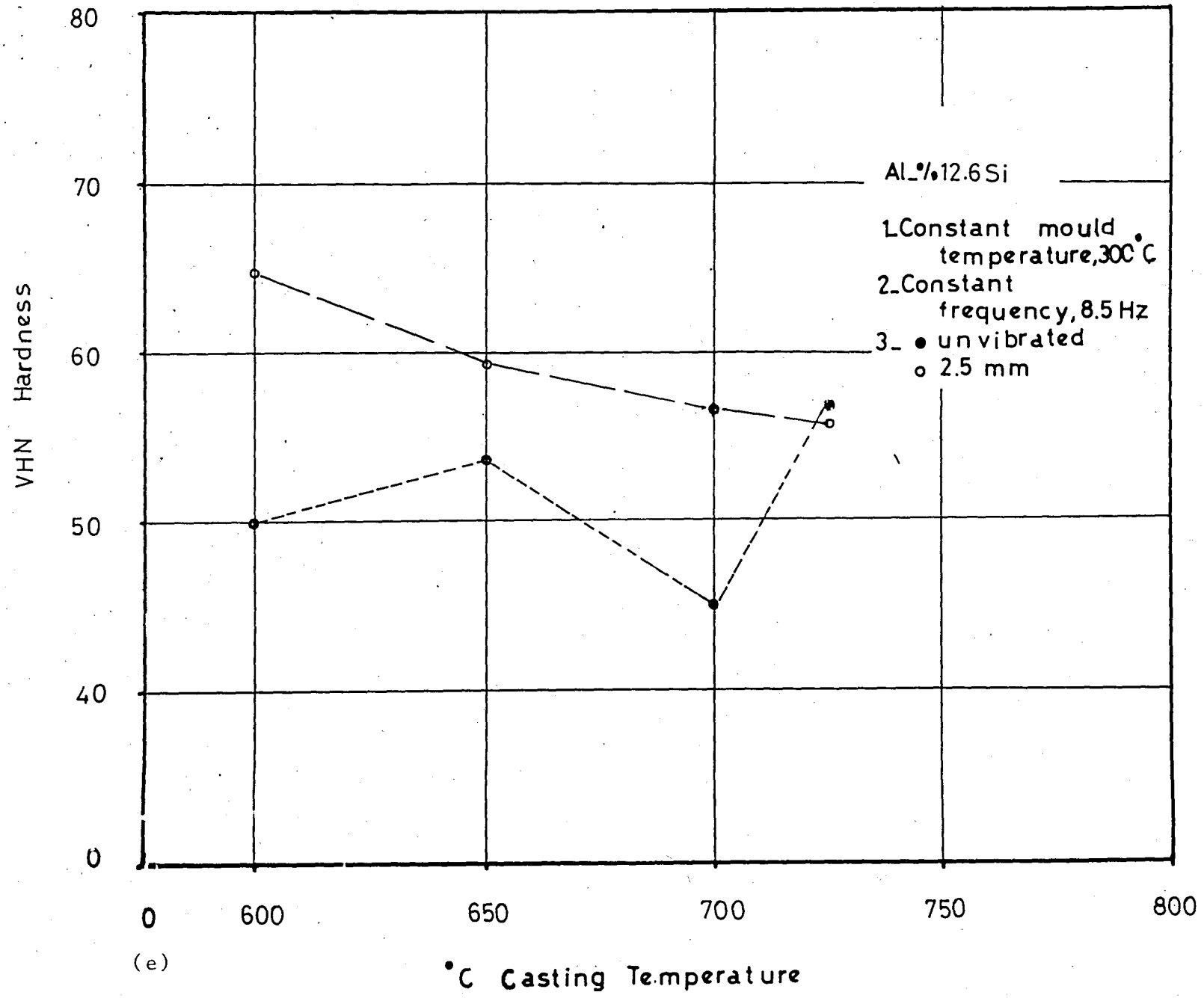
80
70
60
50
40
0
VHN Hardness
Al-%12.6 Si
1.Constant mould temperature, 300°C
2.Constant frequency, 8.5 Hz
3. • unvibrated
o 2.5 mm
0
600
650
700
750
800
°C Casting Temperature

(e)

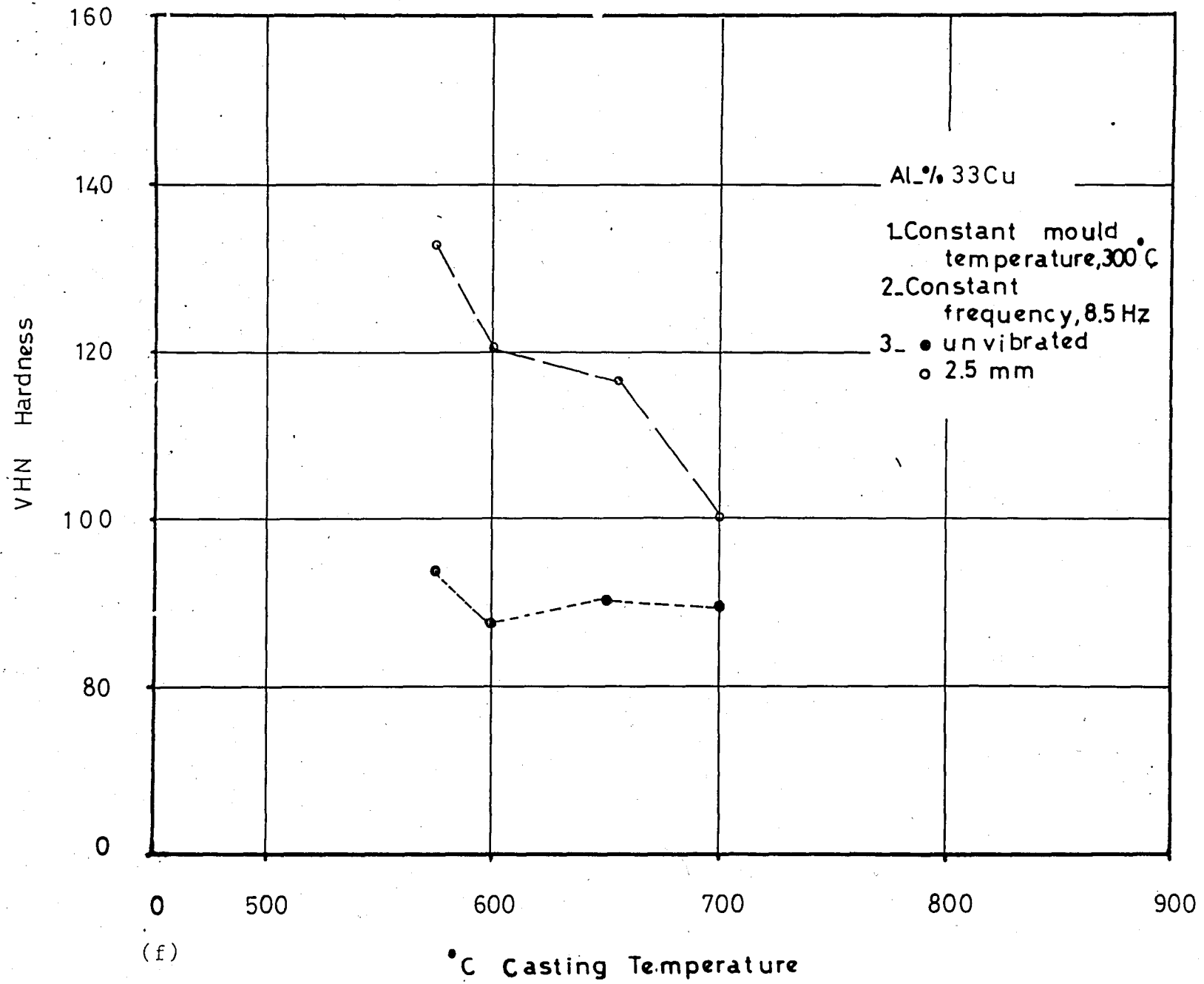
160
140
120
100
80
0
VHN Hardness
Al-% 33Cu
1.Constant mould temperature, 300°C
2.Constant frequency, 8.5 Hz
3. • unvibrated
o 2.5 mm
0
500
600
700
800
900
°C Casting Temperature

(f)

3- Discussion of the Results

The variation of the VHN of the vibrated and unvibrated alloy castings with increasing mould and casting temperatures are oberved in figures 57 a to 57 f.

By the examination of those illustrated data, it is predicted that all the vibrated ingots of Al-% 33 Cu exhibit an improvement in VHN casted with increasing mould temperature and the maximum improvement observed, 73 %, at 600°C. at 1 mm amplitude. Also the decreasing tendency in VHN with increasing mould temperature is clearly illustrated for the vibrated and unvibrated ingot alloys.

When the VHN data of Al-% 5.7 Ni is examined, it is seem to be that there is no any systematic effect of vibration on the VHN of the casted ingots. At only 425°C mould temperature all of the vibrated ingot castings, 1, 2.5 and 4 mm amplitudes, showed superior VHN and also the maximum improvement of 10.8 % observed at 425°C mould temperature. The VHN of the casted alloys, either vibrated or unvibrated, were not systematically effected by the increase in mould temperature.

As the illustrated data for Al-% 12.6 Si is searched, at low mould temperatures, 300°C and 425°C , the superiority of the VHN of vibrated ingot castings, for 1, 2.5 and 4 mm amplitudes, is observed and 8.5 % and 10.7 % maximum improvements observed for 300°C and 425°C respectively. The VHN of the unvibrated and vibrated, 1 and 2.5 mm, ingot castings show an increase and 4 mm amplitude vibrated ingot castings show a decrease with increasing mould temperature after 425°C mould temperature. Also at 600°C mould temperature the worst VHN data obtained for 4 mm vibrated ingot.

Also as the illustrated data in figures 57 d, e f are investigated, it is observed that the vibrated in gots casted with increasing casting temperature present a superior data when compared with the static control ones. The maximum improvements obtained are 45 % for Al-Cu at 575°C, 24 % for Al-Ni at 650°C and 26 % for Al-Si at 600°C, casting temperature.

CHAPTER VII
CONCLUSIONS

The effect of low-frequency vibration on microstructure and mechanical properties when applied to the solidifying melts of various aluminum base eutectics, Al-Cu, Al-Si, and Al-Ni was determined. A mechanical vibrating apparatus has been described in which the mould and casting were vibrated to-gether and a vibration of 9 cycle/sec frequency and 1, 2.5, 4 mm amplitudes were created. The effect of vibration on solidifying metals has been explained by many theories previously and for the case, eutectics solidified with dendritic or planar front, the disturbance in the liquid, interpreted as involving cavitation, is required. For metals which solidify in a dendritic manner, nuclei were formed by fragmentation of dendrite arms under bending stresses and for planar front solidifying metals nuclei were generated by cavitation erosion of the growing solid interface.

Microstructural analysis indicates that the size of the eutectic constituents in the matrix of primary aluminium and eutectic cells formed in the mid-ingot increases with increasing mould and casting temperature for all three aluminium eutectics. Also each eutectic alloy effected differently by vibrational treatment that the decreased eutectic constituent size in the vibrated ingots casted with increasing mould temperature observed for Al-% 5.7 Ni here as for Al-% 33 Cu and Al-% 12.6 Si the eutectic constituent size increases in the vibrated ingots when compared with static control ingots.

The vibrated ingots of Al-% 5.7 Ni present a improved UTS data when ingots casted with increasing mould temperature is considered, and the decreasing trend in UTS with the increase in mould and casting temperature is observed. Vibrated castings of Al-% 33 Cu exhibit a superior data for UTS at high mould temperatures and Al-% 12.6 Si showed an improved UTS data for vibrated ingots casted with increasing casting temperature. Also the obtained elongation data is closely consistent with

the UTS data all though the accuracy in the measurements is not ashigh as desired.

Vickers hardness values obtained from the vibrated ingots exhibit somehow a different behavior. The improvement observed for ingots of Al-% Ni and Al-% 12.6 Si casted with increasing mould temperature is significant at low mould temperatures, where as a superior hardness data presented for Al-% 33 Cu at all mould temperatures. Also the obtained data for vibrated ingots casted with increasing temperature exhibit improvement for all three alloys. The effect of increasing mould and casting temperature also observable from the obtained decreasing data.

Above discussions predict the general lay-out of the effects caused by vibrational treatment that the most beneficial results obtained for Al-Cuand Al-Ni eutectics which do not have any commercial importance. On the other hand the practical importance of the improved UTS and hardness value obtained for Al-Si eutectic alloy in the vibrated ingots casted with increasing casting temperature can be taken into consideration in thin walled, precision castings.

B I B L I O G R A P H Y

1- G.S.Cole and G.F.Bolling; "The Solidification of Innoculated Aluminium ingots", Metallurgical Tarns., Vol.1, May 1970, 1413-1416.

2- W.C.Jonston, G.R.Kotler, S.O'Hara; "Gram Refinement via Electromagnatic Stirring During Solidification", Trans. AIME, Vol.233, Oct. 1965, 1856-1860.

3- A.H.Freedman and J.F.Wallace; "The Influence of Vibration On Solidifying Metals", AFS Trans., 65, 1957, 578-589.

4- R.G.Garlick and J.F.Wallace, "Gram Refinement of Solidifying Metals By Vibration", AFS. Trans., Vol.67, 1959, 366-374.

5- R.I.Southin; "The Influence of Low-Frequency Vibration On the Nucleation of Solidifying Metals", J.Of Inst.Metal, Vol.94, 1966, 401-407.

6- R.S.Richards and W.Rostoker, "The Influence of Vibration On The Solidification of An Aluminium Alloy", Trans. ASM. Vol.48, 1956, 884-903.

7- A.J.Murphy; "Non-Ferrous Foundary Metallurgy", Pergamon Press, New York, 1954.

8- A.Ihsan Telli; "Modification of Al-Si Eutectics Alloy By Antimony", Masters' Thesis, Boğaziçi University, 1984.

9- T.P.Fisher; "Effects of Vibrational Energy on the Soli Solidification of Aluminium Alloys", Br.Foundaryman, 72, 2, 1973, 71-89.

10- Ramesh,R.Burbure; "Influence of Low-Frequency Vibrations on aluminium eutectics", Br.Foundaryman, 1979, 35-38.

11- W.Rostoker and J.R.Dvorak; "Interpritation of Metallographic Structures", Academic Press, New York, 1977.

12- B.Chalmers; "Principles of Solidification", J.Wiley and Sons, New York, 1964.

13- J.Champbell; "Effects of Vibration During Solidification", Int.Metal Rewiev, Vol.26, 2, 1981.

14- E.A.Hiedeman; "Metallurgical Effects of Ultrasonic Waves", J.Of A.Soc.of America, Vol.26, 5, 1954.

15- J.J.Frawley and W.J.Chills; "Dynamic Nucleation of Supercooled Metals", Trans.of the Met.Soc. of AIME, 242, 2, 1968, 256-263.

16- A.Claro; "Effect of Vibration on Solidification of Transperent liquids and Al-Si alloys", F, AFS Trans., Vol. 78, 1970, 324-331.

17- J.H.Gittus; "The Innoculation of Iron and Steel Casting By Means of Vibration", J.of Iron and Steel Inst., June 1959, 118-131.

18- P.D.Southgate; "Action of Vibration on Solidifying Aluminium Allongs", J.of Metals, trans.AIME, Apr. 1957, 514-517.

19- H.A.Steen and A.Hellawel; "Structure and Properties of Al-Si eutectie alloys, Acta Metall., Vol.20, Mar.1972, 363-370.

20- N.Eruslu; "Geniş Katılaşma Aralıklı Al-Cu-Zn alaşımlarında Düşük Frekanslı Titreşim Ulguyarak Döküm Yapısının Kontrolu; Doktora Tezi, İTÜ Metalurji Fakültesi, 1981.

21- Tensile Testing of Metallic Materials, TS 138 March 1978.

22- G.A.Chadwick; "Yield Point analysis in eutectic alloys", Acta Metall., Vol.24, 1976, 1137-1146.

23- W.Rostoker and M.O.Berger; "Effects of Vibration During Solidification of Castings", Foundary, July 1953, 101-105 and 260-265.

24- S.Wojciechowski and B.Chalmers; "The influence of Mechanical Stirring on the Columnar to Equiaxed Transition in Aluminium-Copper Alloys", Trans.ASME Vol.242, Apr.1968, 690-697.

25- A.H.Lane, W.A.Tiller; "Application of Ultrasonic Energy to Ingot Solidification", Trans. AIME, Vol.218, Dec.1960, 985-990.

26- J.C.Johnston, G.R.Kotler; "The Influence of Electromagnetic Stirring in the Nucleation of Tin and Tin-Lead Alloys", Trans. AIME, Vol.227, Dec.1963, 890-896.

27- G.S.Cole and F.Bolling; "Enforced Fluid Motion and The Control of Grain Structures In Metal Castings", Trans. AIME, Vol.239, Nov.1967, 1824-1835.

28- Paul S.Hurd; "Metallic Materials", Holt Rinehart and Winston Inc., New York.

29- Paul G.Shewnon, "Transformations In Metals", McGraw Hill Book Company, New York.

APPENDIX A

Ultimate Tensile Strength Data For Al-Cu Eutectic

Mould temperature °C	Casting temperature °C	Vibration amplitude mm	N/m^2 $x10^5$
300	600	0	2371
425	"	"	1372.8
550	"	"	920.4
600	"	"	530.4
300	"	1	1287
425	"	"	1170
550	"	"	1388.4
600	"	"	1138.8
300	"	2.5	1232.4
425	"	"	780
550	"	"	577.2
600	"	"	1123.2
300	"	4	1778.4
425	"	"	1045.2
550	"	"	1638
600	"	"	1248
300	575	0	2277.6
"	600	"	1521
"	650	"	1154.4
"	700	"	1794
"	575	2.5	1294.8
"	600	"	1544.4
"	650	"	780
"	700	"	624

Ultimate Tensile Strength data for Al-Ni eutectic

Mould temperature °C	Casting temperature °C	Vibration amplitude mm	N/m^2 $x10^5$
300	675	0	1092
425	"	"	577.2
550	"	"	156
600	"	"	280.8
300	"	1	670.8
425	"	"	1326
550	"	"	1123.2
600	"	"	1014
300	"	2.5	1123.2
425	"	"	138.8
550	"	"	936
600	"	"	780
300	"	4	858
425	"	"	1326
550	"	"	1201.6
600	"	"	468
300	700	0	982.8
"	725	"	1170
"	750	"	1170
"	775	"	1170
"	700	2.5	1060.8
"	725	"	764.4
"	750	"	468
"	775	"	468

Ultimate Tensile Strength data for Al-Si eutectic

Mould temperature ^{o}C	Casting temperature ^{o}C	Vibration amplitude mm	$N/m^2 \times 10^5$
300	625	0	1154.4
425	"	"	1497.8
550	"	"	1326
600	"	"	982.8
300	"	1	936
425	"	"	858
550	"	"	1170
600	"	"	1014
300	"	2.5	1170
425	"	"	858
550	"	"	702
600	"	"	546
300	"	4	936
425	"	"	920.4
550	"	"	1294.8
600	"	"	936
300	600	0	936
"	650	"	780
"	700	"	982.8
"	725	"	546
"	600	2.5	1138.8
"	650	"	1638
"	700	"	1123.2
"	725	"	842.4

Elongation data for Al-Cu eutectic

Mould temperature °C	Casting temperature °C	Vibration amplitude mm	%
300	600	0	0.67
425	"	"	0.75
550	"	"	0.25
600	"	"	0.1
300	"	1	0.48
425	"	"	0.58
550	"	"	0.51
600	"	"	0.24
300	"	2.5	0.55
425	"	"	0.33
550	"	"	0.25
600	"	"	0.13
300	"	4	0.41
425	"	"	0.41
550	"	"	0.13
600	"	"	0.11
300	575	0	0.41
"	600	"	0.33
"	650	"	0.16
"	700	"	0.27
"	575	2.5	0.55
"	600	"	0.65
"	650	"	0.5
"	700	"	0.42

Elongation data for Al-Ni eutectic

Mould temperature °C	Casting temperature °C	Vibration amplitude mm	%
300	675	0	3.25
425	"	"	1.16
550	"	"	0.33
600	"	"	0.33
300	"	1	2.6
425	"	"	3
550	"	"	2.4
600	"	"	1.8
300	"	2.5	2.5
425	"	"	2.92
550	"	"	1.6
600	"	"	1.2
300	"	4	2.3
425	"	"	2.4
550	"	"	2.5
600	"	"	2.5
300	700	0	3.8
"	725	"	4
"	750	"	4.58
"	775	"	4.5
"	700	2.5	0.66
"	725	"	1.2
"	750	"	0.16
"	775	"	0.16

Elongation data for Al-Si eutectic

Mould temperature °C	Casting temperature °C	Vibration amplitude mm	%
300	625	0	1.4
425	"	"	2.3
550	"	"	1
600	"	"	0.13
300	"	1	0.74
425	"	"	0.6
550	"	"	0.55
600	"	"	0.3
300	"	2.5	0.5
425	"	"	0.3
550	"	"	0.13
600	"	"	0.1
300	"	4	0.7
425	"	"	0.41
550	"	"	0.37
600	"	"	0.13
300	600	0	0.74
"	650	"	0.34
"	700	"	0.25
"	725	"	0.16
"	600	2.5	2.3
"	650	"	2.5
"	700	"	2.3
"	725	"	1.6

VHN Data for Al-Cu eutectic

Mould temperature °C	Casting temperature °C	Vibration amplitude mm	VHN
300	600	0	152.2
425	"	"	115.58
550	"	"	95.23
600	"	"	88.74
300	"	1	165.7
425	"	"	155.2
550	"	"	150.5
600	"	"	153.2
300	"	2.5	162.2
425	"	"	151.2
550	"	"	149.3
600	"	"	148.2
300	"	4	139.6
425	"	"	152.8
550	"	"	146.7
600	"	"	142
300	575	0	93.23
"	600	"	88.08
"	650	"	90.07
"	700	"	89.85
"	575	2.5	136.02
"	600	"	119.85
"	650	"	118.21
"	700	"	100.06

VHN Data for Al-Ni eutectic

Mould temperature °C	Casting temperature °C	Vibration amplitude mm	VHN
300	675	0	31.66
425	"	"	38.60
550	"	"	40.8
600	"	"	36.7
300	"	1	34.12
425	"	"	34.12
550	"	"	34.44
600	"	"	36.09
300	"	2.5	35.08
425	"	"	39.57
550	"	"	40.84
600	"	"	38.15
300	"	4	34.65
425	"	"	35.75
550	"	"	33.35
600	"	"	32.26
300	700	0	38.10
"	725	"	37.83
"	750	"	37.83
"	775	"	37.99
"	700	2.5	47.5
"	725	"	46.30
"	750	"	45.07
"	775	"	43.52

VHN Data for Al-Si eutectic

Mould temperature °C	Casting temperature °C	Vibration amplitude mm	VHN
300	625	0	49.53
425	"	"	46.29
550	"	"	54.44
600	"	"	51.44
300	"	1	53.78
425	"	"	49.76
550	"	"	51
600	"	"	52.73
300	"	2.5	49.98
425	"	"	48.69
550	"	"	50.87
600	"	"	51.03
300	"	4	50.65
425	"	"	51.25
550	"	"	49.04
600	"	"	47.10
300	600	0	50.87
"	650	"	53.62
"	700	"	45.98
"	725	"	56.06
"	600	2.5	64.21
"	650	"	59.53
"	700	"	57.07
"	725	"	55.13